ASSESSING POTENTIAL APPLICATIONS OF MULTI-COIL AND MULTI-FREQUENCY ELECTROMAGNETIC INDUCTION SENSORS FOR AGRICULTURAL SOILS IN WESTERN NEWFOUNDLAND

by

© Kamaleswaran Sadatcharam

A thesis submitted to the School of Graduate Studies

in partial fulfillment of the requirements for the degree of

Master of Science

Boreal Ecosystems and Agricultural Sciences

School of Science and the Environment

Grenfell Campus

Memorial University of Newfoundland

March 2019

St. John’s Newfoundland and Labrador

Abstract

Ground-based electromagnetic induction (EMI) sensors play a significant role in shallow soil characterization in precision agriculture. Two different types of EMI sensors were used in this study: (i) a multi-coil and (ii) a multi-frequency. The potential applications of both EMI sensors have been assessed through two different studies at the Pynn's Brook Research Station, Pasadena, western Newfoundland. One study was on the development of relationships between apparent electrical conductivity (EC_a) and soil properties, using geostatistical and multivariate statistical approaches, and the second study investigated the depth sensitivity (DS) of multi-coil and multi-frequency EMI sensors using small buried targets of known properties in shallow soils. Soil properties, such as sand, silt, soil moisture content (SMC), cation exchange capacity (CEC), and pore water electrical conductivity (EC_w), were identified as significantly influenced soil properties on EC_a measurements. The multi-frequency EMI sensor is more reliable on EC_a variability for wet soils than dry soils and it could explore deeper soil compared to the multi-coil sensor. The second study revealed that the multi-coil EMI sensor was a more accurate and suitable sensor to detect small metallic targets in the shallow soils than the multi-frequency EMI sensor. Finally, I concluded that the multi-coil EMI sensor is a more appropriate compared to the multi-frequency sensor, to investigate depth sensitivity (DS) analysis as well as the spatiotemporal variability of EC_a as a proxy of soil properties in shallow (agricultural) soils in western Newfoundland.

Acknowledgments

First and foremost, my sincere gratitude to my advisor Dr. Lakshman Galagedara, for the guidance, encouragement and support during field work as well in the successful completion of this research. I would like to express my special thanks to my co-advisor, Dr. Adrian Unc, and advisory committee member, Dr. Manokararajah Krishnapillai, who have provided valuable comments, suggestions, and inputs to my research work.

My special thanks to Dr. Daniel Altdorff for his support and guidance on EMI measurements and analyses. I express my warm thanks to the Research and Development Corporation, NL (RDC-Ignite) and Research Office of the Grenfell Campus, Memorial University of Newfoundland for their financial support. I thank Dr. Tao Yuan for his assistance in the laboratory. My sincere thank to Chameera Illawature for GPR data collection at the field. I especially thank my friends and team members who helped in various aspects of this research, Emmanuel Badewa, Dinushika Wanniarachchi, Ivo Arrey, Gnanakaran Maheswaran, Waqas Ali, Waqar Ashiq, and Abiraami Ramasamy.

I wish to offer my heartfelt thanks to all my family: parents, brothers and sisters, especially my loving wife, for their support and encouragements.

All your support and cooperation are much appreciated.

Kamaleswaran Sadatcharam

Table of Contents

List of Tables

List of Figures

List of Abbreviations and Symbols

ADC	Analog to digital converter
AM	Active microwaves
ASTM	American Society for Testing and Materials
BD	Bulk density
CEC	Cation exchange capacity
cm	Centimeter
CP	Capacitance probe
CR	Cumulative response
CV	Coefficient of variation
DS	Depth sensitivity
DSP	Digital signal processor
EC	Electrical conductivity
EC_a	Apparent electrical conductivity
EC_w	Pore water electrical conductivity
EM	Electromagnetic
EMI	Electromagnetic induction
EPA	Environmental protection agency
ER	Electrical resistivity
f	Frequency
GPR	Ground penetrating radar
GPS	Global positioning system
ha	Hectare
HCP	Horizontal coplanar
Hp	Primary magnetic field
Hs	Secondary magnetic field
ICS, *s*	Inter-coil separation
Kg	Kilogram
LIN	Low induction number
m	Meter
M	Molarity of the solution
Max	Maximum
Min	Minimum
MLR	Multiple linear regression
MS_a	Apparent magnetic susceptibility
N	North
n	Number of samples

NL	Newfoundland and Labrador
NMR	Nuclear magnetic resonance
PBRS	Pynn’s broke research station
PCA	Principal component analysis
PCs	Principal components
PD	Pseudo depth
PDA	Personal digital assistant
PM	Passive microwaves
ppm	Parts per million
ppt	Parts per thousand
r	Pearson's correlation
R^2	Coefficient of determination
R^2p	Predicted R^2
RNE	Relative nugget effects
RR	Relative response
Rx	Receiver
S	Siemens
SD	Standard deviation
SE	Standard error
SMC	Soil moisture content
TDR	Time domain reflectometry
TDS	Total dissolved solids
Tx	Transmitter
USA	United States of America
USDA	United States Department of Agriculture
V5	Corn variety (DKC26-28RIB)
VCP	Vertical coplanar
W	West
z	Normalized depth
°C	Degree Celsius

Chapter 1: Introduction and Overview

1.1. Background

Understanding spatiotemporal variability of the soil and water is necessary to develop site-specific management practices to achieve sustainable agriculture in Newfoundland and Labrador (NL); it is also a required and fundamental assessment for precision agriculture. Soil spatiotemporal variability studies in support of sustainable agricultural development for the future food production in the province of NL are gaining attention (Quinlan, 2012).

Around 55% of the landmass in the NL province is covered by Podzolic soil (Sanborn et al., 2011). Western Newfoundland is predominantly covered by soils classified in the great Podzol group of “Orthic Humo-Ferric Podzol,” which are brownish-colored and have low organic matter (Kirby, 1988; Sanborn et al., 2011). General characterizations of Podzol are acidic, well to rapid drainage, low nutrients, coarse to medium texture, and shallow (Kirby, 1988). These soil characterizations limit agricultural production for most of the agricultural soils in NL. Therefore, soil quality needs to be improved through practices such as adding organic matter to improve the structure and increase water holding capacity and using fertilizers to make the soil fertile for agricultural activities. Soil moisture content (SMC) is a fundamental soil property that highly influences crop production, and, therefore, its spatiotemporal variability has to be monitored under field conditions to support site-specific agricultural management. Not only SMC, but other physiochemical properties--such as texture, bulk density (BD), porosity, pore water electrical conductivity (EC_w) and cation exchange capacity (CEC)--of soils should be monitored rapidly to avoid minor temporal variabilities for large-scale agriculture. Near-surface geophysical techniques are called for to understand, characterize, and monitor the spatiotemporal variability of soil properties in shallow soils.

The spatiotemporal variability of soil properties in an agricultural field can be characterized by many geophysical methods, such as electrical resistivity (ER), time domain reflectometry (TDR), ground penetrating radar (GPR), electromagnetic induction (EMI), capacitance probes (CPs), active microwaves (AM), passive microwaves (PM), neutron thermalization, nuclear magnetic resonance (NMR), gamma-ray attenuation, and near-surface seismic reflection (Corwin, 2008). However, all these methods follow different operating principles and perform at various scales. EMI is an established and widely-used technology for soil studies, and it can be used in precision agriculture to map soil heterogeneity at both spatial and temporal scales over relatively larger fields (Corwin and Allred, 2008; Doolittle and Brevik, 2014; Lesch et al., 2005). Traditional methods (*i.e.* TDR and soil sampling) for measuring soil properties (SMC, texture, BD, etc.) are inadequate to fulfill present-day research. These methods are generally invasive, provide only point measurements, and are costly due to the need for repeated measurements and temporal monitoring for a large-scale. On the other hand, EMI technology is a non-invasive, cost-effective, and rapid method which can provide continuous measurements to investigate the spatiotemporal variability of physiochemical properties of soils (Corwin, 2008; Corwin and Lesch, 2005; Doolittle and Brevik, 2014).

An EMI sensor measures soil's apparent electrical conductivity (EC_a) as a proxy of soil properties (Altdorff and Dietrich, 2014; Corwin, 2005; Huang et al., 2016; McNeill and Bosnar, 1999; Pedrera-Parrilla et al., 2015). EC_a is a popular and accepted parameter for studying a variety of physical and chemical soil properties that directly or indirectly influence the EC_a readings (Corwin, 2008; Corwin and Lesch, 2005b, 2005a, 2003; Doolittle et al., 2014). EMI sensors can be used to measure and map various soil properties, including: soil salinity, soil texture, SMC, soil BD, porosity, CEC, EC_w water table depth, and soil depth sounding (Altdorff et al., 2017; Bouksila et al., 2012; Brevik et al., 2006; Brevik and Fenton, 2004; Buchanan and Triantafilis, 2009; Corwin and Lesch, 2014; Corwin and Scudiero, 2016; Friedman, 2005; Huang et al., 2015; Lück et al., 2009; Misra and Padhi, 2014; Rodrigues et al., 2015; Vitharana et al., 2008). EC_a data encompass subsoil information at a range of depths, information which is directly correlated with plant growth and crop production (Kaffka et al., 2005; Kravchenko et al., 2003).

Altdorff et al. (2018) studied the effects of agronomic treatments and different soil amendments on EC_a, while also investigating the prediction accuracy of SMC using EC_a data. Besides, the researchers found that different management zones could be identified with EC_a variability on a large-scale.

Sensitivity (response from soil) of EMI instruments is a non-linear function with soil depth. Therefore, depth-weighted measurements are fundamental to EC_a. A depth of investigation of EMI instruments, called *Depth Sensitivity* (DS), and accuracy of DS in field-scale, needs further investigation. Accuracy of DS is still debated among researchers while it shows dissimilarity from a sensor to sensor. The DS of EMI instruments in shallow soils, which are relevant for agricultural soils, must be evaluated for the particular site and their conditions (Boaga, 2017). An effective DS can be used as an assessing tool to measure the capability of EMI sensors in terms of sampling depth accuracy.

Responses of EMI from subsurface soil are different for EC_a and apparent magnetic susceptibility (MS_a). Theoretical EMI response models (DS models) were developed with a function of the soil depth for EC_a and MS_a separately (Keller and Frischknecht, 1966; McNeill, 1980). MS_a is more effective to identify metal objects or highly conductive materials in the subsurface. However, parameters like soil/sediment layers, amount of air, water, magnetic minerals, stone and pottery fragments, may change the MS_a variations in the field (Dalan and Banerjee, 1998; Simon and Moffat, 2015). Similar to EC_a, MS_a also has potential applications for soil related investigations.

I investigated and assessed the potential applications of two types of EMI sensors, namely multi-coil and multi-frequency, for shallow Podzolic soil characterization, and depth sensitivity analysis, by using small buried targets in western Newfoundland. This research was conducted in a silage corn field at the Pynn's Brook Research Station (PBRS), managed by the Department of Fisheries and Land Resources of the Government of NL, Canada.

1.2. Aim and Objectives

This thesis explores the potential applications of two different types of EMI sensors for understanding and mapping spatiotemporal variability of properties in shallow soils in terms of the EC_a variability, and examines the depth sensitivity of MS_a measurements. The MS_a field data were evaluated with MS_a depth response models. The key objectives of the study were to:

i. Assess the correlation between soil physiochemical properties (*i.e.* SMC, BD, soil texture, pH, CEC and EC_w) and EC_a using multi-coil or multi-frequency EMI sensors.

ii. Characterize the spatiotemporal variability of EC_a as a proxy for soil properties.

iii. Evaluate and compare the depth sensitivity of multi-coil or multi-frequency EMI sensors through small buried targets in shallow soil.

iv. Interpret field MS_a data and theoretical MS_a depth response models.

This research study employed with CMD–MiniExplorer (multi-coil) and GEM–2 (multi-frequency) for manual EMI surveys at PBRS, Pasadena, western Newfoundland. To achieve the objectives, two main field studies were carried out. One was undertaken to quantify soil physiochemical properties, such as SMC, BD, soil texture, pH, CEC and EC_w, along with EMI surveys in a silage corn field. Soil samples were analyzed at the Boreal Ecosystem Research Facility at the Grenfell Campus-Memorial University of Newfoundland. The second study focused on the depth sensitivity of two EMI sensors in shallow Podzolic soil. For achieving these depth sensitivity goals, different conductivity materials were systematically buried in a separate experimental field (fallow) with uniform soil conditions next to the silage corn field, and several EMI grid surveys were carried out over the field. In general, the EMI method produces two parameters known as EC_a and MS_a. The first two objectives were related to EC_a while the other two were related to MS_a study.

1.3. Thesis Organization

This thesis explores the applicability and potential of multi-coil and multi-frequency EMI sensors for characterizing Podzolic soils in western Newfoundland. It is presented in four chapters:

Chapter 1 is the general introduction and overview of the EMI method in soil studies, along with EMI principles, a brief literature review outlining EMI applications, and sensor specifications.

Chapter 2 establishes geostatistical and multivariate statistical techniques for monitoring the spatiotemporal variability of EC_a data, with measured soil physiochemical properties. This chapter includes variogram analysis, principal component analysis (PCA), multiple linear regression (MLR), kriging interpolation, and mapping soil EC_a variability.

Chapter 3 describes the depth sensitivity of multi-coil and multi-frequency EMI sensors using small buried targets. MS_a data were used for mapping and detecting metallic targets. It includes the assessment of which EMI sensor is more suitable for metal detection in shallow soils.

Chapter 4 is the general summary and conclusion of the overall research and the identification of research gaps for future studies.

1.4. Overview of the EMI Method for Soil Studies

1.4.1 Operating Principle of EMI

The basic operating principle of the EMI instruments is transmitting electromagnetic (EM) energy into the ground and receiving the secondary EM energy from the subsoil. The instrument is commonly composed of a transmitter (Tx) coil and a receiver (Rx) coil connected by a cable of varying length (Figure **1.1**). According to Maxwell’s equations, an alternating electric current produces perpendicular alternating primary magnetic fields from the Tx coil. The primary magnetic fields induce circular electrical currents (eddy currents) below the surface. These eddy currents generate secondary magnetic fields, and they are captured by a Rx coil along with primary magnetic fields (Bonsall et al., 2013; Keller and Frischknecht, 1966; McNeill and Bosnar, 1999; McNeill, 1980).

The Rx measures the phase and amplitude of the secondary fields, which is different from the primary fields, mainly due to the subsurface properties. The secondary field can be divided into an in-phase component and an out of phase (quadrature) component compared with the phase of the primary field. When the EMI instrument operates at a low induction number and homogenous half-space approximation, the in-phase component is directly proportional to the soil MS_a, while the quadrature component is directly proportional to the soil's EC_a (Huang et al., 2003; McNeill, 1980).

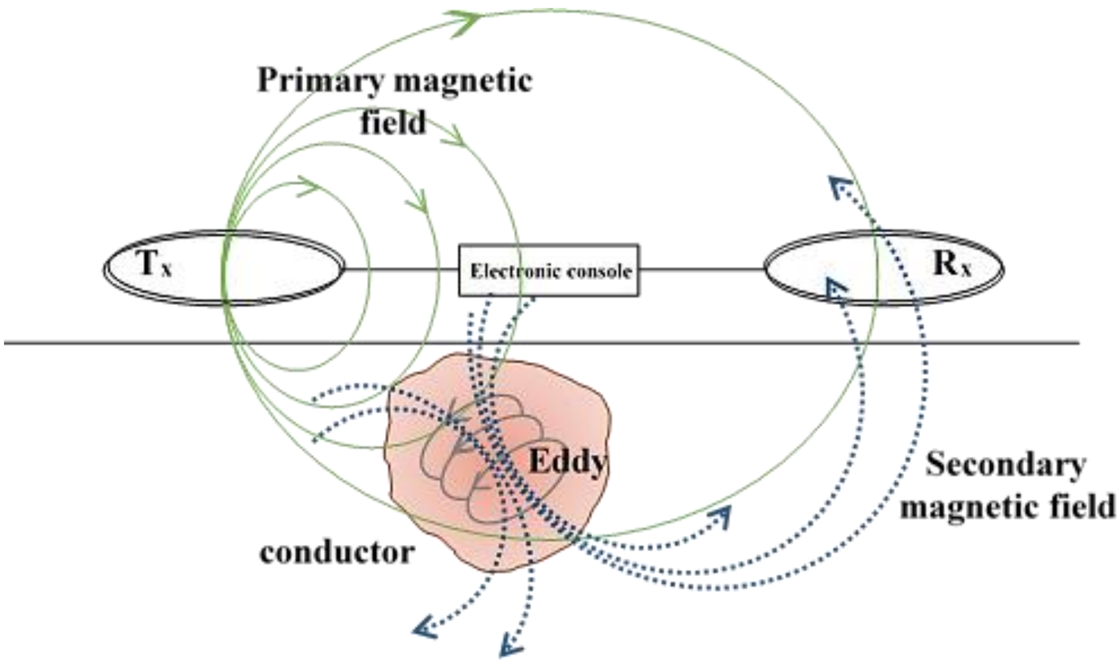

Figure **1.1**: Schematic view of EMI operating principles. Tx is the transmitter coil and Rx is the receiver coil.

The typical coil orientations of an EMI sensor (Figure **1.2**) are vertical dipole mode or horizontal coplanar (HCP) mode, and horizontal dipole mode or vertical coplanar (VCP) mode, which influences EM field penetration and, therefore, the sampling depth.

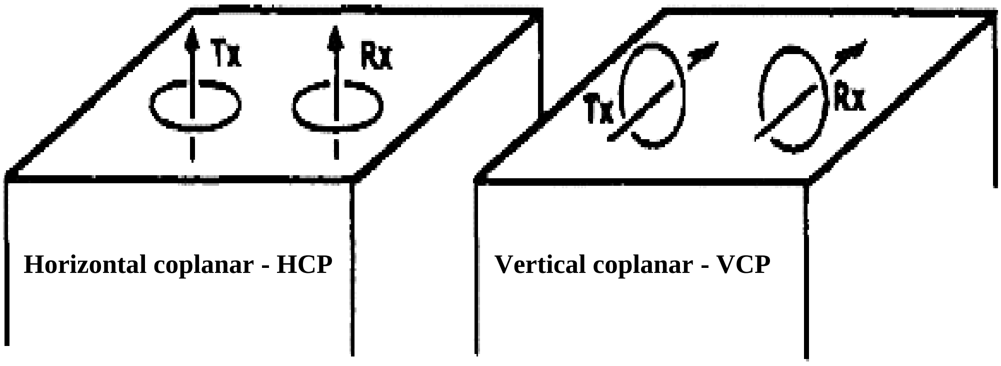

Figure **1.2**: The HCP and VCP mode of operation, where Tx is the transmitter coil and Rx is the receiver coil (McNeill, 1980).

1.4.2 Apparent Electrical Conductivity (EC_a)

EC_a of soil (millisiemens per meter - mS/m) is a depth-weighted average of the bulk soil electrical conductivity within a volume of the subsurface, mostly between the Tx and Rx (Figure **1.3**) (Cook and Walker, 1992; McNeill, 1980). According to McNeill's (1980) approximation, EMI based EC_a is given by:

$$ECa = \frac{2}{\pi f \mu_o s^2}\left(\frac{(Hs)_{quadrature}}{Hp}\right) \qquad \text{Eq. 1.1}$$

where f is the frequency (Hz), μ_o is the magnetic permeability of free space ($4\ \pi\ 10^{-7}$ H/m), s is the inter-coil separation (m), and Hp and Hs are primary and secondary EM fields at the receiver coil, respectively.

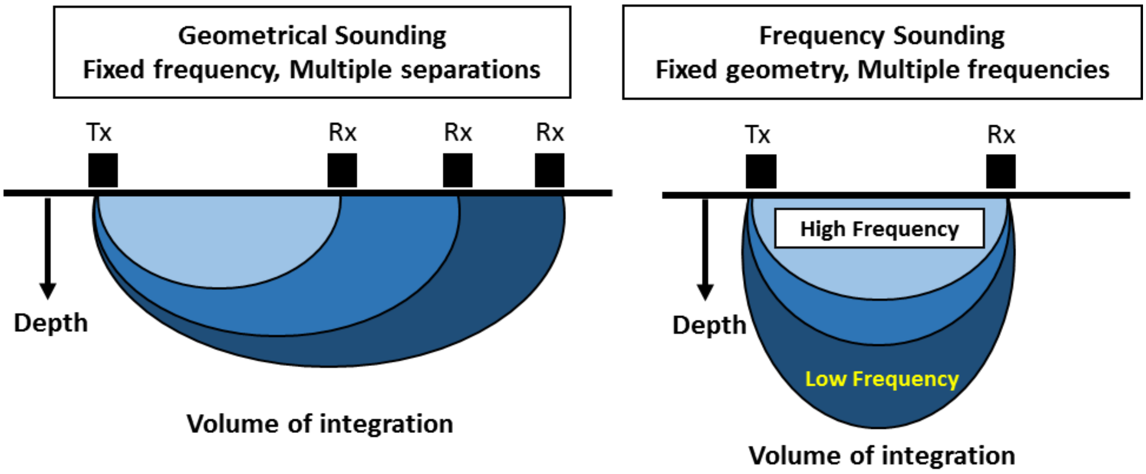

Figure **1.3**: Depth sensitivity using geometry (left) and frequency (right) sounding methods of EMI (modified from Keiswetter and Won, 1997)

Rhoades et al. (1999) explained in detail the factors influencing EC_a measurements under field conditions. Electrical conductivity (EC) refers to the ability to transmit an electrical current within a material (in soil, for example). In general, three pathways of current flow contribute to the EC_a of subsoils, and those are (Figure **1.4**):

1. Solid-Liquid phase pathway	:	predominantly, exchangeable cations linked with clay minerals
2. Liquid phase pathway	:	soil water in macropores contained dissolved solutes
3. Solid phase pathway	:	soil particles interconnected each other

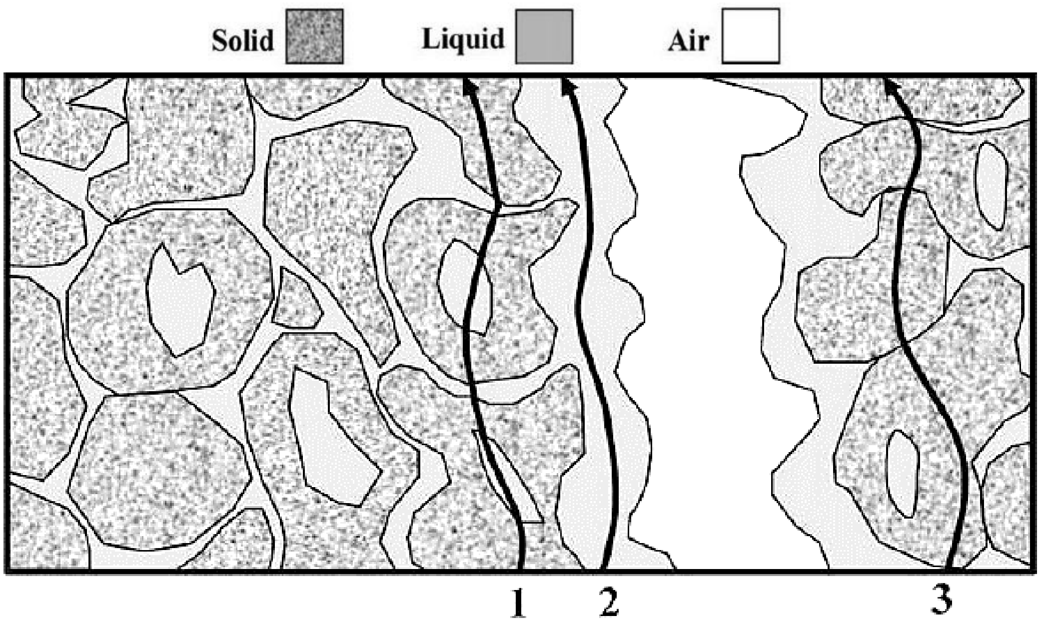

Figure **1.4**: Schematic representation of electrical conductivity pathways of the EC_a measurements (modified from Corwin and Lesch, 2005).

1.4.3 Apparent Magnetic Susceptibility (MS_a)

Apparent magnetic susceptibility, MS_a (parts per thousand - ppt), measures the ability of materials to be magnetized by applied magnetic fields. MS_a depends on the presence of magnetic minerals, but in order to characterize the amount, the shape and type of the minerals must be taken into account (Thompson et al., 1975). MS_a is not often a usable component like EC_a (Dalan, 2008; Simpson et al., 2010), because MS_a gives completely different outputs (negative anomalies from HCP mode) based on coil configuration of the EMI sensor and the target depth (Linford, 1998; Simpson et al., 2010). Anthropogenic activities, such as humanmade underground structures, soil disturbance at industrial sites and management practices including leaching fraction in agricultural fields --can influence soil MS_a measurements (Bonsall et al., 2014;

Delefortrie et al., 2018; Simpson, 2009; Van De Vijver et al., 2015). Also, bacterial activities and fire can result in higher MS_a values in topsoils than subsoils (Bevan and Rinita, 2003).

1.5. Depth Sensitivity of EMI Measurements

Here, depth sensitivity (DS) is indicating depth of investigation (or depth of penetration) of EMI instruments, and it is mainly dependent on the frequency of the primary field, the electrical structure of the subsurface soil, inter-coil separation (ICS), and coil configurations – VCP or HCP mode (Monteiro Santos et al., 2010). Fitterman and Labson (2005) pointed out some basic conditions that should be satisfied for EMI sensors to detect a target:

i. Primary EM fields should induce a current in the target. In case of resistive targets, the induced current flows around the targets.
ii. EM properties should be different between the target and surroundings.
iii. The anomalous responses from the EMI sensors must be larger than noise signals received.

DS could be inferred from geometry soundings or frequency soundings by changing ICS or frequencies, respectively (Figure **1.3**). Generally, 'skin depth' is a standard measure for the penetration depth of frequency sounding EMI sensors. The skin depth (δ) is the depth where the primary EM wave is attenuated by a factor of 1/e, or to about 37% of the original amplitude (Spies, 1989). However, when conditions are less than ideal, skin depth underestimates the DS of the EMI data, and overestimates in environmentally noisy or geologically complex areas (Bongiovanni et al., 2008; Huang, 2005). Therefore, accurate prediction of DS cannot yet be achieved.

$$\delta = \sqrt{\frac{1}{\sigma \mu_o \pi f}} \qquad \text{Eq. 1.2}$$

where, σ is the EC of the medium, μ_o is the magnetic permeability of free space, and f is the frequency of the primary EM signal.

Theoretical DS response models available for EMI sensors that only depend on the ICS and coil orientations, are based on the low induction approximation of a homogenous subsurface (McNeill, 1980; Saey et al., 2015). These theoretical models were developed for relative and cumulative responses of the induced signals (secondary fields) of EMI sensors (McNeill, 1980). The relative response (RR) describes the contribution of an induced signal from a thin layer at different depths, and the cumulative response (CR) is the volume of integration between a certain depth and infinite depth. These models give equations for quadrature (EC_a) (McNeill, 1980; Saey et al., 2015) and in-phase (MS_a) (Keller and Frischknecht, 1966; Simpson et al., 2010) components of induced responses. EC_a depth sensitivity models are more popular in many applications compared to MS_a models. HCP mode response changes from positive to negative in the MS_a model, so interpretations of MS_a data are difficult. Some researchers have used the same equation of EC_a depth model for the MS_a depth model (Santos and Porsani, 2011), but only a few studies have been conducted for the interpretation of data using a MS_a DS model.

1.6. Multi-coil EMI Sensor

The multi-coil EMI device operates at a fixed frequency of 30 kHz, with three coil separations. The instrument has one Tx and three Rxs with fixed offsets of 0.32 m, 0.71 m, and 1.18 m (Figure **1.5**). The sensor can be used at both HCP and VCP coil orientations, and it gives six different effective depths of subsoil (Altdorff et al., 2018). The sensor is well adapted to outside temperatures between -10℃ and +50℃, and the temperature stability is ±1 mS/m per 10℃ change in temperature (GF-Instruments, 2011).

1.7. Multi-frequency EMI Sensor

1.7.1 Sensor Specifications

The multi-frequency EMI sensor is a handheld, digital, programmable, and multi-frequency broadband EM sensor (Tang et al., 2018; Won et al., 1996). The multi-frequency package consists of the ski that encloses all sensing elements, an electronics enclosure that plugs onto the ski, a detachable IPaq for display, and a shoulder strap, as shown in Figure **1.6.** Features and specifications of the instrument can be listed as following (User's Manual, Geophex Ltd):

- Operating frequency range 0.3 kHz to 90 kHz
- Single or multiple frequency survey
- Maximum sampling rate selectable 30 Hz or 25 Hz
- Lightweight 3.6 kg
- ICS between Tx and Rx coils is 1.67 m
- Easy replaceable and extends battery life, that eliminates cooling fans
- Personal digital assistant (PDA) digital display with WinGEM software
- Windows based operating software for easy use
- External GPS connector
- Bluetooth connection to IPaq and RS232 serial ports for other devices
- Real-time painting a quick data look in the survey area

- Data stored internal memory as well as SD memory card as external memory
- Environmental noise spectrum displays or stores it in SD card
- The output is taken as In-phase and Quadrature in ppm at each frequency, EC_a and MS_a and Powerline amplitude

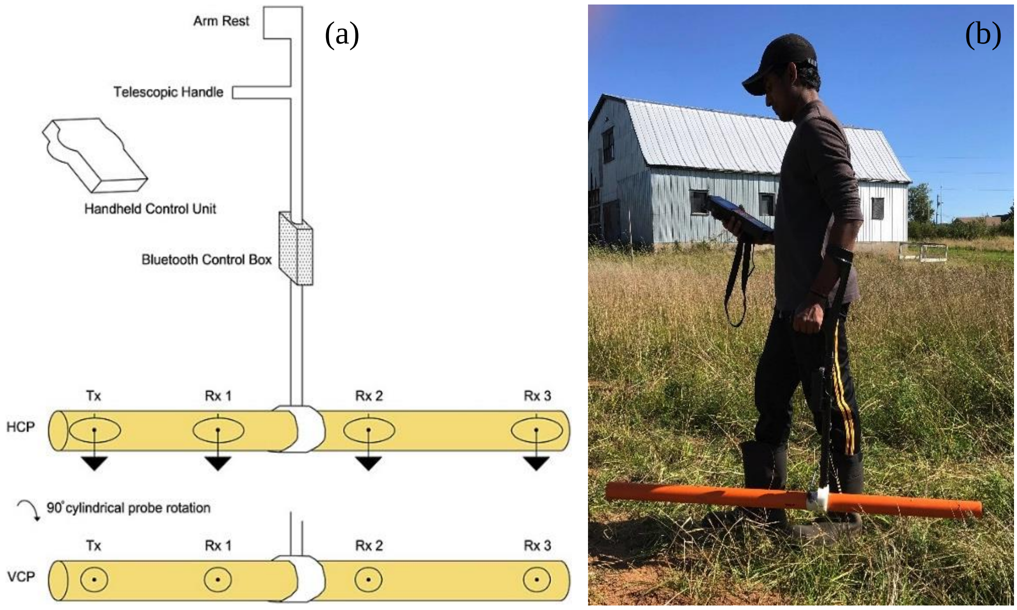

Figure **1.5**: (a) Coil geometry, configuration and orientation of the multi-coil EMI sensor. (Offsets 0.32m, 0.71m and 1.18m respectively for Rx 1, Rx 2 and Rx 3 from the Tx coil) (Bonsall et al., 2013); (b) Multi-coil sensor operation at PBRS field.

Figure **1.6**: Components of the multi-frequency EMI instrument

1.7.2 Operating Principle of the multi-frequency EMI sensor

The multi-frequency instrument consists of three coils. A fixed coil separation between Tx and Rx is 1.67 m and the third one is a bucking coil at 1.035 m from the Tx to cut off the primary field from the Rx (Huang, 2005; Simon et al., 2015). Figure **1.7** shows the electronic block diagram of the multi-frequency EMI sensor. The built-in software converts the desired Tx frequency into a digital bit-stream, which is selected by the operator. This bit-stream comprises instructions on how to control a set of digital switches (called H-bridge) connected across the Tx coil and generates a complex waveform that contains all frequencies specified by the operator (Won et al., 1996).

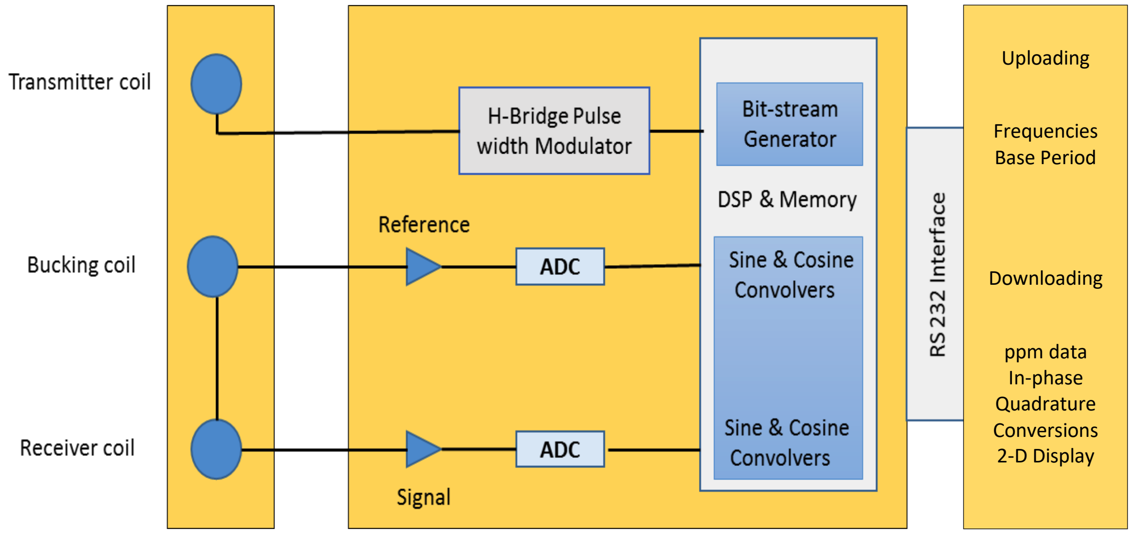

Figure **1.7**: Electronic Block Diagram of the multi-frequency EMI sensor. (modified from Won et al., 1996). DSP – digital signal processor; ADC – analog to digital converter.

Ten frequencies can be used simultaneously in the multi-frequency EMI sensor. If a higher number of frequencies is used, the strength of each frequency will be reduced, and consequently lowering the resolution (Bongiovanni et al., 2008; Tang et al., 2018). The multi-frequency EMI sensor can be used at both HCP and VCP modes of operation: that means a single frequency can sample two different integral depths of subsoil based on the coil orientation. The frequency is inversely proportional to the skin depth (Eq. 2); therefore, multiple frequencies are equivalent to measuring the earth response at multiple depths (Won et al., 1996). The data acquisition by the multi-frequency EMI device is at 10 Hz. The basic output from the multi-frequency EMI data logger is parts per million (ppm) for both in-phase and quadrature components. The unit ppm is defined as in Eq. 1.3 (Keiswetter and Won, 1997).

$$\text{ppm} = 10^6 \times \frac{\text{secondary magnetic field at receiver coil}}{\text{primary magnetic field at receiver coil}} \qquad \text{Eq. 1.3}$$

1.8. References

Altdorff, D., Dietrich, P., 2014. Delineation of areas with different temporal behavior of soil properties at a landslide affected Alpine hillside using time-lapse electromagnetic data. Environ. Earth Sci. 72, 1357–1366. https://doi.org/10.1007/s12665-014-3240-7

Altdorff, D., Galagedara, L., Nadeem, M., Cheema, M., Unc, A., 2018. Effect of agronomic treatments on the accuracy of soil moisture mapping by electromagnetic induction. Catena 164, 96–106. https://doi.org/10.1016/j.catena.2017.12.036

Altdorff, D., von Hebel, C., Borchard, N., van der Kruk, J., Bogena, H., Vereecken, H., Huisman, J.A., 2017. Potential of catchment-wide soil water content prediction using electromagnetic induction in a forest ecosystem. Environ. Earth Sci. 76, 111. https://doi.org/10.1007/s12665-016-6361-3

Bevan, B., Rinita, D., 2003. Magnetic Susceptibility Sounding. Weems, VA. https://doi.org/10.13140/RG.2.2.10891.28962

Boaga, J., 2017. The use of FDEM in hydrogeophysics: A review. J. Appl. Geophys. 139, 36–46. https://doi.org/10.1016/j.jappgeo.2017.02.011

Bongiovanni, M. V., Bonomo, N., de la Vega, M., Martino, L., Osella, A., 2008. Rapid evaluation of multifrequency EMI data to characterize buried structures at a historical Jesuit Mission in Argentina. J. Appl. Geophys. 64, 37–46. https://doi.org/10.1016/j.jappgeo.2007.11.006

Bonsall, J., Fry, R., Gaffney, C., Armit, I., Beck, A., Gaffney, V., 2013. Assessment of the CMD mini-explorer, a new low-frequency multi-coil electromagnetic device, for archaeological investigations. Archaeol. Prospect. 20, 219–231. https://doi.org/10.1002/arp.1458

Bonsall, J., Gaffney, C., Armit, I., 2014. Preparing for the future: A reappraisal of archaeo-geophysical surveying on Irish National Road Schemes 2001-2010. https://doi.org/10.13140/RG.2.1.1706.9202

Bouksila, F., Persson, M., Bahri, A., Berndtsson, R., 2012. Electromagnetic induction prediction of soil salinity and groundwater properties in a Tunisian Saharan oasis. Hydrol. Sci. J. 57, 1473–1486. https://doi.org/10.1080/02626667.2012.717701

Brevik, E.C., Fenton, T.E., 2004. The Effect of Changes in Bulk Density on Soil Electrical Conductivity as Measured with the Geonics EM-38. Soil Horizons 45, 96–102. https://doi.org/10.2136/sh2004.3.0096

Brevik, E.C., Fenton, T.E., Lazari, A., 2006. Soil electrical conductivity as a function of soil water content and implications for soil mapping. Precis. Agric. 7, 393–404. https://doi.org/10.1007/s11119-006-9021-x

Buchanan, S., Triantafilis, J., 2009. Mapping water table depth using geophysical and environmental variables. Ground Water 47, 80–96. https://doi.org/10.1111/j.1745-6584.2008.00490.x

Cook, P.G., Walker, G.R., 1992. Depth Profiles of Electrical Conductivity from Linear Combinations of Electromagnetic Induction Measurements. Soil Sci. Soc. Am. J. 56, 1015–1022. https://doi.org/10.2136/sssaj1992.03615995005600040003x

Corwin, D.L., 2005. Geospatial Measurements of Apparent Soil Electrical Conductivity for Characterizing Soil Spatial Variability, in: Soil-Water-Solute Process Characterization: An Integrated Approach. CRC Press, Boca Raton, FL, pp. 639–672. https://doi.org/10.1201/9781420032086.ch18

Corwin, D.L., Allred, B.J., 2008. Past, Present, and Future Trends of Soil Electrical Conductivity Measurement Using Geophysical Methods, in: Handbook of Agricultural Geophysics. CRC Press, Taylor & Francis Group, New York, pp. 17–44. https://doi.org/doi:10.1201/9781420019353.ch2

Corwin, D.L., Lesch, S.M., 2014. A simplified regional-scale electromagnetic induction - Salinity calibration model using ANOCOVA modeling techniques. Geoderma 230–231, 288–295. https://doi.org/10.1016/j.geoderma.2014.03.019

Corwin, D.L., Lesch, S.M., 2005a. Apparent soil electrical conductivity measurements in agriculture. Comput. Electron. Agric. 46, 11–43. https://doi.org/10.1016/j.compag.2004.10.005

Corwin, D.L., Lesch, S.M., 2005b. Characterizing soil spatial variability with apparent soil electrical conductivity: Part II. Case study. Comput. Electron. Agric. 46, 135–152. https://doi.org/10.1016/j.compag.2004.11.003

Corwin, D.L., Lesch, S.M., 2005c. Apparent soil electrical conductivity measurements in agriculture. Comput. Electron. Agric. 46, 11–43. https://doi.org/10.1016/j.compag.2004.10.005

Corwin, D.L., Lesch, S.M., 2003. Application of Soil Electrical Conductivity to Precision Agriculture. Agron. J. 95, 455–471. https://doi.org/10.2134/agronj2003.0455

Corwin, D.L., Scudiero, E., 2016. Field-Scale Apparent Soil Electrical Conductivity, in: Logsdon, S. (Ed.) Methods of Soil Analysis. Soil Science Society of America, Madison, USA. https://doi.org/10.2136/methods-soil.2015.0038

Dalan, R.A., 2008. A Review of the Role of Magnetic Susceptibility in Archaeogeophysical Studies in the USA: Recent Developments and Prospects. Archaeol. Prospect. 15, 1–31. https://doi.org/10.1002/arp

Dalan, R.A., Banerjee, S.K., 1998. Techniques of Soil Magnetism. Geoarchaeology 13, 3–36.

Delefortrie, S., Hanssens, D., De Smedt, P., 2018. Low signal-to-noise FDEM in-phase data: Practical potential for magnetic susceptibility modelling. J. Appl. Geophys. 152, 17–25. https://doi.org/10.1016/j.jappgeo.2018.03.003

Doolittle, J.A., Brevik, E.C., 2014. The use of electromagnetic induction techniques in soil studies. Geoderma 223, 33–45. https://doi.org/10.1016/j.geoderma.2014.01.027

Fitterman, D. V, Labson, V.F., 2005. 10. Electromagnetic Induction Methods for Environmental Problems, in: Butler, D.K. (Ed.), Near-Surface Geophysics. Society of Exploration Geophysicists, Oklahoma, U.S.A, pp. 301–356. https://doi.org/10.1190/1.9781560801719.ch10

Friedman, S.P., 2005. Soil properties influencing apparent electrical conductivity: A review. Comput. Electron. Agric. 46, 45–70 https://doi.org/10.1016/j.compag.2004.11.001

Huang, H., 2005. Depth of investigation for small broadband electromagnetic sensors.

Geophysics 70, 135–142. https://doi.org/10.1190/1.2122412

Huang, H., Won, I.J., San Filipo, B., 2003. Detecting buried nonmetal objects using soil magnetic susceptibility measurements, in: Proceedings of SPIE. pp. 1181–1188. https://doi.org/10.1117/12.485952

Huang, J., Scudiero, E., Choo, H., Corwin, D.L., Triantafilis, J., 2016. Mapping soil moisture across an irrigated field using electromagnetic conductivity imaging. Agric. Water Manag. 163, 285–294. https://doi.org/10.1016/j.agwat.2015.09.003

Huang, J., Subasinghe, R., Malik, R.S., Triantafilis, J., 2015. Salinity hazard and risk mapping of point source salinisation using proximally sensed electromagnetic instruments. Comput. Electron. Agric. 113, 213–224. https://doi.org/10.1016/j.compag.2015.02.013

Kaffka, S.R., Lesch, S.M., Bali, K.M., Corwin, D.L., 2005. Site-specific management in salt-affected sugar beet fields using electromagnetic induction. Comput. Electron. Agric. 46, 329–350. https://doi.org/10.1016/j.compag.2004.11.013

Keiswetter, D.A., Won, I.J., 1997. Multifrequency Electromagnetic Signature of the Cloud Chamber, Nevada Test Site. J. Environ. Eng. Geophys. 2, 99–103. https://doi.org/10.4133/JEEG2.2.99

Kirby, G.E., 1988. Soils of the Pasadena-Deer Lake area, Newfoundland [WWW Document]. URL http://sis.agr.gc.ca/cansis/publications/surveys/nf/nf17/nf17_report.pdf (accessed 11.8.17).

Kravchenko, A.N., Thelen, K.D., Bullock, D.G., Miller, N.R., 2003. Relationship among Crop Grain Yield, Topography, and Soil Electrical Conductivity Studied with Cross-Correlograms. Agron. J. 95, 1132–1139. https://doi.org/10.2134/agronj2003.1132

Lesch, S.M., Corwin, D.L., Robinson, D.A., 2005. Apparent soil electrical conductivity mapping as an agricultural management tool in arid zone soils. Comput. Electron. Agric. 46, 351–378. https://doi.org/10.1016/j.compag.2004.11.007

Linford, N.T., 1998. Geophysical Survey At Boden Vean, Cornwall, Including an Assessment of the Microgravity Technique for the Location of Suspected Archaeological Void Features. Archaeometry 40, 187–216. https://doi.org/10.1111/j.1475-4754.1998.tb00833.x

Lück, E., Gebbers, R., Ruehlmann, J., Spangenberg, U., 2009. Electrical conductivity mapping for precision farming. Near Surf. Geophys. 7, 15–25. https://doi.org/10.3997/1873-0604.2008031

McNeill, J.D., 1980. Electromagnetic Terrain Conductivity Measurement at Low Induction Numbers, Technical note TN-06. Mississauga, ON.

McNeill, J.D., Bosnar, M., 1999. Application of dipole–dipole electromagnetic systems for geological depth sounding, Technical Note TN-31. Mississauga, ON.

Misra, R.K., Padhi, J., 2014. Assessing field-scale soil water distribution with electromagnetic induction method. J. Hydrol. 516, 200–209. https://doi.org/10.1016/j.jhydrol.2014.02.049

Monteiro Santos, F.A., Triantafilis, J., Bruzgulis, K.E., Roe, J.A.E., 2010. Inversion of Multiconfiguration Electromagnetic (DUALEM-421) Profiling Data Using a One-

Dimensional Laterally Constrained Algorithm. Vadose Zo. J. 9, 117–125. https://doi.org/10.2136/vzj2009.0088

Pedrera-Parrilla, A., Brevik, E.C., Vijver, E. Van De, Espejo, A.J., Taguas, E. V, Giráldez, J. V, Martos, S., Vanderlinden, K., 2015. Effects of different topsoil properties on apparent electrical conductivity under varying soil water contents. Estud. en la Zo. No Saturada 12, 25–32.

Quinlan, J., 2012. Building agricultural capacity in newfoundland and labrador, The Harris Centre. St. John's.

Rhoades, J.D., Chanduvi, F., Lesch, S.M., 1999. Soil salinity assessment: methods and interpretation of electrical conductivity measurements. FAO Irrig. Drain. Pap. No. 57.

Rodrigues, F.A., Bramley, R.G. V, Gobbett, D.L., 2015. Proximal soil sensing for Precision Agriculture: Simultaneous use of electromagnetic induction and gamma radiometrics in contrasting soils. Geoderma 243, 183–195. https://doi.org/10.1016/j.geoderma.2015.01.004

Saey, T., De Smedt, P., Delefortrie, S., Van De Vijver, E., Van Meirvenne, M., 2015. Comparing one- and two-dimensional EMI conductivity inverse modeling procedures for characterizing a two-layered soil. Geoderma 241, 12–23. https://doi.org/10.1016/j.geoderma.2014.10.020

Sanborn, P., Lamontagne, L., Hendershot, W., 2011. Podzolic soils of Canada: Genesis, distribution, and classification. Can. J. Soil Sci. 91, 843–880. https://doi.org/10.4141/cjss10024

Santos, V.R.N., Porsani, J.L., 2011. Comparing performance of instrumental drift correction by linear and quadratic adjusting in inductive electromagnetic data. J. Appl. Geophys. 73, 1–7. https://doi.org/10.1016/j.jappgeo.2010.10.004

Simon, F.-X., Moffat, I., 2015. Identification of shapes and uses of past landscapes through EMI survey, in: Sarris, A. (Ed.), Best Practices of Geoinformatic Technologies for the Mapping of Archaeolandscapes. Archaeopress, Oxford, pp. 25–34.

Simpson, D., Van Meirvenne, M., Lück, E., Rühlmann, J., Saey, T., Bourgeois, J., 2010. Sensitivity of multi-coil frequency domain electromagnetic induction sensors to map soil magnetic susceptibility. Eur. J. Soil Sci. 61, 469–478. https://doi.org/10.1111/j.1365-2389.2010.01261.x

Spies, B.R., 1989. Depth of investigation in electromagnetic sounding methods. Geophysics 54, 872–888. https://doi.org/10.1190/1.1442716

Tang, P., Chen, F., Jiang, A., Zhou, W., Wang, H., Leucci, G., de Giorgi, L., Sileo, M., Luo, R., Lasaponara, R., Masini, N., 2018. Multi-frequency Electromagnetic Induction Survey for Archaeological Prospection: Approach and Results in Han Hangu Pass and Xishan Yang in China. Surv. Geophys. 1–18. https://doi.org/10.1007/s10712-018-9471-5

Thompson, R., Battarbee, R.W., O'Sullivan, P.E., Oldfield, F., 1975. Magnetic susceptibility of lake sediments. Limnol. Oceanogr. 20, 687–698. https://doi.org/10.4319/lo.1975.20.5.0687

Vitharana, U.W.A., Saey, T., Cockx, L., Simpson, D., Vermeersch, H., Van Meirvenne, M., 2008. Upgrading a 1/20,000 soil map with an apparent electrical conductivity survey. Geoderma 148, 107–112. https://doi.org/10.1016/j.geoderma.2008.09.013

Won, I.J., Keiswetter, D.A., Fields, G.R., Sutton, L.C., 1996. GEM-2: A New Multifrequency Electromagnetic Sensor. J. Environ. Eng. Geophys. 1, 129–138. https://doi.org/10.4133/JEEG1.2.129

Zungalia, E.J., Tuck, F.C., Spariosu, D.J., 1989. Geophysical Investigations of a Ground Water Contaminant Plume-Electrical and Electromagnetic Methods, in: Hatcher, K.J. (Ed.), Georgia Water Resources Conference. Institute of Natural Resources, The University of Georgia, Georgia, pp. 165–168.

Chapter 2: Developing Relationships between Apparent Electrical Conductivity and Soil Properties Using Geostatistical and Multivariate Statistical Approaches

2.1. Co-authorship Statement

A manuscript based on Chapter 2, entitled "*Developing Relationships between Apparent Electrical Conductivity and Soil Properties Using Geostatistical and Multivariate Statistical Approaches*" has been prepared for submission to Precision Agriculture (Sadatcharam, K., Unc, A., Krishnapillai, M. and Galagedara, L., 2018). Kamaleswaran Sadatcharam, the thesis author was the primary author and Dr. Galagedara (supervisor), was the corresponding and the fourth author. Dr. Unc (co-supervisor) and Dr. Krishnapillai (committee member) were second and third authors, respectively. All authors were part of the research project on "*Hydrogeophysical Characterization of Agricultural Fields in Western Newfoundland using Integrated GPR-EMI*", which was led by Dr. Galagedara. For the work in Chapter 2, the overall research strategy was developed by Dr. Galagedara with input from all members of the group. Mr. Sadatcharam was responsible for the specific methodology, data collection, analysis, and interpretation and writing of the manuscript. Dr. Unc and Dr. Krishnapillai provided inputs for the field experiment, data interpretation, and manuscript editing.

2.2. Abstract

An electromagnetic induction (EMI) sensor measures soil's apparent electrical conductivity (EC_a) as a proxy of subsoil properties. Relationships between EC_a and soil properties (physiochemical properties) under wet and dry conditions are needed to understand the spatiotemporal variability of EC_a across the agricultural fields. Geostatistical and multivariate statistical approaches can be used to screen the relationship of EC_a and soil properties to improve the prediction accuracy by eliminating weakly correlated variables. The objectives of this study were to: (i) identify the significant soil properties influencing EC_a measured with multi-coil and multi-frequency EMI sensors on dry and wet days; and (ii) assess the potential coil separations, frequencies, and coil orientations of EMI sensors on measuring EC_a variability, using detailed geostatistical and multivariate statistical techniques in a shallow Podzolic soil. A field experiment was conducted on a silage-corn field (8 x 42 m^2) at Pynn's Brook Research Station, in western Newfoundland. Soil samples were collected on two different days – a dry day (August) and a wet day (October) – and soil physiochemical properties, such as soil texture, bulk density, soil moisture content (SMC), cation exchange capacity (CEC), pore water electrical conductivity (EC_w) and soil pH, were analyzed in the laboratory. EC_a data points were digitized according to the soil sampling locations from the ordinary block kriging interpolated EC_a maps. The statistical analyses, *i.e.* variograms, principal component analysis (PCA), and backward elimination of multiple linear regression (MLR), were applied to the EC_a and soil properties data. The EMI–EC_a increases with the increasing soil moisture of the field, and as well, the accuracy of the MLR model predictions also increases from dry to wet days. Anticipated significantly influenced factors of EC_a were identified as silt, SMC, CEC, EC_w, and sand of the shallow sandy loam soils. The multi-frequency EMI surveys were more reliable on moist soils; in particular, VCP–49kHz of the multi-frequency is appropriate to investigate soil variability, while VCP–C3 and HCP–C2 are the most appropriate coil separations and orientation of the multi-coil EMI sensor. The multi-coil is a more suitable EMI sensor than the multi-frequency for investigating the spatiotemporal variability of EC_a in Podzols at the test site.

Keywords: apparent electrical conductivity, electromagnetic induction, geostatistical analysis, multivariate statistical analyses, soil properties

2.3. Introduction

Characterization of spatiotemporal variability of shallow soil properties is crucial for precision agriculture (Allred, 2011). Usually, soil samples and laboratory analyses are carried out to understand the soil's spatiotemporal variability. The conventional sampling and analysis of physiochemical properties of soils involves invasive sampling and provides only point measurements. This is expensive and not feasible for large-scale and extended temporal monitoring (Doolittle and Brevik, 2014; Mahmood et al., 2012; Serrano et al., 2013). More currently available sensing technologies may be implemented to avoid such issues. In addition, non-invasive in-situ techniques may allow a reduction in the excessive use of environmentally unfriendly chemical-based laboratory analyses.

Electromagnetic induction (EMI) is an established and widely used technology for soil studies. Various EMI sensors have been adopted for the measurement of apparent electrical conductivity (EC_a), due to their non-invasive nature, cost-effectiveness, and their ability to provide rapid, continuous measurements. The EC_a can be used to map spatiotemporal soil heterogeneities (Corwin, 2008; Corwin and Lesch, 2005; Doolittle and Brevik, 2014). Moreover, for characterization of soil variability, EC_a maps can be used to delineate management zones (Moral et al., 2010; Ruser et al., 2008). However, EC_a varies from site to site. Therefore, interpretation of EC_a measurements for a particular site requires detailed statistical analyses (Bronson et al., 2005).

EC_a measured by an EMI sensor has been used as a proxy of subsoil properties (Altdorff and Dietrich, 2014; Corwin, 2004; Huang et al., 2016; Pedrera-Parrilla et al., 2015). The EC_a is a standard and accepted parameter to study a variety of soil properties that directly or indirectly influence the EC_a readings (Corwin, 2008; Doolittle and Brevik, 2014). EMI sensors can be employed to measure and map various soil properties, including: soil salinity (Corwin and Lesch, 2014; Huang et al., 2015); soil texture ; soil moisture content – SMC (Brevik et al., 2006; Misra and Padhi, 2014); water table depth (Bouksila et al., 2012; Buchanan and Triantafilis, 2009; Doolittle et al., 2000; Hall et al., 2004; Schumann and Zaman, 2003); bulk density (BD) and porosity of soil (Brevik and Fenton, 2004;Corwin and Lesch, 2005); cation exchange capacity – CEC (Corwin and Scudiero, 2016; Rodrigues et al., 2015) and pore water electrical conductivity (EC_w) (Altdorff et al., 2017; Friedman, 2005). Recently, Altdorff et al. (2018) studied the effects of agronomic treatments and different soil amendments on EC_a; they also investigated prediction accuracy of SMC using EC_a data. In addition, different management zones could be identified with EC_a variability on a large-scale. When the EMI instrument was coupled with a Global Positioning System (GPS), it offered quicker and easier EMI surveys for the large-scale (Heil and Schmidhalter, 2017; Priori et al., 2013; Vitharana et al., 2006).

Geostatistical and multivariate statistical approaches including variogram analysis, principal component analysis (PCA), and multiple linear regression (MLR), are more suitable for relating EC_a with multiple soil properties (Jolliffe, 2002; Moral et al., 2010). Variogram analysis is a basic geostatistical approach for characterizing the spatial correlations of data (Baroni et al., 2013; MacCormack et al., 2017; Oliver and Webster, 2015). The experimental variogram (measured data) fitted with theoretical variogram models (e.g. exponential and spherical models) can establish accurate spatially dependent data sets. The ordinary block kriging is one of the most suitable spatial interpolation techniques for agricultural landscapes (Altdorff and Dietrich, 2014; Li and Heap, 2014; Scudiero et al., 2016; Zhu and Lin, 2010). A fitted experimental variogram is required for the ordinary block kriging interpolation technique, since the relationships between EC_a and soil properties are spatially dependent (D Altdorff et al., 2017; Altdorff et al., 2018; Bronson et al., 2005; Taylor et al., 2010), variogram analysis is a potential way for developing accurate mapping of soil properties using the measured EC_a data.

PCA avoids multi-collinearity effects among the variables and generates new uncorrelated variables called principal components (PCs) (Bronson et al., 2005; Heiniger et al., 2003; Martini et al., 2017). PCA helps to identify uncorrelated variables and, therefore, selects the most influencing variables for further analysis. Backward elimination of MLR is an accepted method to identify significantly correlated variables, while removing statistically non-significant variables. Therefore, geostatistical and multivariate statistical approaches will be very effective for characterizing the soil physiochemical variables and their relationships with soil EC_a.

The EC_a variations are primarily responsive to the presence of soil properties, such as texture (clay), SMC, and CEC when measured under non-saline conditions (De Smedt et al., 2013; Doolittle and Brevik, 2014; Pedrera-Parrilla et al., 2016b). Some soils, such as Orthic Humo-Ferric Podzol, found in western Newfoundland, contain a very low amount of clay, typically less than 10% (Altdorff et al., 2018; Farooque et al., 2012). This low clay percentage limits the CEC of the soils. Therefore, in those particular soils, SMC plays a major role in influencing EC_a variability. SMC measurements can be used to differentiate between wet and dry days, so relationships between EC_a and soil properties under wet and dry conditions are needed in order to understand, at least, the spatiotemporal variability of SMC. The objectives of this study were to identify the significant soil properties influencing EC_a measured with multi-coil and multi-frequency EMI sensors on dry and wet days, and assess the potential coil separations, frequencies, and coil orientations of EMI sensors on measuring EC_a variability, using detailed geostatistical and multivariate statistical techniques in a shallow Podzolic soil.

2.4. Methodology

2.4.1 Study Area

The research was conducted at the Pynn's Brook Research Station (PBRS) managed by the Department of Fisheries and Land Resources, of the Government of Newfoundland and Labrador, Canada. The PBRS is located (49°04'23"N, 57°33'39"W) in the Humber Valley Watershed in the western part of the island of Newfoundland (Figure **2.1**a). Sandy fluvial and glacio-fluvial deposits are spread over a very gentle slope at the research site (Kirby, 1988). Figure **2.1**b & c show the silage-corn agronomic experimental area, with different soil amendments as treatments, and the adjacent grassed field, all covering approximately 0.4 ha. The silage-corn experiment was conducted using five different silage-corn hybrid varieties to evaluate the biomass production potentials and greenhouse gases emission (Altdorff et al., 2018; Waqar, 2018). A detailed study using EMI instruments was focused on one variety (DKC26-28RIB, DEKALB, Canada) of the silage-corn experiment, which covers approximately 350 m^2 area. The soil texture in the top 0–15 cm soil layer showed sandy loam to loamy fine sand: sand 73.2% (± 5.2), silt 20.8% (± 4.6), and clay 6.0% (± 1.2), according to the United States Department of Agriculture (USDA) soil classification. Based on last 30 years (2016−1986) of weather data from the nearby weather station in Deer Lake

(49°12'33"N, 57°23'40"W), the mean annual precipitation and temperature are 1113 mm and 4^{o}C, respectively (http://climate.weather.gc.ca/). Generally, July is recognized as the hottest month and February as the coldest month in the western Newfoundland region (Daniel Altdorff et al., 2017).

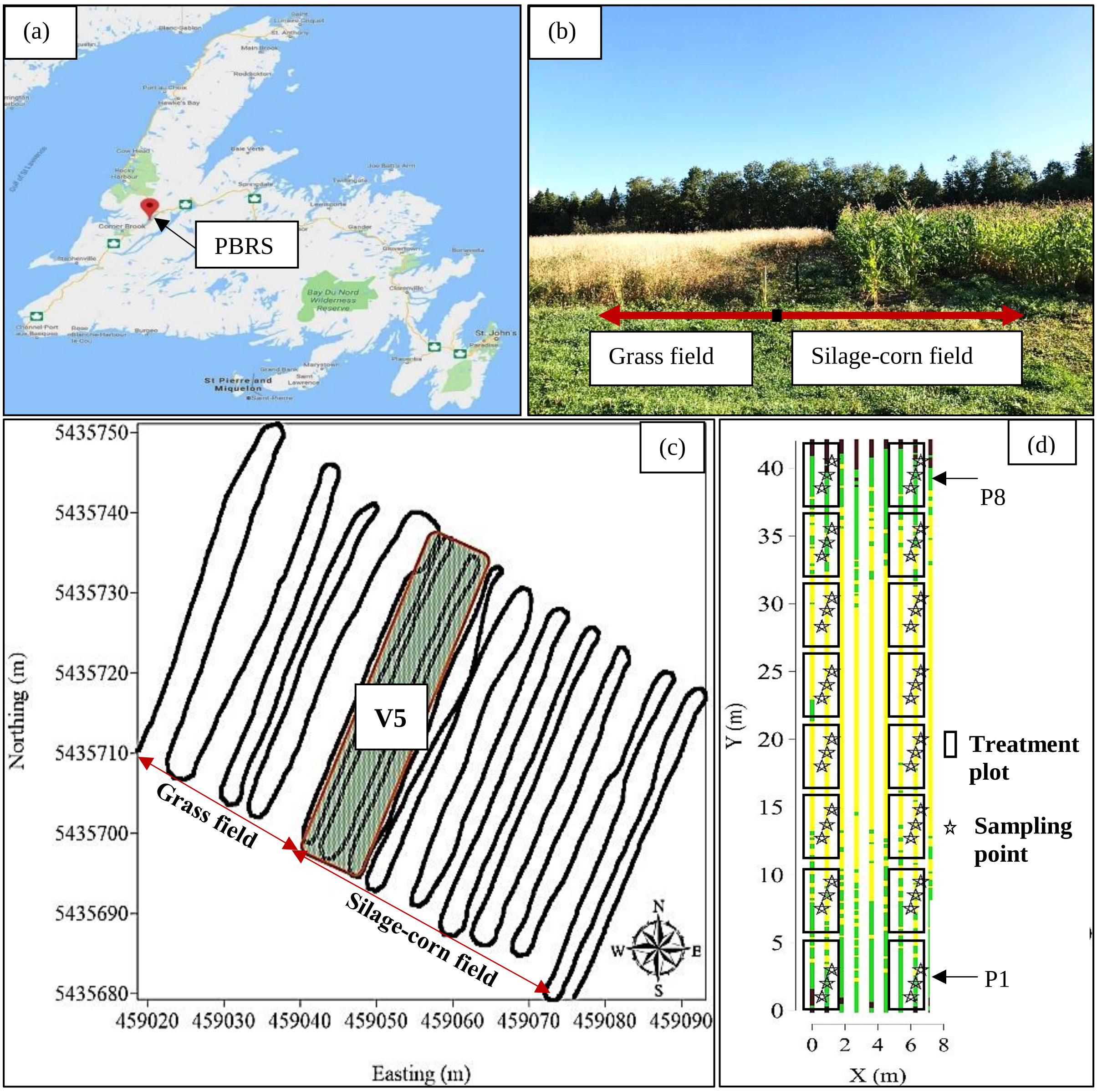

Figure **2.1**: Study site, field layout, and sampling locations. (a) Location of PBRS, (b) Grass and silage-corn fields, (c) Entire experimental field indicating the location of the DKC26-28RIB variety -V5, EMI survey coupled with GPS are showed in the black lines (d) Soil and EC_a sampling points on two transects of V5.

2.4.2 Soil Sampling and Analysis

A detailed soil investigation was carried out in the variety DKC26-28RIB section (hereafter called V5) of the silage-corn field (8 x 42 m^2). The V5 is comprised of four replicates (2 crop rows per replicate) and each replicate row was divided into 8 treatment plots (P1 to P8); each plot area was 1 x 5 m^2 (Figure **2.1**d). Soil samples were collected to measure soil properties such as soil texture, BD, CEC, pH, EC_w, and soil moisture content–gravimetric (SMC). Standard soil analytical procedures (Gregorich and Carter, 2007) were employed (Table **2.1**) at the Boreal Ecosystem Research Facility laboratory of Grenfell Campus-Memorial University of Newfoundland. Soil texture and BD were measured only once in this study. For soil texture, 28 undisturbed core samples were collected at a depth 0–15 cm to cover the entire V5 field. Air dried and sieved soils from <2 mm were used for the hydrometer analysis to measure the soil particle size distributions, then the soil textures were calculated according to the USDA soil taxonomy classifications. As for BD, undisturbed core samples (n=48) were collected, along with two transects, as shown in Figure **2.1**d. A sliding hammer fitted with a core sampler containing a plastic liner (diameter 3.5 cm and length 15 cm) was used to collect cores at the same depth (0–15 cm). The variogram models and ordinary block kriging were applied to soil textures (sand, silt, and clay) and BD data, in order to create interpolated maps for the V5 area. Then, the point data were digitized (extract data from maps) from interpolated maps according to the location where other soil samples were collected (Zhu et al., 2010).

Other soil properties, such as SMC, CEC, pH and EC_w were measured using composite soil samples collected at two depths (0–10 cm and 10–20 cm) and then depth weighted averages were calculated for the depth 0–20 cm. Each composite sample consisted of three samples collected in each treatment plot on a diagonal direction, with 1 m distance and 0.3 m spacing (Figure **2.1**d). These four soil properties were measured from the samples collected on August 18 and October 13, 2017, to represent dry and wet days, respectively. Average soil temperatures for the August 18 and October 13 were 17°C (dry day) and 8°C (wet day), respectively (Figure **2.2**).

Table **2.1**: Soil property measured, instrument used and the method

Soil Properties	**Instruments**	**Standard method**
Soil texture	Standard hydrometer (ASTM, USA)	Hydrometer method (Kroetsch and Wang, 2007)
BD (g/cm^3)	Core sampler with a sliding hammer	Core method (Hao et al., 2007)
SMC (%)	Convection Oven (Thermo Scientific, USA)	Gravimetric with oven drying (Topp et al., 2007)
CEC (cmol/kg)	Ion Chromatography- Dionex™ ICS-5000+ DC-5 Detector/Chromatography (Thermo Scientific, USA)	Sodium Acetate method-EPA 9081 (Chapman, 1965)
pH	HI9813-6 portable pH/EC/TDS/Temperature meter (HANNA instruments, USA)	0.01 M $CaCl_2$ method (Hendershot et al., 2007)
EC_w (mS/cm)	HI9813-6 portable pH/EC/TDS/Temperature meter (HANNA instruments, USA)	$EC_{1:2,}$ soil: deionized water (Miller and Curtin, 2007)

ASTM – American Society for Testing and Materials; EPA – Environmental Protection Agency; EC – electrical conductivity; TDS – Total dissolved solids; M – molarity of the solution

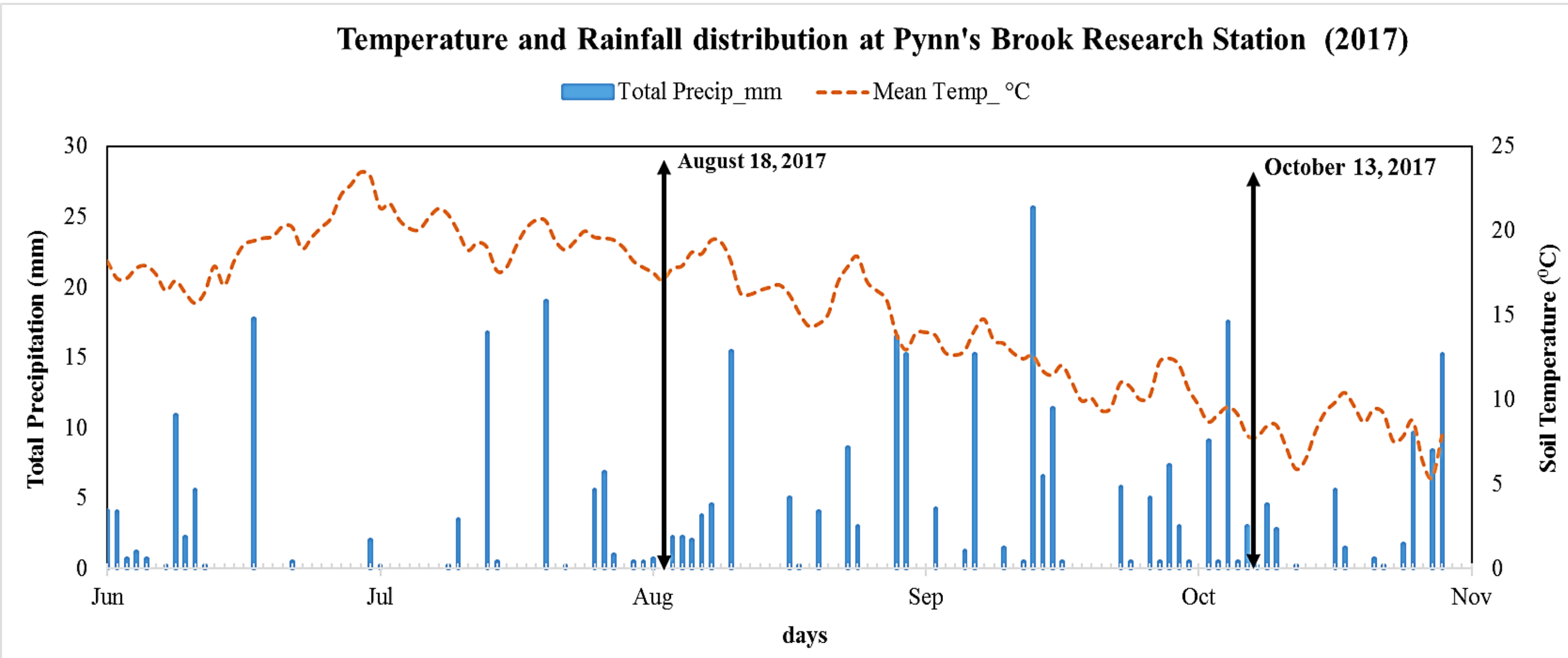

Figure **2.2**: Weather data, daily total precipitation in mm, and averaged soil temperature at a depth 20 cm. Vertical black arrows indicate the EMI measurements: August 18, 2017 and October 13, 2017.

2.4.3 Electromagnetic Induction Surveys

EMI grid surveys were carried out on the V5 of the silage-corn field using a multi-coil, and a multi-frequency at least once a month from July 2017 to October 2017. However, soil samples were taken only two days, along with EMI surveys, as mentioned above, on a dry day and a wet day. A 1 m line spacing was used during grid surveys, covering 8 x 42 m^2 area, using both EMI sensors. Orientation of the probe of both instruments was parallel to the transect lines and with the transmitter coil (Tx) always front facing in each survey. The number of EC_a readings in a survey were stretched according to the transect length (42 m) and walking speed, then the EC_a and relative coordinates were recorded by inbuilt software. GPS was not used when data were collected on the V5 area. EC_a data were collected by using both vertical coplanar (VCP) and horizontal coplanar (HCP) coil orientations. The multi-coil and multi-frequency EMI sensors were warmed up for approximately 20–30 min at the beginning of each survey.

According to McNeil's approximation (McNeil, 1980), the sampling depth of the multi-coil EMI probe provides six different integral depths of subsurface for both VCP and HCP coil orientations. These depths denoted here as: VCP–C1 (25 cm), VCP–C2 (50s cm – shallow), VCP–C3 (90 cm), HCP−C1 (50d cm - deep), HCP−C2 (100 cm) and HCP−C3 (180 cm) (D Altdorff et al., 2017; Bonsall et al., 2013). Similarly, three factory-calibrated frequencies were employed with the multi-frequency EMI sensor for both VCP and HCP coil orientations to provide 6 sampling depths; hereafter these depths are denoted as VCP−18kHz, VCP−38kHz, VCP−49kHz, HCP−18kHz, HCP−38kHz and HCP−49kHz.

Based on the analysis of raw data from both EMI sensors, noise data--such as negative values (*i.e.* mean of C1 for VCP and HCP modes) and unusual observations (*i.e.* mean of 18 kHz for VCP and HCP modes)--were removed as outliers of EMI sensors (APPENDIX 1). Therefore, VCP−C1 and HCP−C1 were ignored from the multi-coil instruments (Altdorff et al., 2018; Thiesson et al., 2017), and VCP−18kHz and HCP−18kHz were also omitted for statistical analysis.

2.4.3.1 Multi-coil EMI Sensor

The multi-coil EMI sensor operates at a fixed frequency of 30 kHz with three coil separations. The instrument has one transmitter coil (Tx) and three receiver coils (Rx) with fixed offsets of 0.32 m, 0.71 m and 1.18 m. Operating sensor height is approximately 20 cm from the ground surface (Altdorff et al., 2018), which maximizes depth sensitivity. The sensor is well adapted to outside temperatures between -10℃ and +50℃; the temperature stability is ±1 mS/m per 10℃ change in air temperature (GF-Instruments, 2011). The multi-coil EMI surveys were always carried out in one direction over the grid lines of the V5 field.

2.4.3.2 Multi-frequency EMI Sensor

The multi-frequency device has fixed coil separation between Tx and Rx, which is 1.67 m, and there is a bucking coil at ~1m from the Tx to cut off the primary field from the Rx (Simon et al., 2015a). Typically, operating frequencies have to be specified and selected by the user for each survey. Up to ten frequencies can be used simultaneously. However, since the power provided by the internal battery is distributed equally among the selected frequencies, power reduces in strength when more frequency signals are selected, consequently lowering the resolution. Free-air calibration (or 'zero') and amplitude calibration have been done at the factory and stored in multi-frequency operating software. An approximately 1 m sensor height was maintained for bi-directional grid surveys.

2.4.4 EMI Data Processing

Temperature corrections for the EC_a raw data collected from instruments were done using Eq. 2.1 to 25℃ (Sheets and Hendrickx, 1995).

$$EC_{25} = EC_a \times \left[0.4470 + 1.4034 \times e^{-T/26.815}\right] \qquad \text{Eq. 2.1}$$

where EC_a is the collected data, and T is the soil temperature measured (℃). EC_{25} is the temperature corrected EC_a.

The soil temperature was recorded at a depth of 20 cm below the surface. Daily average temperature was calculated for the daily EMI survey duration (from 9 am to 4 pm) using minimum and maximum temperature recorded at the weather station at the site. Temperature corrected EC_a data were used to create interpolated maps, using an ordinary block kriging interpolating technique in the Surfer11 software (Golden Software Inc., USA) (De Smedt et al., 2013). Two variogram models (exponential and spherical) were applicable for the V5 site, and these were used in the ordinary block kriging technique, in order to achieve high resolution spatially interpolated data (Altdorff et al., 2018). Point data were digitized from interpolated maps with respect to the soil sampling locations in the field (*i.e.* three points per treatment plot in a diagonal direction). Finally, an averaged point data was calculated from each treatment plot. Thus, 16 points were obtained for both the dry day and the wet day.

2.4.5 Statistical Analysis

A variogram analysis was used to develop spatial correlations among EC_a data, and helps to determine unknown EC_a points (from interpolated locations) with respect to spatial locations in both dry and wet days. Figure **2.3** shows a typical variogram consisting of three important parameters, namely nugget, range, and sill. The nugget represents variability at distances smaller than the sample spacing, including measurement error. A higher sill or shorter range suggests greater variations of measured data (Zhu and Lin, 2010). Exponential and spherical (theoretical variogram) models were fitted to measured EC_a datasets (experimental variogram) from the test site. Ordinary least squares method was applied to fit an experimental variogram with an approximated model variogram (Baroni et al., 2013). A small lag distance was used in the variogram analysis, because measurements were taken from a small experimental field.

A small lag distance can be used with 30–50 pairs of samples or greater (APPENDIX 2), when the lag distance is less than half of the maximum distance of the field (Journel and Huijbregts, 1978; Li and Heap, 2014). A 90-degree directional tolerance, called omni-direction, was used to cover all directions (Variogram Tutorial, Golden Software, Inc., USA). The relative nugget effects (RNE) were calculated by the ratio of nugget to sill for both dry and wet days in order to characterize spatial dependency of EC_a data (Moral et al., 2010; Oliver and Webster, 2015). An RNE value (variability) describes unexplainable or random variation related to total variation in a short-range (Nayanaka et al., 2011; Zhu and Lin, 2010).

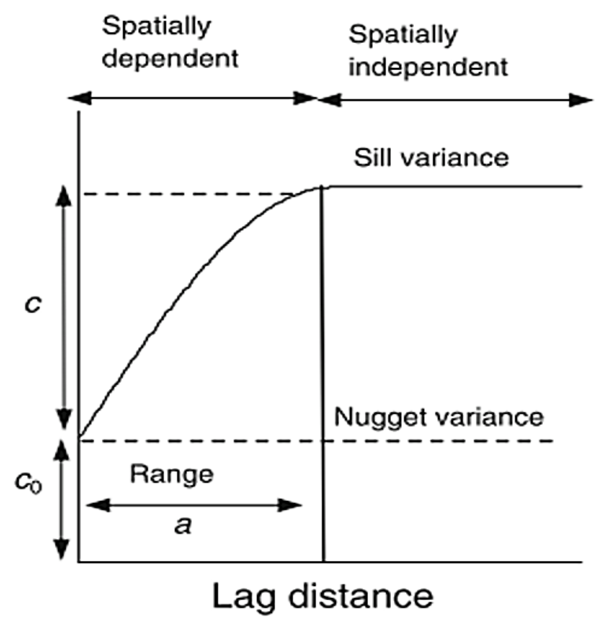

Figure **2.3**: Typical structure of a (semi) variogram model; Sill ($C+C_0$), range (a) and Nugget (C_0) (Oliver and Webster, 2015)

Simple Pearson's correlation (*r*) coefficients were calculated between soil properties and digitized EC_a data, using the statistical software Minitab 17 (Minitab Inc., 2010). A principal component analysis (PCA) was used to reduce the number of significant soil properties (uncorrelated variables), and also to avoid multi-collinearity effects among the correlated variables (Bronson et al., 2005; Heiniger et al., 2003). The PCA analysis was performed with XLSTAT v2018.3 software (Addinsoft, Paris, 2018), and bi-plots were created to show a graphical representation of correlations among the variables measured in the field. In order to identify the significant dependence of EC_a on tested soil properties, a stepwise (backward elimination) MLR analysis followed by the Pearson's correlation and the PCA were done (De Caires et al., 2015).

Finally, separate MLR models were developed for pre-selected coil separations of the multi-coil and the frequencies of the multi-frequency EMI sensors for this particular Podzolic soil in western Newfoundland. These MLR models were assessed by properties of model summary, especially standard error (SE), coefficient of determination (R^2), and predicted coefficient of determination (R^2p). The R^2p value indicates how a regression model better predicts new observations by avoiding overfitting a model, which contains many predictor variables. Therefore, R^2p values can be used to determine the best regression models when comparing the different number of predictors in each regression model. The developed regression models were used here to identify suitable coils or frequencies of EMI sensors to characterize soil variability using ECa. ECa readings can be influenced by several soil properties, and those soil properties vary from site to site.

A few assumptions were made for this study. In general, a quadrature component of secondary field proportional to EC_a under low induction number condition. Soil samples for texture and BD were collected at the depth 0–15 cm, but other soil properties were measured at 0–20 cm depth soil samples. Soil texture and BD data were taken only once, so the same data were used for both dry and wet day analyses.

Assumptions Made:

- The McNeill's approximations for EC_a measurements obtained under low induction number applies.

- Homogenous distribution of the soil texture and BD within the depth of 0–20 cm, and there are no temporal changes of soil texture and BD throughout the study period (August 18 to October 13, 2017).
- There were no external power line disturbances when doing the EMI surveys.

2.5. Results and Discussion

2.5.1 Descriptive Analysis of Soil Physiochemical Properties

The soil samples were collected from shallow depths (0–10 cm and 10–20 cm) due to the stony nature and shallow soil with a hardpan of Podzols, which consequently made it hard to collect samples, especially in the dry season. Measured samples were converted to a depth weighted average of 0–20 cm to make a spatially homogeneous depth sample (Pedrera-Parrilla et al., 2016). The research was conducted on an Orthic Humo-Ferric Podzolic soil, which has low organic matter (<5%) and clay content (Kirby, 1988; Smith et al., 2011), and consequently low EC_a measurements. A very low clay percentage was reported (6.0 ± 0.8) with a coefficient of variation (CV) of 13.1% in the V5 silage-corn field at PBRS. A similar variability was observed for silt (CV = 15.3%), but sand content showed a low variability (CV = 4.7%) as shown in Table **2.2**. Among the clay, silt, and sand content, silt becomes one of the influencing factors of EC_a variability, since clay content was very low in the tested field. Domsch and Giebel (2004) reported that silt content also influences EC_a similar to clay content.

Khan et al. (2016) found low EC_a (mean, 4.4 mS/m) for the same soil type (Podzol) using a DualEM–2 EMI sensor. This value matched the EC_a measured here with the multi-coil EMI in this research field. Another finding by Waine et al. (2000) classified EC_a readings according to soil textural classes, whereas sandy loam soils were categorized by 0–10 mS/m; the authors also suggested that coarse-textured soils give EC_a <15 mS/m. These EC_a values and findings were more similar to EC_a data measured at the PBRS site.

BD showed lower CV (5.1%) compared to other soil properties, except for sand and pH, which shows the uniform compaction across the field. The same soil texture and BD measurements were used for both days and were assumed to be unchanged within this short period. Therefore, except for EC_w, mean values of other tested soil properties are higher in the wet day compared to the dry day (Table **2.2**). EC_w shows the highest CV (41.2%) in the dry day than any other soil properties from both days. The pH value exhibits acidity (< 7) of Orthic Humo-Ferric Podzols (Farooque et al., 2012) in the PBRS. Soil moisture content (SMC) plays a major role in comparing the EC_a variability of both days. The CVs of SMC is 12.9% and 15.0% for dry and wet days, respectively. At the same time, the average SMC is 12.3% (±1.6) for dry sampling and 19.9% (±3.0) for wet sampling, illustrating that wet day SMC was high in the tested field.

2.5.2 Descriptive Analysis for EC_a Data of the Multi-coil and Multi-frequency EMI Sensors

Descriptive statistics of the raw EC_a data of the EMI sensors are given in APPENDIX 1. After removal of some raw EC_a data, new descriptive statistical values were calculated for EC_a and soil properties, shown in Table **2.2**. Measured EC_a values were higher on the wet day than the dry day, as expected. The second coil separation (C2) of the multi-coil EMI the highest EC_a values; EC_a, 4.0 (±0.3) mS/m from HCP–C2 for the dry day, and 6.2 (±0.8) mS/m from VCP–C2 for the wet day. Interestingly, a high CV of EC_a is reported on the wet day for the multi-coil, and on the dry for the multi-frequency EMI sensor. However, CV differences between dry and wet days were much smaller for the multi-coil compared to the multi-frequency EMI sensor.

Average EC_a measured from VCP–49kHz is 20.3 (±0.7) mS/m with a CV of 3.7%, which is the highest mean and the lowest CV from among all the measured EC_a using both instruments and coil orientations. The 38 kHz frequency data of the multi-frequency show very high CVs on both days compared to all other values (Table **2.2**). On the other hand, the EC_a measurements by 49 kHz frequency show a relatively higher mean EC_a value, ranging from 7.5 (±0.7) to 20.3 (±0.7) mS/m for both days (Table **2.2**). The VCP mode of the multi-frequency EMI gives a higher EC_a compared to the HCP mode on the dry day. Additionally, a higher variability (high CV) of EC_a is found on the dry day compared to the wet day from multi-frequency EMI. A similar pattern of high variability in dry days has been found by Korres et al. (2010) and Pedrera-Parrilla et al. (2016b).

EC_a measurements from VCP and HCP coil orientations could be influenced by how soil layers are characterized with different conductive properties. A good example was given by Corwin and Scudiero (2016) with respect to the salinity profile along with a depth: if EC_a of VCP>HCP, salinity decreases with depth; VCP<HCP, salinity increases with depth, and if VCP>>>HCP, salinity is uniformly distributed to a certain depth.

Likewise, EC_a data from the multi-coil EMI sensor can be categorized as EC_a of VCP<HCP on the dry day, and VCP>HCP on the wet day. It reveals that high SMC in shallow soil (near the surface) increases EC_a values in VCP mode measurements. Furthermore, the mean value of the EC_a of VCP–C2 was doubled on the wet day compared to dry day (Table **2.2**).

Overall, 38 kHz data from multi-frequency EMI, and soil properties including silt, clay, SMC, and CEC were showed similar variability from the wet day. Likewise, EC_a data measured by 49 kHz frequency were showed closer range of variability with the same soil properties for the dry day. All multi-coil EMI data were showed adequate variability range with the aforementioned soil properties for both days compared to multi-frequency EMI sensor.

Table **2.2**: Descriptive statistics of soil properties and EMI-EC_a (mS/m) data for both dry and wet days (n=16),

Variable	Dry day Mean	SD	CV	Min	Max	Wet day Mean	SD	CV	Min	Max
Multi-frequency EMI										
VCP–38kHz	1.9	0.8	39.2	0.9	3.3	3.9	0.7	18.5	2.8	5.2
VCP–49kHz	11.4	1.1	9.2	9.5	13.5	20.3	0.7	3.7	19.1	21.8
HCP–38kHz	1.6	1.0	58.7	0.7	3.8	6.3	0.8	12.8	5.2	7.7
HCP–49kHz	7.5	0.7	9.5	6.6	8.8	16.6	0.7	4.2	15.7	17.9
Multi-coil EMI										
VCP–C2	3.4	0.3	7.5	2.9	3.9	6.2	0.8	12.8	5.3	7.7
VCP–C3	3.1	0.3	8.0	2.6	3.5	3.5	0.4	11.0	2.7	4.1
HCP–C2	4.0	0.3	6.6	3.6	4.5	4.4	0.4	9.0	3.7	5.0
HCP–C3	3.6	0.3	8.9	3.1	4.1	4.2	0.4	10.2	3.5	5.1
Soil properties										
Sand (%)	74.2	3.5	4.7	68.0	81.7	74.2	3.5	4.7	68.0	81.7
Silt (%)	19.9	3.1	15.3	13.7	25.4	19.9	3.1	15.3	13.7	25.4
Clay (%)	6.0	0.8	13.1	4.7	7.5	6.0	0.8	13.1	4.7	7.5
BD (g/cm^3)	1.4	0.1	5.1	1.3	1.5	1.4	0.1	5.1	1.3	1.5
SMC (%)	12.3	1.6	12.9	9.3	15.5	19.7	3.0	15.0	15.1	23.8
pH	5.4	0.2	3.7	4.9	5.7	5.7	0.2	4.2	5.3	6.1
CEC (cmol/kg)	11.0	2.1	19.3	8.0	14.3	12.2	1.9	15.8	9.4	15.1
EC_w (mS/cm)	0.2	0.1	41.2	0.1	0.5	0.1	0.0	26.8	0.1	0.1

SD – standard deviation; CV – coefficient of variation (%); Min – minimum; Max – maximum, all values were rounded for one decimal

Table **2.3**: Experimental variogram model parameters of EC_a data for dry and wet days

Variables	Dry day Model	Nugget	Sill	Range (m)	RNE (%)	Wet day Model	Nugget	Sill	Range (m)	RNE (%)
Multi-frequency EMI										
VCP–38kHz	Exp	0.100	0.830	0.3	12.0	Exp	0.030	0.250	0.4	12.0
VCP–49kHz	Sph	0.500	2.700	0.5	18.5	Exp	0.020	0.160	0.3	12.5
HCP–38kHz	Exp	0.050	0.350	0.6	14.3	Exp	0.020	0.170	1.6	11.8
HCP–49kHz	Exp	0.050	0.260	0.4	19.2	Exp	0.010	0.110	1.4	9.1
Multi-coil EMI										
VCP–C2	Exp	0.001	0.070	1.0	1.4	Exp	0.005	0.056	0.8	8.9
VCP–C3	Sph	0.001	0.046	1.4	2.2	Exp	0.005	0.067	1.0	7.5
HCP–C2	Exp	0.001	0.058	0.7	1.7	Exp	0.005	0.056	2.0	8.9
HCP–C3	Sph	0.001	0.048	1.1	2.1	Exp	0.005	0.050	0.8	10.0

Exp – exponential model; Sph – Spherical model; RNE – relative nugget effect

Descriptive statistics do not provide spatial variability of soil properties or EC_a. Therefore, a geostatistical analysis was required for spatial data analysis (Farooque et al., 2012). Kriging is a better interpolation technique to estimate values in unknown locations from the spatial data (Arun, 2013; Shahid et al., 2013). The ordinary block kriging uses a weighted average of adjacent values, which are optimized using variogram models (Martini et al., 2017; Oliver and Webster, 2015). Therefore, accurate interpolation could be established using variogram models of EC_a data, and, consequently, mapping the variability of EC_a for both dry and wet days could be accomplished. APPENDIX 3 shows EC_a maps of the multi-coil sensor which were created using variogram and ordinary block kriging interpolation techniques.

2.5.3 Variogram Analysis

A summary of experimental variogram analysis for dry and wet days is shown in Table **2.3**. Exponential and spherical theoretical variogram models were fitted to EC_a data with a small lag distance (5 m) due to the 42 m by 8 m (a small) study area. Watson et al. (2017) fitted an exponential variogram model with a 10 m lag distance on a 40 m by 50 m study site. Based on the variogram models, higher variability was found on the dry day compared to the wet day, irrespective of the sensor type or coil orientation. The nugget and sill (EC_a data) are very low for the multi-coil (≤ 0.005 and <0.07) compared to the multi-frequency EMI sensor (> 0.05 and > 0.26). The highest sill is reported for VCP–49kHz (2.7), followed by VCP–38kHz (0.83) on the dry day. Figure **2.4** clearly depicts that the nugget values vary between the frequencies and coil orientations of the multi-frequency, while the multi-coil EMI has a consistent nugget for coil separations and coil orientations.

From the experimental variogram, the VCP mode showed higher variability than the HCP mode for EC_a measurements of both instruments. Figure **2.4** shows that VCP and HCP are separated from each other on the dry day (multi-frequency) and the wet day (multi-coil). The multi-frequency data display has almost identical spatial variability (and also low) on the wet day compared to the dry day.

Strong spatial dependency by both EMI sensors was exhibited through RNE%. According to Moral et al. (2010), RNE < 25% indicated strong spatial dependence; between 25 and 75% denoted moderate spatial dependence; greater than 75% indicated weak spatial dependence. However, both instruments showed a robust spatial dependency because RNE is less than 25%. The RNEs of the multi-coil EMI sensor are higher on the wet day compared to dry day. Oppositely, the RNEs were higher on the dry day compared to wet day for the multi-frequency sensor, except VCP–38kHz. The overall RNE values of the multi-coil were lower than the multi-frequency sensor. HCP–49kHz and VCP–49kHz showed the highest RNEs (19.2% and 18.5%) for the dry day, while VCP–C2 had the lowest RNE (1.4%) on the same day. The multi-coil EMI instrument has stronger spatial dependency compared to the multi-frequency, due to a very low RNE of the multi-coil sensor (Moral et al., 2010).

With the knowledge of geometrical and frequency sounding of EMI (Figure **1.3**), the effective depth from the ground surface to deeper subsoil can be arranged as VCP–C2 < VCP–C3 < HCP–C2 < HCP–C3 for the multi-coil EMI device, and as VCP–49kHz < VCP–38kHz < HCP–49kHz < HCP–38kHz for the multi-frequency EMI device. If these depth sensitivity patterns were compared with experimental variogram models (Figure

2.4), it would reveal that a high variability exists in the near-surface soil (*i.e.* VCP mode shows high variability from both sensors); that is true for an agricultural field.

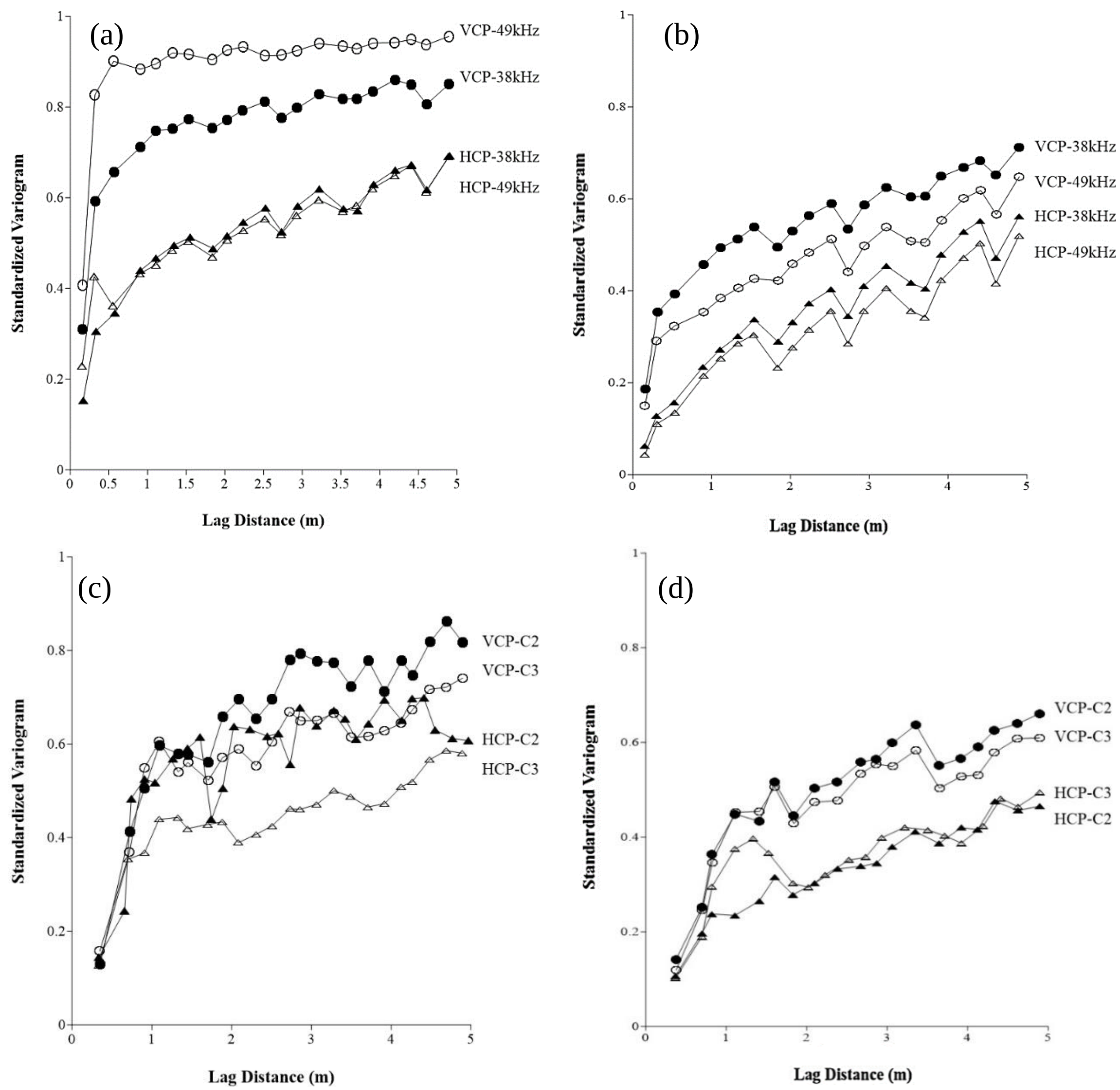

Figure **2.4**: Experimental variogram of EC_a data: (a-b) multi-frequency EMI sensor for dry and wet days, respectively; (c-d) multi-coil EMI sensor for dry and wet days, respectively.

2.5.4 Pearson's Correlation

The simple correlation coefficient *r* between the digitized EC_a data and eight soil properties is shown in Table **2.4**. The correlation strength between EC_a and soil properties can be divided, according to Zhu and Lin (2010), *i.e.* if $r < 60\%$, this means weak correlation, and if $r > 60\%$ this means strong correlation. Huang et al. (2018) recently reported that a weak *r* (VCP−40% and HCP−30%) was obtained when the field was very dry (nearly a permanent wilting point) and a strong *r* (VCP−74% and HCP−75%) was found after an irrigation event (wet field). Therefore, correlation strengths can change due to wetting and drying patterns of the field.

Significant ($p<0.05$) correlation was found between SMC and all EC_a data for the dry and wet days, except the 38 kHz frequency data of the multi-frequency on the wet day. Only EC_a of VCP−C3, HCP−C2 and VCP−49kHz showed higher *r* with SMC towards the wet day. Overall, the highest correlation for the dry day was found between VCP–38kHz and SMC (r = 83%), and concurrently for the wet day between VCP–C3 and SMC (r = 81%) among all soil properties tested. Interestingly, VCP−38kHz established a weak and non-significant correlation (r = 47%) with SMC for the wet day.

Silt also correlated significantly with all EC_a data for both days, except HCP−38kHz from the dry day. All dry day EC_a data were significantly correlated with CEC, while only VCP−C3 and HCP−C2 were significant for the wet day (Table **2.4**). There were significant correlations found with EC_w and all EMI–EC_a --one on the dry day, and three on the wet day. It was also noted that the EC_w had a significant correlation with the VCP‒C3, HCP‒C2, and VCP‒49kHz in the wet day survey.

Some soil properties, such as sand, clay, BD, and pH, have a negative correlation with EC_a data on both days. However, only the sand has a significant (p<0.05) correlation with EC_a data. Negative correlations with sand and EC_a were reported by several studies (Heiniger et al., 2003; Pedrera-Parrilla et al., 2015; Serrano et al., 2014). A study by Bronson et al. (2005) confirmed the negative correlation between EC_a and clay content in the Ropesville test site, and the negative correlation was established due to low clay content. Likewise, the authors observed negative correlations among EC_a, CEC, and pH.

Table **2.4**: Pearson's correlation coefficient (*r*) summary between soil properties (0‒20 cm depth), and temperature corrected EC_a data for both wet and dry days (n=16)

	VCP–38kHz	**VCP–49kHz**	**HCP–38kHz**	**HCP–49kHz**	**VCP–C2**	**VCP–C3**	**HCP–C2**	**HCP–C3**
Dry day								
Sand (%)	-0.48	-0.48	-0.34	-0.41	**-0.75*****	**-0.69****	**-0.68****	-0.43
Silt (%)	**0.61***	**0.59***	0.48	**0.55***	**0.73*****	**0.72****	**0.73*****	**0.55***
Clay (%)	-0.26	-0.20	-0.38	-0.33	0.45	0.20	0.18	-0.24
BD (g/cm^3)	-0.40	-0.150	-0.17	-0.40	-0.16	-0.33	-0.34	-0.46
SMC (%)	**0.83*****	**0.50***	**0.65****	**0.76*****	**0.55***	**0.74*****	**0.71****	**0.79*****
pH	-0.17	-0.33	-0.06	-0.16	0.10	0.02	-0.22	-0.20
CEC (cmol/kg)	**0.70****	**0.51***	**0.61***	**0.65****	**0.60***	**0.77****	**0.79*****	**0.78*****
EC_w (mS/cm)	0.21	0.005	0.11	0.062	0.47	0.44	**0.60***	0.38
Wet day								
Sand (%)	-0.38	**-0.60***	-0.41	-0.47	-0.48	**-0.72****	**-0.61***	**-0.53***
Silt (%)	**0.51***	**0.69****	**0.55***	**0.60***	**0.62****	**0.76*****	**0.66****	**0.62****
Clay (%)	-0.31	-0.07	-0.35	-0.29	-0.29	0.24	0.11	-0.06
BD (g/cm^3)	-0.43	-0.28	-0.33	-0.37	-0.37	-0.28	-0.34	-0.39
SMC (%)	0.47	**0.63****	0.47	**0.56***	**0.55***	**0.81*****	**0.77*****	**0.68****
pH	0.09	-0.08	-0.03	-0.10	-0.07	-0.15	-0.11	0.02
CEC (cmol/kg)	0.25	0.43	0.29	0.39	0.37	**0.68****	**0.63****	0.49
EC_w (mS/cm)	0.37	**0.60***	0.39	0.37	0.38	**0.63****	**0.50***	0.46

Bold numbers correspond to significant correlations (*** p<0.001, ** p<0.01, * p<0.05) BD – bulk density; SMC – soil moisture content (gravimetric); CEC – cation exchange capacity; EC_w – pore water electrical conductivity

EMI sensors are not a reliable tool to measure BD, soil pH (Corwin and Scudiero, 2016; Korsaeth, 2005; Scudiero et al., 2016), and some macronutrients (Adamchuk et al., 2004; Korsaeth, 2005; Lobsey et al., 2010). Weak correlations obtained on both days between EC_a and soil properties, such as clay content, BD, and soil pH, implies that further statistical analyses are not necessary (Bronson et al., 2005; Heiniger et al., 2003).

2.5.5 Principal Component Analysis

The first two principal components (PC1 and PC2) together exhibit a larger portion of the total variability of all soil properties and EMI–EC_a data. Both PCs include approximately 71% and 77% variances for the dry day and the wet day, respectively, of all the aforementioned soil properties including clay, BD, and pH, and EC_a data. These two values show strong spatial relationships between some of the soil properties and EC_a data. Good spatial correlations concerning the first two PCs (De Caires et al., 2015) are shown in Table **2.5**. Almost every EC_a (both sensors and modes) had stronger correlations with PC1 for both days. However, among the soil properties, only clay was strongly correlated with PC2 on both days, but PC2 only contributes 16% (dry day) and 18% (wet day) from the total variance of the data (Table **2.5**). The correlation strengths between the PC1 and soil properties are: CEC > SMC > silt for the dry day, and silt > SMC > CEC for the wet day.

The graphical explanation of correlations is displayed in bi-plots for both days (Figure **2.5**). A bi-plot simultaneously provides a relative position of variables and observations in a graphical relationship (Jolliffe, 2002). Only predominant predictors (soil properties) were clustered with positively correlated EC_a data, as shown in Figure **2.5**.

The correlation strength is evaluated by an angle between the two arrows in the bi-plot: <90^o for positive correlation and >90^o for negative correlation (Mahmood et al., 2012). VCP–C3 and HCP–C2 of the multi-coil EMI sensor exhibit strong positive correlations with silt, CEC, and SMC on both days, but EC_w shows strong correlations on the wet day only. In the bi-plot, the length (from the origin) of each arrow represents the measure of fit for a variable. A shorter and longer length symbolizes poor and good representation of measured data, respectively (Mahmood et al., 2012). The BD, pH, and EC_w show poor representation on both days in the bi-plots.

Table **2.5**: Correlations between measured variables and the first two PCs at the study site

Variables	Dry day		Wet day	
	PC1	**PC2**	**PC1**	**PC2**
VCP–38kHz	0.882	-0.289	0.837	-0.495
VCP–49kHz	0.706	-0.345	**0.947**	-0.236
HCP–38kHz	0.800	-0.458	0.851	-0.477
HCP–49kHz	0.855	-0.425	0.891	-0.396
VCP–C2	0.717	0.506	0.894	-0.404
VCP–C3	0.890	0.213	0.916	0.143
HCP–C2	0.894	0.161	0.893	0.022
HCP–C3	**0.896**	-0.261	0.924	-0.226
Sand	-0.733	-0.546	-0.761	-0.576
Silt	0.823	0.377	0.841	0.434
Clay	0.032	**0.950**	0.086	**0.854**
BD	-0.458	0.069	-0.421	0.047
SMC	0.865	-0.163	0.824	0.418
pH	-0.302	0.142	-0.234	-0.514
CEC	0.887	0.063	0.653	0.505
EC_w	0.397	0.465	0.564	0.292

Highest correlation values in each PC are showed in bold.

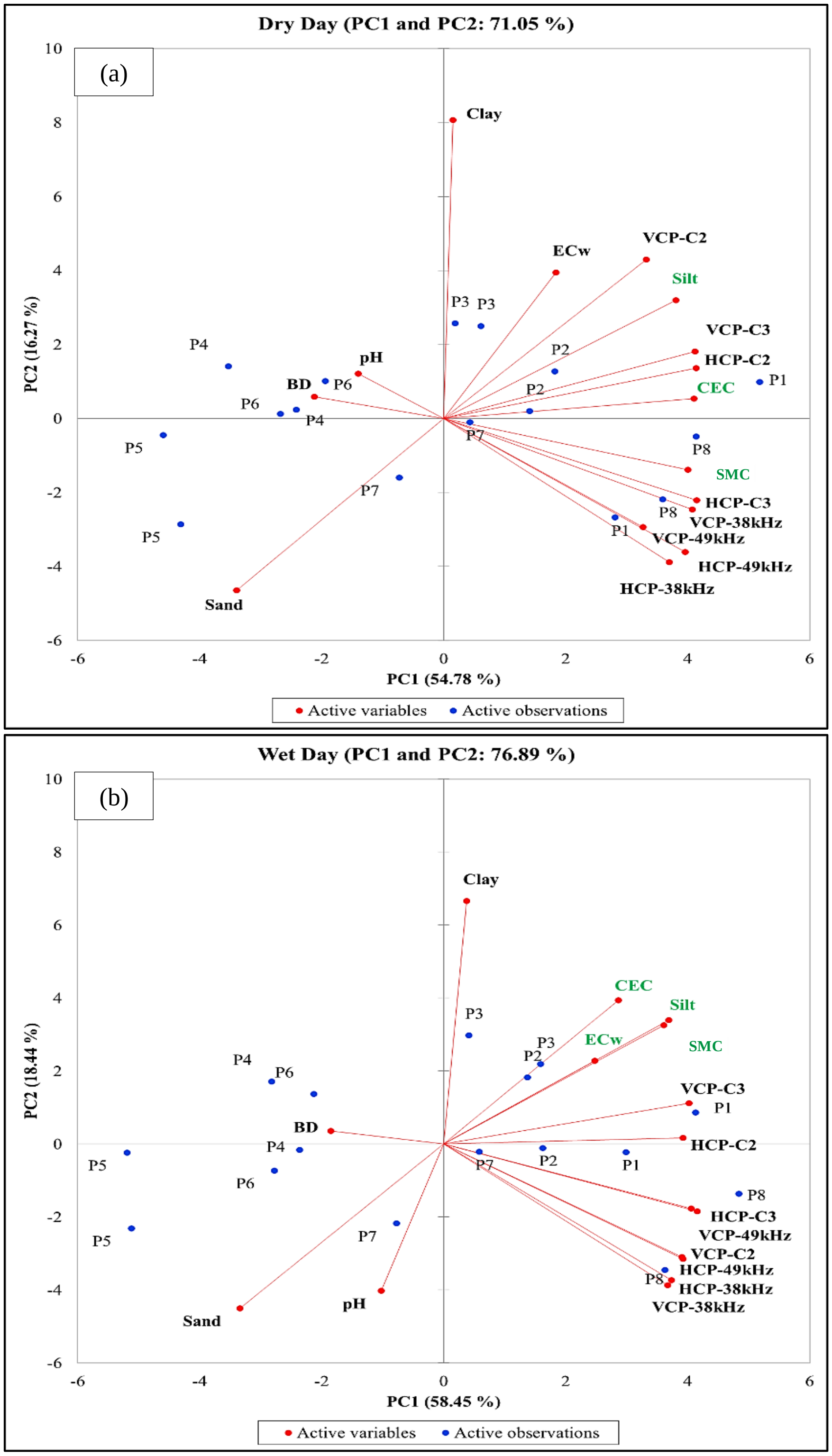

Figure **2.5**: PCA biplots of measured soil properties with respect to 8 treatment plots (P1-P8). (a) - dry day; (b) - wet day; Green colored soil properties represent positive significant correlation with most of the EC_a data.

The treatment plots, P4, P5 and P6, were located in the center of the V5 silage-corn field. These plots showed low SMC and high stony texture (by field observation), resulting in high BD. This is reflected in Figure **2.5**, BD and sand mostly spread over P4, P5, and P6 plots. The V5 has small elevation differences between the center (higher) of the field and both outer ends. Therefore, surface runoff and interflow can cause nutrients, organic matters, and finer particles (clay) to transport and accumulate towards both ends of the V5 field (field observations also revealed this pattern). This variability could be observed in interpolated EC_a maps by using both EMI sensors (Figure **2.6** and **2.7**).

Soil properties such as sand, silt, SMC, CEC, and EC_w were selected for backward multiple linear regression (MLR) analysis, based on the results of both *r* and PCA.

2.5.6 Multiple Linear Regression (Backward Elimination of MLR)

Results from the above geostatistical and statistical analyses were ratified by backward elimination of MLR. The MLR indicates the most influencing predictors for EC_a among the tested soil properties (i.e. sand, silt, SMC, CEC, and EC_w). Huang et al. (2018) used a similar set of EC_a data (EM38h and EM38v) in different regression models for predicting SMC at different depths. My study was slightly different, because measured EC_a is represented by depth weighted soil EC_a, corresponding to different coil separations or frequencies with VCP and HCP modes of operation. Completely different regression models were developed for dry and wet days by the backward elimination analysis of MLR.

A summary result of MLR analysis is shown in Table **2.6**. The SE values are in the range of 0.14–0.18 with the multi-coil and 0.37–0.71 with the multi-frequency EMI on the dry day data. However, from the wet day, almost a narrow range of values are observed for both sensors (for the multi-coil sensor, SE=0.19–0.26 and for the multi-frequency, SE=0.21–0.28). The coefficient of determination (R^2) of each model was higher on the wet day compared to the dry day, except HCP coil pairs of the multi-coil EMI device (Table **2.6**).

Predicted coefficient of determination (R^2_p) is a crucial parameter in comparing regression models which have different predictors. Overall prediction of EC_a from soil properties is lower in the dry day surveys compared to the wet day. In the dry day, more than 50% prediction accuracy is given by VCP−38kHz and HCP−49kHz of the multi-frequency EMI sensor, as well as VCP−C3, HCP−C2 and C3 of the multi-coil EMI sensor. All multi-frequency sensor data and all VCP mode of the multi-coil developed strong prediction models on the wet day. The highest R^2p values on the dry day (62%) and the wet day (87%), respectively, are from HCP−C2 and HCP−38kHz (Table **2.6**).

The multi-frequency EMI sensor explores sampling depth for more than 4 m (Tang et al., 2018), but there is an impact from shallow soil properties since the EC_a measurements are integrated from the surface. The shallow (0–20 cm) soil samples also have significant impacts on the EC_a readings (Bronson et al., 2005; Farooque et al., 2012). The multi-frequency EMI data established better regression models with significantly correlated soil properties when the soil was wet (Table **2.7**). In other words, R^2p>50% was shown by VCP−38kHz and HCP−49kHz surveys on the dry day as well as all surveys on the wet day. Overall, soil textures (sand and silt) mainly influenced the multi-frequency EMI-EC_a data for both days (Table **2.7**).

The multi-coil EMI sensor is less complicated for interpreting the depth sensitivity of EC_a measurements compared to the multi-frequency device. Clearly, when the soil becomes wet, the VCP mode (shallow depths) has a high predicted R^2p (>70%) for EC_a of the multi-coil on the wet day. At the same time, the HCP mode of operation on the dry day is moderately suitable to predict some soil properties (*i.e.* sand, silt, EC_w and SMC).

The wet day regression model equations of both sensors consist of more soil properties (predictor variables). SMC is the most influential soil property for this study, since the EMI data is a comparison between dry and wet days. Especially in the wet day, all regression model equations of both sensors have SMC as a predictor. However, in the dry day, only the VCP–38kHz of the multi-frequency, as well as the VCP–C3 and HCP–C2 of the multi-coil EMI, show SMC as one of the predictors in their regression models.

De Smedt et al. (2013) reported that EC_a measurements under the non-saline conditions can be directly related to soil texture (sand, silt, clay) and is influenced by SMC and organic matter. Sudduth et al. (2005) found that soil texture, SMC, and CEC are primarily responsible for EC_a variation. This study also showed similar soil properties (such as SMC, sand, and silt), CEC, and EC_w influenced EMI–EC_a in the tested Podzolic soils.

Table **2.6**: Summary of backward elimination MLR between soil and hydraulic properties and EC_a data of multi-frequency and multi-coil EMI sensors on the dry and wet days (p<0.05 and n=16)

Variables	**Dry day**				**Wet day**			
	SE	R^2	R^2adj	R^2p	SE	R^2	R^2adj	R^2p
Multi-frequency EMI								
VCP–38kHz	0.37	0.80	0.75	0.53	0.28	0.90	0.85	0.74
VCP–49kHz	0.71	0.60	0.54	0.46	0.23	0.93	0.90	0.77
HCP–38kHz	0.61	0.65	0.60	0.46	0.21	0.96	0.93	0.87
HCP–49kHz	0.42	0.70	0.66	0.56	0.27	0.90	0.85	0.66
Multi-coil EMI								
VCP–C2	0.18	0.56	0.52	0.43	0.25	0.93	0.90	0.80
VCP–C3	0.15	0.69	0.64	0.54	0.19	0.79	0.75	0.71
HCP–C2	0.14	0.78	0.72	0.62	0.26	0.59	0.56	0.49
HCP–C3	0.18	0.73	0.66	0.56	0.25	0.75	0.66	0.41

SE – Standard error of the regression, R2 – coefficient of determination, R^2adj – adjusted R^2; R^2p – predicted R^2

Table **2.7**: Backward elimination MLR models for dry and wet day surveys (p<0.05)

Dry Day	Wet Day
Multi-frequency EMI	
VCP-38kHz = -39.6 + 0.386 Sand + 0.510 Silt + 0.2210 **SMC**	VCP-38kHz = -74.8 + 0.793 Sand + 0.866 Silt + 0.2738 **SMC** - 0.3220 CEC + 14.75 EC_w
VCP-49kHz = -64.7 + 0.749 Sand + 1.034 Silt	VCP-49kHz = -46.04 + 0.6524 Sand + 0.713 Silt + 0.2313 **SMC** - 0.2085 CEC + 20.46 EC_w
HCP-38kHz = -87.3 + 0.893 Sand + 1.143 Silt	HCP-38kHz = -87.33 + 0.9434 Sand + 1.0665 Silt + 0.2259 **SMC** - 0.2779 CEC + 16.52 EC_w
HCP-49kHz = -57.2 + 0.646 Sand + 0.846 Silt	HCP-49kHz = -57.6 + 0.742 Sand + 0.837 Silt + 0.2063 **SMC** - 0.2051 CEC + 12.05 EC_w
Multi-coil EMI	
VCP-C2 = 7.543 - 0.0555 Sand	VCP-C2 = -78.95 + 0.852 Sand + 0.992 Silt + 0.2244 **SMC** - 0.2622 CEC + 12.73 EC_w
VCP-C3 = 4.35 - 0.0307 Sand + 0.0839 **SMC**	VCP-C3 = 1.233 + 0.0877 **SMC** + 6.78 EC_w
HCP-C2 = 2.329 + 0.0368 Silt + 0.0583 **SMC** + 1.077 EC_w	HCP-C2 = 2.374 + 0.1027 **SMC**
HCP-C3 = -24.97 + 0.2838 Sand + 0.3611 Silt + 1.396 EC_w	HCP-C3 = -28.42 + 0.317 Sand + 0.303 Silt + 0.1108 **SMC** + 10.62 EC_w

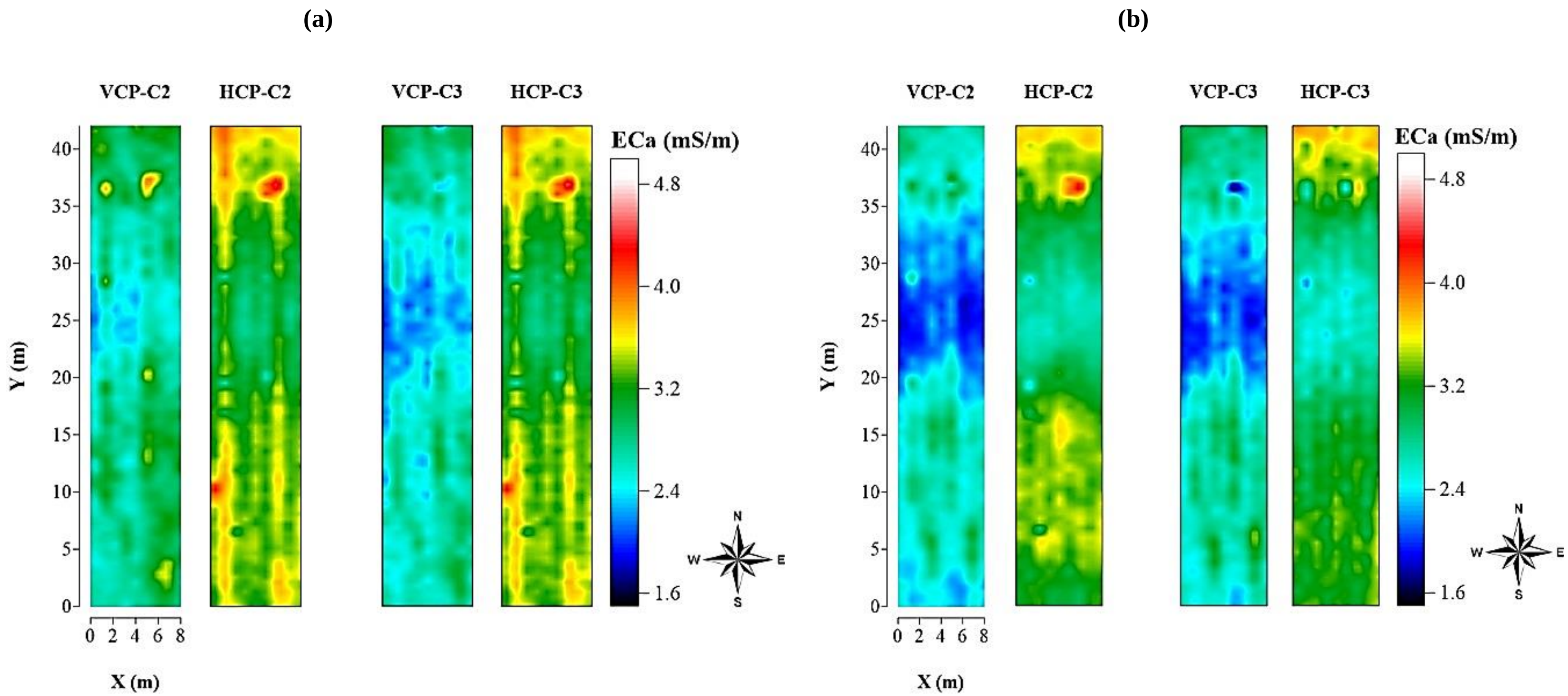

Figure **2.6**: Interpolated maps of EC_a using the multi-coil EMI sensor (a) dry day (b) wet day

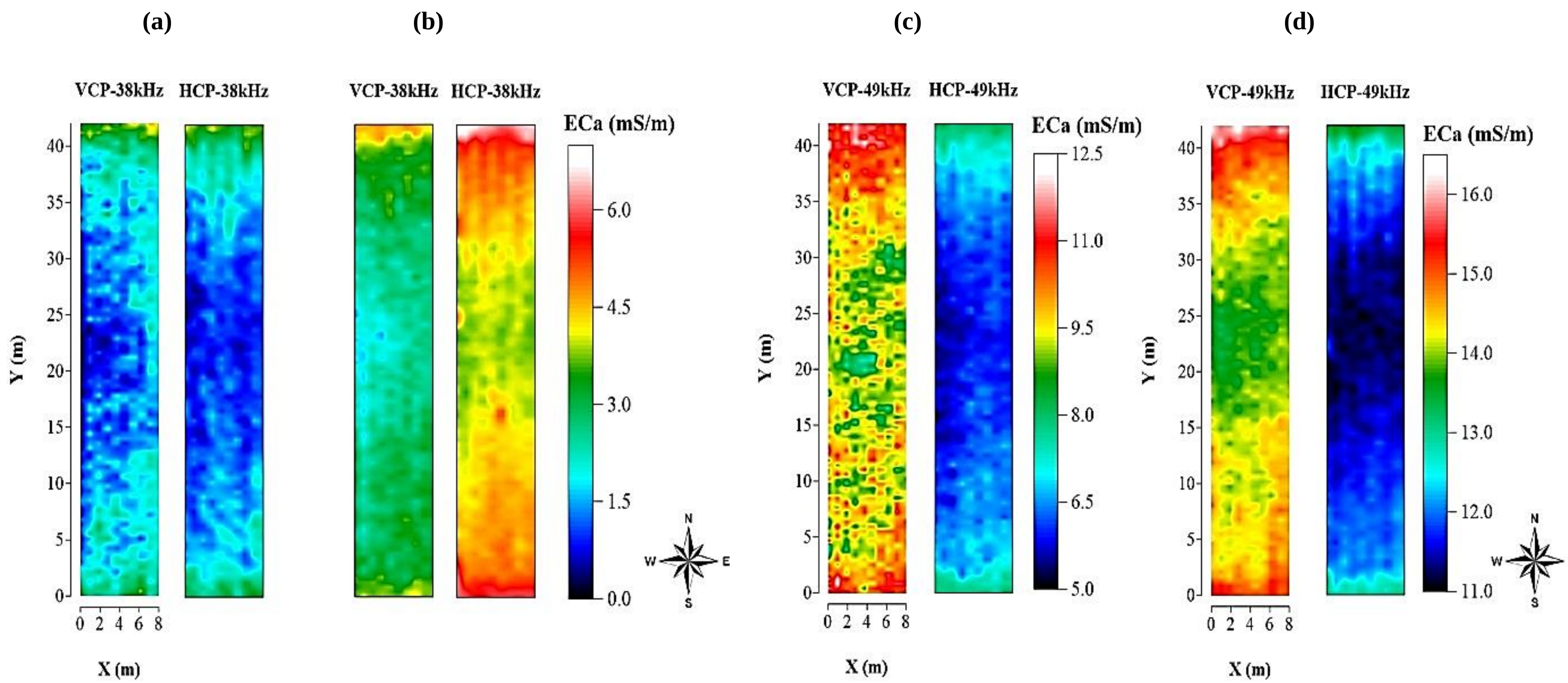

Figure **2.7**: Interpolated maps of EC_a using the multi-frequency EMI sensor: (a) dry day and (b) wet day with 38kHz frequency, (c) dry day and (d) wet day with 49kHz frequency

2.6. Conclusions

Geostatistical and multivariate statistical methods could establish optimal approaches to relate EC_a with relevant soil physiochemical properties. In this study, the EC_a interpolated maps showed the spatiotemporal variability of EC_a in the tested site. Both multi-coil and multi-frequency EMI sensors showed high spatial dependency on EC_a measurements. The EC_a values of both the multi-coil and the multi-frequency EMI sensors increase with increasing SMC of the field from the dry to wet day. The most significantly influenced factor of EC_a out of all other measured soil properties at the PBRS site is SMC. Not only the SMC, but also a few other soil properties (*i.e.* sand, silt, CEC, EC_w), significantly contributed to the EC_a variability.

The PCA clustered soil properties according to the EC_a surveys. The PCA and *r* showed only significant positive correlations between all EC_a measurements and soil properties (such as silt, SMC, and CEC) on either the dry or wet day surveys. Due to low clay content, silt influenced the EC_a measurements, and this influence was similar to the reports of clay's influence on EC_a, as cited in the literature. Based on the backward elimination of MLR models, the significantly influenced soil properties on measured EC_a from both EMI sensors are: sand, silt, SMC, CEC, and EC_w. Prediction accuracy of the MLR model increases when the soil is wet. The EC_a variability due to wet and dry conditions was successfully assessed for both EMI sensors.

The multi-frequency sensor is a more reliable instrument to characterize wet soils compared to dry soils, and it could explore deeper soil than the multi-coil EMI sensor. The VCP mode and high frequency (49 kHz) of the multi-frequency device are appropriate for soil investigation, while VCP−C3 and HCP−C2 are the more appropriate coil separations and orientations of the multi-coil sensor. The multi-coil device is a more suitable EMI sensor compared to the multi-frequency to investigate the spatiotemporal variability of EC_a as a proxy of shallow soil properties (agricultural soils) in western Newfoundland.

2.7. References

Adamchuk, V.I., Hummel, J.W., Morgan, M.T., Upadhyaya, S.K., 2004. On-the-go soil sensors for precision agriculture. Comput. Electron. Agric. 44, 71–91. https://doi.org/10.1016/j.compag.2004.03.002

Allred, B.J., 2011. Agricultural Geophysics: Past/Present Accomplishments and Future Advancements, in: The Second Global Workshop on Proximal Soil Sensing - Montreal 2011. Montreal, pp. 24–31.

Altdorff, D., Dietrich, P., 2014. Delineation of areas with different temporal behavior of soil properties at a landslide affected Alpine hillside using time-lapse electromagnetic data. Environ. Earth Sci. 72, 1357–1366. https://doi.org/10.1007/s12665-014-3240-7

Altdorff, D., Galagedara, L., Nadeem, M., Cheema, M., Unc, A., 2018. Effect of agronomic treatments on the accuracy of soil moisture mapping by electromagnetic induction. Catena 164, 96–106. https://doi.org/10.1016/j.catena.2017.12.036

Altdorff, D., Galagedara, L., Unc, A., 2017. Impact of projected land conversion on water balance of boreal soils in western newfoundland. J. Water Clim. Chang. 8, 613–626. https://doi.org/10.2166/wcc.2017.016

Altdorff, D., von Hebel, C., Borchard, N., van der Kruk, J., Bogena, H., Vereecken, H., Huisman, J.A., 2017. Potential of catchment-wide soil water content prediction using electromagnetic induction in a forest ecosystem. Environ. Earth Sci. 76, 111. https://doi.org/10.1007/s12665-016-6361-3

Archie, G.E., 1942. The Electrical Resistivity Log as an Aid in Determining Some Reservoir Characteristics. Trans. AIME 146, 54–62. https://doi.org/10.2118/942054-G

Arun, P. V, 2013. A comparative analysis of different DEM interpolation methods. Egypt. J. Remote Sens. Sp. Sci. 16, 133-139. https://doi.org/10.1016/j.ejrs.2013.09.001

Baroni, G., Ortuani, B., Facchi, A., Gandolfi, C., 2013. The role of vegetation and soil properties on the spatio-temporal variability of the surface soil moisture in a maize-cropped field. J. Hydrol. 489, 148–159. https://doi.org/10.1016/j.jhydrol.2013.03.007

Bonsall, J., Fry, R., Gaffney, C., Armit, I., Beck, A., Gaffney, V., 2013. Assessment of the CMD mini-explorer, a new low-frequency multi-coil electromagnetic device, for archaeological investigations. Archaeol. Prospect. 20, 219–231. https://doi.org/10.1002/arp.1458

Bouksila, F., Persson, M., Bahri, A., Berndtsson, R., 2012. Electromagnetic induction prediction of soil salinity and groundwater properties in a Tunisian Saharan oasis. Hydrol. Sci. J. 57, 1473–1486. https://doi.org/10.1080/02626667.2012.717701

Brevik, E.C., Fenton, T.E., 2004. The Effect of Changes in Bulk Density on Soil Electrical Conductivity as Measured with the Geonics EM-38. Soil Horizons 45, 96–102. https://doi.org/10.2136/sh2004.3.0096

Brevik, E.C., Fenton, T.E., Lazari, A., 2006. Soil electrical conductivity as a function of soil water content and implications for soil mapping. Precis. Agric. 7, 393–404. https://doi.org/10.1007/s11119-006-9021-x

Bronson, K.F., Booker, J.D., Officer, S.J., Lascano, R.J., Maas, S.J., Searcy, S.W., Booker, J., 2005. Apparent electrical conductivity, soil properties and spatial covariance in the U.S. Southern High Plains. Precis. Agric. 6, 297–311. https://doi.org/10.1007/s11119-005-1388-6

Buchanan, S., Triantafilis, J., 2009. Mapping water table depth using geophysical and environmental variables. Ground Water 47, 80–96. https://doi.org/10.1111/j.1745-6584.2008.00490.x

Chapman, H.D., 1965. Cation-Exchange Capacity, in: Black, C.A. (Ed.), Methods of Soil Analysis. Part 2. Chemical and Microbiological Properties. American Society of Agronomy, Soil Science Society of America, Madison, Wisconsin, pp. 891–900. https://doi.org/10.2134/agronmonogr9.2.c6

Corwin, D.L., 2005. Geospatial Measurements of Apparent Soil Electrical Conductivity for Characterizing Soil Spatial Variability, in: Soil-Water-Solute Process Characterization: An Integrated Approach. CRC Press, Boca Raton, FL, pp. 639–672. https://doi.org/10.1201/9781420032086.ch18

Corwin, D.L., Allred, B.J., 2008. Past, Present, and Future Trends of Soil Electrical Conductivity Measurement Using Geophysical Methods, in: Handbook of Agricultural Geophysics. CRC Press, Taylor & Francis Group, New York, pp. 17–44. https://doi.org/doi:10.1201/9781420019353.ch2

Corwin, D.L., Lesch, S.M., 2014. A simplified regional-scale electromagnetic induction - Salinity calibration model using ANOCOVA modeling techniques. Geoderma 230, 288–295. https://doi.org/10.1016/j.geoderma.2014.03.019

Corwin, D.L., Lesch, S.M., 2005a. Apparent soil electrical conductivity measurements in agriculture. Comput. Electron. Agric. 46, 11–43. https://doi.org/10.1016/j.compag.2004.10.005

Corwin, D.L., Lesch, S.M., 2005b. Characterizing soil spatial variability with apparent soil electrical conductivity: Part II. Case study. Comput. Electron. Agric. 46, 135–152. https://doi.org/10.1016/j.compag.2004.11.003

Corwin, D.L., Lesch, S.M., 2003. Application of Soil Electrical Conductivity to Precision Agriculture. Agron. J. 95, 455–471. https://doi.org/10.2134/agronj2003.0455

Corwin, D.L., Scudiero, E., 2016. Field-Scale Apparent Soil Electrical Conductivity, in: Logsdon, S. (Ed.) Methods of Soil Analysis. Soil Science Society of America, Madison, USA. https://doi.org/10.2136/methods-soil.2015.0038

De Caires, S.A., Wuddivira, M.N., Bekele, I., 2015. Spatial analysis for management zone delineation in a humid tropic cocoa plantation. Precis. Agric. 16, 129–147. https://doi.org/10.1007/s11119-014-9366-5

De Smedt, P., Van Meirvenne, M., Herremans, D., De Reu, J., Saey, T., Meerschman, E., Crombé, P., De Clercq, W., 2013. The 3-D reconstruction of medieval wetland reclamation through electromagnetic induction survey. Sci. Rep. 3, 1–5. https://doi.org/10.1038/srep01517

Domsch, H., Giebel, A., 2004. Estimation of soil textural features from soil electrical conductivity recorded using the EM38. Precis. Agric. 5, 389–409. https://doi.org/10.1023/B:PRAG.0000040807.18932.80

Doolittle, J.A., Brevik, E.C., 2014. The use of electromagnetic induction techniques in soil studies. Geoderma 223, 33–45. https://doi.org/10.1016/j.geoderma.2014.01.027

Doolittle, J.A., Noble, C., Leinard, B., 2000. An Electromagnetic Induction Survey of a Riparian Area in southwest Montana. Soil Surv. horizons 41, 27–36. https://doi.org/10.1520/D0850-11.1

Farooque, A.A., Zaman, Q.U., Schumann, A.W., Madani, A., Percival, D.C., 2012. Delineating Management Zones for Site Specific Fertilization in Wild Blueberry Fields. Appl. Eng. Agric. 28, 57–70.

Friedman, S.P., 2005. Soil properties influencing apparent electrical conductivity: A review. Comput. Electron. Agric. 46, 45–70 https://doi.org/10.1016/j.compag.2004.11.001

Gregorich, E.G., Carter, M.R., 2007. Soil Sampling and Methods of Analysis, Second. ed. CRC Press.

Hall, L.M., Brainard, J.R., Bowman, R.S., Hendrickx, J.M.H., 2004. Determination of Solute Distributions in the Vadose Zone Using Downhole Electromagnetic Induction. Vadose Zo. J. 3, 1207–1214. https://doi.org/10.2136/vzj2004.1207

Hao, X., Ball, B.C., Culley, J.L.B., Carter, M.R., Parkin, G.W., 2007. Soil Density and Porosity, in: Gregorich, E.G., Carter, M.R. (Eds.), Soil Sampling and Methods of Analysis. CRC Press, pp. 743–759.

Heil, K., Schmidhalter, U., 2017. The application of EM38: Determination of soil parameters, selection of soil sampling points and use in agriculture and archaeology. Sensors (Switzerland) 17, 2540. https://doi.org/10.3390/s17112540

Heiniger, R.W., McBride, M.B., Clay, D.E., 2003. Using soil electrical conductivity to improve nutrient management. Agron. J. 95, 508–519.

Hendershot, W.H., Lalande, H., Duquette, M., 2007. Soil Reaction and Exchangeable Acidity, in: Gregorich, E.G., Carter, M.R. (Eds.), Soil Sampling and Methods of Analysis. CRC Press, pp. 173–178.

Huang, J., Purushothaman, R., McBratney, A., Bramley, H., 2018. Soil Water Extraction Monitored Per Plot Across a Field Experiment Using Repeated Electromagnetic Induction Surveys. Soil Syst. 2, 11. https://doi.org/10.3390/soilsystems2010011

Huang, J., Scudiero, E., Choo, H., Corwin, D.L., Triantafilis, J., 2016. Mapping soil moisture across an irrigated field using electromagnetic conductivity imaging. Agric. Water Manag. 163, 285–294. https://doi.org/10.1016/j.agwat.2015.09.003

Huang, J., Subasinghe, R., Malik, R.S., Triantafilis, J., 2015. Salinity hazard and risk mapping of point source salinisation using proximally sensed electromagnetic instruments. Comput. Electron. Agric. 113, 213–224. https://doi.org/10.1016/j.compag.2015.02.013

Jolliffe, I.T., 2002. Principal Component Analysis, Second Edi. ed. Springer-Verlag, New York.

Journel, A.G., Huijbregts, C.J., 1978. Mining Geostatistics. Academic Press, London.

Kachanoski, R.G., Gregorich, E.G., Wesenbeeck, I.J. VAN, 1988. Estimating Spatial Variations of Soil Water Content Using Noncontacting Electromagnetic Inductive Methods. Can. J. Soil Sci. 68, 715–722.

Kaffka, S.R., Lesch, S.M., Bali, K.M., Corwin, D.L., 2005. Site-specific management in salt-affected sugar beet fields using electromagnetic induction. Comput. Electron. Agric. 46, 329–350. https://doi.org/10.1016/j.compag.2004.11.013

Khan, F.S., Zaman, Q.U., Chang, Y.K., Farooque, A.A., Schumann, A.W., Madani, A., 2016. Estimation of the rootzone depth above a gravel layer (in wild blueberry fields) using electromagnetic induction method. Precis. Agric. 17, 155–167. https://doi.org/10.1007/s11119-015-9413-x

Kirby, G.E., 1988. Soils of the Pasadena-Deer Lake area, Newfoundland [WWW Document]. URL http://sis.agr.gc.ca/cansis/publications/surveys/nf/nf17/nf17_report.pdf (accessed 11.8.17).

Korres, W., Koyama, C.N., Fiener, P., Schneider, K., 2010. Analysis of surface soil moisture patterns in agricultural landscapes using Empirical Orthogonal Functions. Hydrol. Earth Syst. Sci. 14, 751–764. https://doi.org/10.5194/hess-14-751-2010

Korsaeth, A., 2005. Soil apparent electrical conductivity (ECa) as a means of monitoring changesin soil inorganic N on heterogeneous morainic soils in SE Norway during two growing seasons. Nutr. Cycl. Agroecosystems 72, 213–227. https://doi.org/10.1007/s10705-005-1668-6

Kroetsch, D., Wang, C., 2007. Particle Size Distribution, in: Gregorich, E.G., Carter, M.R. (Eds.), Soil Sampling and Methods of Analysis. CRC Press, pp. 713–726.

Li, J., Heap, A.D., 2014. Spatial interpolation methods applied in the environmental sciences: A review. Environ. Model. Softw. 53, 173–189. https://doi.org/10.1016/j.envsoft.2013.12.008

Lobsey, C.R., Rossel, R.A. V, McBratney, A.B., 2010. Proximal Soil Nutrient Sensing Using Electrochemical Sensors, in: Proximal Soil Sensing. Springer, Dordrecht, pp. 77–88. https://doi.org/10.1007/978-90-481-8859-8

MacCormack, K., Arnaud, E., Parker, B.L., 2017. Using a Multiple Variogram Approach to Improve the Accuracy of Subsurface Geological Models. Can. J. Earth Sci. 55, 786–801. https://doi.org/10.1139/cjes-2016-0112

Mahmood, H.S., Hoogmoed, W.B., van Henten, E.J., 2012. Sensor data fusion to predict multiple soil properties. Precis. Agric. 13, 628–645. https://doi.org/10.1007/s11119-012-9280-7

Martini, E., Wollschläger, U., Musolff, A., Werban, U., Zacharias, S., 2017. Principal Component Analysis of the Spatiotemporal Pattern of Soil Moisture and Apparent Electrical Conductivity. Vadose Zo. J. 16, 1–12. https://doi.org/10.2136/vzj2016.12.0129

McNeill, J.D., Bosnar, M., 1999. Application of dipole–dipole electromagnetic systems for geological depth sounding, Technical Note TN-31. Mississauga, ON.

Miller, J.J., Curtin, D., 2007. Electrical Conductivity and Soluble Ions, in: Gregorich, E.G., Carter, M.R. (Eds.), Soil Sampling and Methods of Analysis. CRC Press, pp. 161–172.

Misra, R.K., Padhi, J., 2014. Assessing field-scale soil water distribution with electromagnetic induction method. J. Hydrol. 516, 200–209. https://doi.org/10.1016/j.jhydrol.2014.02.049

Moral, F.J., Terrón, J.M., Silva, J.R.M. da, 2010. Delineation of management zones using mobile measurements of soil apparent electrical conductivity and multivariate geostatistical techniques. Soil Tillage Res. 106, 335–343. https://doi.org/10.1016/j.still.2009.12.002

Nayanaka, V.G.D., Vitharana, W.A.U., Mapa, R.B., 2011. Geostatistical Analysis of Soil Properties to Support Spatial Sampling in a Paddy Growing Alfisol. Trop. Agric. Res. 22, 34–44. https://doi.org/10.4038/tar.v22i1.2668

Oliver, M.A., Webster, R., 2015. Basic Steps in Geostatistics: The Variogram and Kriging. SpringerBriefs in Agriculture, Landon.

Pedrera-Parrilla, A., Brevik, E.C., Giráldez, J. V, Vanderlinden, K., 2016a. Temporal stability of electrical conductivity in a sandy soil. Int. Agrophysics 30, 349–357. https://doi.org/10.1515/intag-2016-0005

Pedrera-Parrilla, A., Brevik, E.C., Vijver, E. Van De, Espejo, A.J., Taguas, E. V, Giráldez, J. V, Martos, S., Vanderlinden, K., 2015. Effects of different topsoil properties on apparent electrical conductivity under varying soil water contents. Estud. en la Zo. No Saturada 12, 25–32.

Pedrera-Parrilla, A., Van De Vijver, E., Van Meirvenne, M., Espejo-Pérez, A.J., Giráldez, J. V, Vanderlinden, K., 2016b. Apparent electrical conductivity measurements in an olive orchard under wet and dry soil conditions: significance for clay and soil water content mapping. Precis. Agric. 17, 531–545.

https://doi.org/10.1007/s11119-016-9435-z

Priori, S., Martini, E., Andrenelli, M.C., Magini, S., Agnelli, A.E., Bucelli, P., Biagi, M., Pellegrini, S., Costantini, E.A.C., 2013. Improving Wine Quality through Harvest Zoning and Combined Use of Remote and Soil Proximal Sensing. Soil Sci. Soc. Am. J. 77, 1338–1348. https://doi.org/10.2136/sssaj2012.0376

Rodrigues, F.A., Bramley, R.G. V, Gobbett, D.L., 2015. Proximal soil sensing for Precision Agriculture: Simultaneous use of electromagnetic induction and gamma radiometrics in contrasting soils. Geoderma 243, 183–195. https://doi.org/10.1016/j.geoderma.2015.01.004

Ruser, R., Gerl, G., Kainz, M., Ebertseder, T., Reents, H.J., Schmid, H., Munch, J.C., Gutser, R., 2008. Management of Heterogeneous Systems, in: Schröder, P., Pfadenhauer, J., Munch, J.C. (Eds.), Perspectives for Agroecosystem Management : Balancing Environmental and Socio-Economic Demands. Elsevier B.V., pp. 41–200.

Schumann, A.W., Zaman, Q.U., 2003. Mapping water table depth by electromagnetic induction. Appl. Eng. Agric. 19, 675–688. https://doi.org/10.13031/2013.15663

Scudiero, E., Corwin, D.L., Wienhold, B.J., Bosley, B., Shanahan, J.F., Johnson, C.K., 2016. Downscaling Landsat 7 canopy reflectance employing a multi-soil sensor platform. Precis. Agric. 17, 53–73. https://doi.org/10.1007/s11119-015-9406-9

Serrano, J., Shahidian, S., da Silva, J.M., 2014. Spatial and temporal patterns of apparent electrical conductivity: DUALEM vs. Veris sensors for monitoring soil properties. Sensors (Switzerland) 14, 10024–10041. https://doi.org/10.3390/s140610024

Serrano, J.M., Shahidian, S., da Silva, J.R.M., 2013. Apparent electrical conductivity in dry versus wet soil conditions in a shallow soil. Precis. Agric. 14, 99–114. https://doi.org/10.1007/s11119-012-9281-6

Shahid, S.A., Abdelfattah, M.A., Taha, F.K., 2013. Developments in Soil Salinity Assessment and Reclamation: Innovative Thinking and Use of Marginal Soil and Water Resources in Irrigated Agriculture. Springer Science+Business Media, Dordrecht.

Sheets, K.R., Hendrickx, J.M.H., 1995. Noninvasive soil water content measurement using electromagnetic induction. Water Resour. Res. 31, 2401–2409.

Simon, F.X., Sarris, A., Thiesson, J., Tabbagh, A., 2015. Mapping of quadrature magnetic susceptibility/magnetic viscosity of soils by using multi-frequency EMI. J. Appl. Geophys. 120, 36–47. https://doi.org/10.1016/j.jappgeo.2015.06.007

Smith, C.A.S., Webb, K.T., Kenney, E., Anderson, A., Kroetsch, D., 2011. Brunisolic Soils of Canada: Genesis, ditribution and classification. Can. J. Soil Sci. 91, 695–717. https://doi.org/10.4141/cjss10024

Sudduth, K.A., Kitchen, N.R., Wiebold, W.J., Batchelor, W.D., Bollero, G.A., Bullock, D.G., Clay, D.E., Palm, H.L., Pierce, F.J., Schuler, R.T., Thelen, K.D., 2005. Relating apparent electrical conductivity to soil properties across the north-central USA. Comput. Electron. Agric. 46, 263–283. https://doi.org/10.1016/j.compag.2004.11.010

Tang, P., Chen, F., Jiang, A., Zhou, W., Wang, H., Leucci, G., de Giorgi, L., Sileo, M., Luo, R., Lasaponara, R., Masini, N., 2018. Multi-frequency Electromagnetic Induction Survey for Archaeological Prospection: Approach and Results in Han

Hangu Pass and Xishan Yang in China. Surv. Geophys. 1–18. https://doi.org/10.1007/s10712-018-9471-5

Taylor, J.A., Short, M., McBratney, A.B., Wilson, J., 2010. Comparing the Ability of Multiple Soil Sensors to Predict Soil Properties in a Scottish Potato Production System, in: Proximal Soil Sensing. Springer Netherlands, Dordrecht, pp. 387–396. https://doi.org/10.1007/978-90-481-8859-8_33

Thiesson, J., Tabbagh, A., Simon, F.X., Dabas, M., 2017. 3D linear inversion of magnetic susceptibility data acquired by frequency domain EMI. J. Appl. Geophys. 136, 165–177. https://doi.org/10.1016/j.jappgeo.2016.10.038

Topp, G.C., Parkin, G.W., Ferre, T.P.A., 2007. Soil Water Content, in: Gregorich, E.G., Carter, M.R. (Eds.), Soil Sampling and Methods of Analysis. CRC Press, pp. 939–961.

Vitharana, U.W.A., Van Meirvenne, M., Cockx, L., Bourgeois, J., 2006. Identifying potential management zones in a layered soil using several sources of ancillary information. Soil Use Manag. 22, 405–413. https://doi.org/10.1111/j.1475-2743.2006.00052.x

Waine, T.W., Blackmore, B.S., Godwin, R.J., 2000. Mapping available water content and estimating soil textural class using electro-magnetic induction, in: EurAgEng. Warwick.

Waqar, A., 2018. Evaluating the potential of biochar in mitigating greenhouse gases emission and nitrogen retention in dairy manure based silage corn cropping systems. Memorial University of Newfoundland.

Watson, H.D., Neely, H.L., Morgan, C.L.S., McInnes, K.J., Molling, C.C., 2017. Identifying subsoil variation associated with gilgai using electromagnetic induction. Geoderma 295, 34–40. https://doi.org/10.1016/j.geoderma.2017.01.029

Williams, B.G., Baker, G.C., 1982. An electromagnetic induction technique for reconnaissance surveys of soil salinity hazards. Aust. J. Soil Res. 20, 107–118. https://doi.org/10.1071/SR9820107

Zhu, Q., Lin, H., Doolittle, J.A., 2010. Repeated Electromagnetic Induction Surveys for Improved Soil Mapping in an Agricultural Landscape. Soil Water Manag. Conserv. 74, 1763–1774. https://doi.org/10.2136/sssaj2010.0056

Zhu, Q., Lin, H.S., 2010. Comparing ordinary kriging and regression kriging for soil properties in contrasting landscapes. Pedosphere 20, 594–606. https://doi.org/10.1016/S1002-0160(10)60049-5

Zungalia, E.J., Tuck, F.C., Spariosu, D.J., 1989. Geophysical Investigations of a Ground Water Contaminant Plume-Electrical and Electromagnetic Methods, in: Hatcher, K.J. (Ed.), Georgia Water Resources Conference. Institute of Natural Resources, The University of Georgia, Georgia, pp. 165–168.

Chapter 3: Investigating the Depth Sensitivity of Multi-Coil and Multi-Frequency Electromagnetic Induction Methods Using Small Buried Targets in Shallow Soils

3.1. Co-authorship Statement

Chapter 3 is on "*Investigating the Depth Sensitivity of Multi-Coil and Multi-Frequency Electromagnetic Induction Methods Using Small Buried Targets in Shallow Soils*" has been prepared for submission to Journal of Applied Geophysics (Sadatcharam, K., Unc, A., Krishnapillai, M. and Galagedara, L., 2018). Kamaleswaran Sadatcharam, the thesis author was the primary author and Dr. Galagedara (supervisor), was the corresponding and the fourth author. Dr. Unc (co-supervisor) and Dr. Krishnapillai (committee member) were second and third authors, respectively. All authors were part of the same research project on "*Hydrogeophysical Characterization of Agricultural Fields in Western Newfoundland using Integrated GPR-EMI*", which was led by Dr. Galagedara. For the work in Chapter 3, the overall research strategy was developed by Dr. Galagedara with input from all members of the group. Mr. Sadatcharam was responsible for the specific methodology, data collection, analysis, and interpretation and writing of the manuscript. Dr. Unc and Dr. Krishnapillai provided inputs for the field experiment, data interpretation, and manuscript editing. Dr. Galagedara as the project lead and the main supervisor provided research plans and guidance for the entire process.

3.2. Abstract

Knowledge about the depth sensitivity (DS) of apparent electric conductivity (EC_a) and apparent magnetic susceptibility (MS_a) recorded by electromagnetic induction (EMI) is essential for shallow soil investigations. As EC_a is commonly the established value and its DS function widely accepted, investigations about the DS of MS_a are less prominent in literature. MS_a is a desirable property to investigate DS of EMI if using buried targets of known depths and conductivities. However, the sign-changing behavior of some MS_a measurements of horizontal coplanar (HCP) coil orientation is a matter of debate among researchers. The theoretical DS models of EMI are also complicated to interpret with field measurements. Therefore, I investigated the DS of EMI instruments using small buried targets and assessed it with theoretical DS models. Also, the DS of EMI was evaluated with integrated EMI and ground penetrating radar analyses. A small plot experiment over a 4 x 15 m^2 area was carried out in a sandy loam soil in western Newfoundland. Materials of different conductivities (4-metal and 4-plastic targets) were buried at eight distinct locations within a 30 to 80 cm depth range. Three coil separations (32, 71, and 118 cm) from the multi-coil EMI sensor were used in two coil orientations: vertical coplanar (VCP) and HCP for the multi-coil EMI surveys. Simultaneously, four factory-calibrated frequencies (18, 38, 49, and 80 kHz) and both coil orientations were used for measuring MS_a (in ppt) using the multi-frequency EMI probe. High-resolution ordinary block kriging-interpolated maps were created using absolute deviation of the measured MS_a from the background data to identify anomalies from the buried targets. The multi-coil device clearly detected all of the four metal targets from three coil separations in both coil orientations. Only three of the metal targets were identified from the multi-frequency EMI data with

weak anomalies. HCP operations produced stronger anomalies compared to VCP, in both sensors. A guideline was developed to understand and evaluate the negative MS_a value of HCP of multi-coil EMI with the theoretical DS models. The multi-coil EMI sensor shows better accuracy predicting the depth of targets than the multi-frequency in the shallow soils of the tested field in western Newfoundland.

Keywords: apparent magnetic susceptibility, depth sensitivity, electromagnetic induction (EMI), horizontal coplanar (HCP), metal targets

3.3. Introduction

Understanding the near-surface characterization of soil is an essential requirement for shallow soil studies and agricultural activities (Hubbard and Linde, 2011; Moghadas et al., 2010). Shallow soils are highly heterogeneous, and their properties and processes are intricate to interpret (Boaga, 2017). Integrated use of geophysical instruments, such as electromagnetic induction (EMI) sensors and ground penetrating radar (GPR), can provide more detailed information on shallow soils (Corwin, 2005; Drive, 2007; Kadiolu and Daniels, 2008; Moghadas et al., 2010; Rubin and Hubbard, 2005; Saey et al., 2014). One of the particular applications of these methods is to detect buried metallic and non-metallic targets in shallow soils (Allred et al., 2004). This method provides target depths (depth sensitivity) in order to locate the targets below the ground surface.

EMI is commonly used for obtaining the apparent electrical conductivity (EC_a) of soil (Corwin, 2005; McNeill, 1980). Further, it can be used to characterize rapid apparent magnetic susceptibility (MS_a) variations across the field (Barrowes and Douglas, 2016; Benech et al., 2016; Bongiovanni et al., 2008; Simpson et al., 2009).

Similar to EC_a, MS_a can be affected by several parameters, such as soil/sediment layers, amount of air, water, stone, metal and pottery fragments in soils (Dalan and Banerjee, 1998; Simon and Moffat, 2015). In particular, MS_a is responsive to highly conductive objects, such as metals, but less sensitive to small changes in bulk conductivity (Barrowes and Douglas, 2016). For instance, larger nonmetallic targets could be detected by MS_a due to the contrasts between the non-metallic targets and the host medium (Huang et al., 2003).

There are two different types of EMI instruments that can deal with the depth resolution of the integral signals: multi-coil and multi-frequency. The multi-coil EMI sensors are comprised of various coil separations (one transmitter and few receivers) and were used to explore different depth layers in the soil profile (Altdorff et al., 2016; De Smedt et al., 2013; Keiswetter and Won, 1997). Likewise, multi-frequency EMI sensors could, in general, explore depth layers (Boaga, 2017; Tang et al., 2018) while operating with different frequencies. However, the success of both operating methods is highly test-site and target related. Generally, higher frequencies provide shallow penetrations and lower frequencies provide deeper penetrations (Allred et al., 2005; Keiswetter and Won, 1997; Tang et al., 2018; Witten et al., 2000). There are some basic conditions that should be satisfied for EMI sensors to detect a target, namely: primary electromagnetic (EM) fields should induce a current in the target; in case of resistive targets, the induced current flows around the targets; EM properties should be different between the target and its surroundings; the anomalous responses from the EMI sensors must be larger than the noise signals received (Fitterman and Labson, 2005).

In general, GPR is able to provide high-resolution subsurface images and more accurate DS compared to EMI at a field scale (Fitterman and Labson, 2005). The depth of the buried target can be estimated by manually fitting the hyperbola in a GPR data processing software (Annan, 2003; Huisman et al., 2003; Jol, 2009). Integrated use of EMI–GPR can differentiate metallic and non-metallic targets in the sub-surface (Kadiolu and Daniels, 2008).

Depth sensitivity (depth of investigation) models of EMI sensors depend on the inter-coil separation (ICS) and coil orientations under a low induction number (McNeill, 1980; Saey et al., 2015) as well on the employed frequencies (Bongiovanni et al., 2008; Keiswetter and Won, 1997; Noh et al., 2016). The interpretation of MS_a , however, is more complex, because some parts of the horizontal coplanar (HCP) responses show a switch of the algebraic sign from positive to negative values – “sign-changing” (Benech et al., 2016; Noh et al., 2016; Saey et al., 2013; Simpson et al., 2010, 2009; Thiesson et al., 2011) or else, values less than the background MS_a of the EMI survey. This complexity depends on the depth of the buried targets. The HCP mode of operation is less sensitive for MS_a than the vertical coplanar (VCP) mode (Saey et al., 2013; Simpson et al., 2009).

Apparent magnetic susceptibility (MS_a) generates different DS responses than EC_a, and its use is constrained to shallow soil (Linford, 1998; Simpson et al., 2010, 2009). Hence, the amount of MS_a related field studies is limited. Moreover, the accuracy of soil DS is related to the sensors used and is still under discussion. Accurate predictions of DS for the multi-frequency EMIs are not fully achievable yet (Badewa et al., 2018). Furthermore, ‘skin depth’ leads to overestimation or underestimation of the DS of multi-frequency EMI sensors (Bongiovanni et al., 2008).

Theoretical DS models of MS_a and their applications are rarely noticed in previous research. (Bevan and Rinita, 2003; Dalan, 2008; Delefortrie et al., 2018; Simpson et al., 2010). However, many studies recognized the negative values of MS_a measurements from the HCP coil orientation. For example: Sasaki et al. (2010) found that the shallowest target may contain negative MS_a values for lower frequencies (<10 kHz) using multi-frequency EMI sensors. Two similar studies suggested the negative MS_a anomalies can be used as an indicator to identify shallow underground targets using a HCP-1m coil orientation of the DUALEM-21S (Simpson et al., 2010) and the EM38 (Santos and Porsani, 2011). Simon et al. (2014) suggested that the HCP mode of operation may produce negative MS_a from shallow soil layers. Noh et al. (2016) found the negative values produced by shorter offsets (<2 m) of the HCP mode were generated in the near surface due to the effect of a downward polarization of the magnetic targets. However, the problem with negative MS_a from the HCP coil orientation is not fully addressed yet. Therefore, the issue of negative measurements of MS_a could be evaluated with theoretical DS models and field data.

DS could be used as an assessing tool to measure the capability of EMI sensors regarding sampling depth accuracy (Boaga, 2017). The DS of such instruments in shallow soils, for example in agricultural soils, need to be evaluated for particular soils and their conditions (Saey et al., 2016). Here, I hypothesized that the DS of EMI sensors in shallow soils could be evaluated by assessing the performance of EMI and GPR to detect small buried targets of known conductivity.

3.4. Materials and Methodology

3.4.1 Study Area

The research was conducted at the Pynn's Brook Research Station (PBRS), managed by the Department of Fisheries and Land Resources, of the Government of Newfoundland and Labrador, Canada. The PBRS is located (49°04'23"N, 57°33'39"W) in the Humber Valley Watershed in the western part of the island of Newfoundland (Figure **3.1**). Sandy fluvial and Glacio-fluvial deposits are spread dominantly over very gentle slope of the research site (Kirby, 1988). The soil texture in the top 15 cm soil layer showed sandy loam to loamy fine sand soils: sand 73.2% (± 5.2), silt 20.8% (± 4.6), and clay 6.0% (± 1.2).

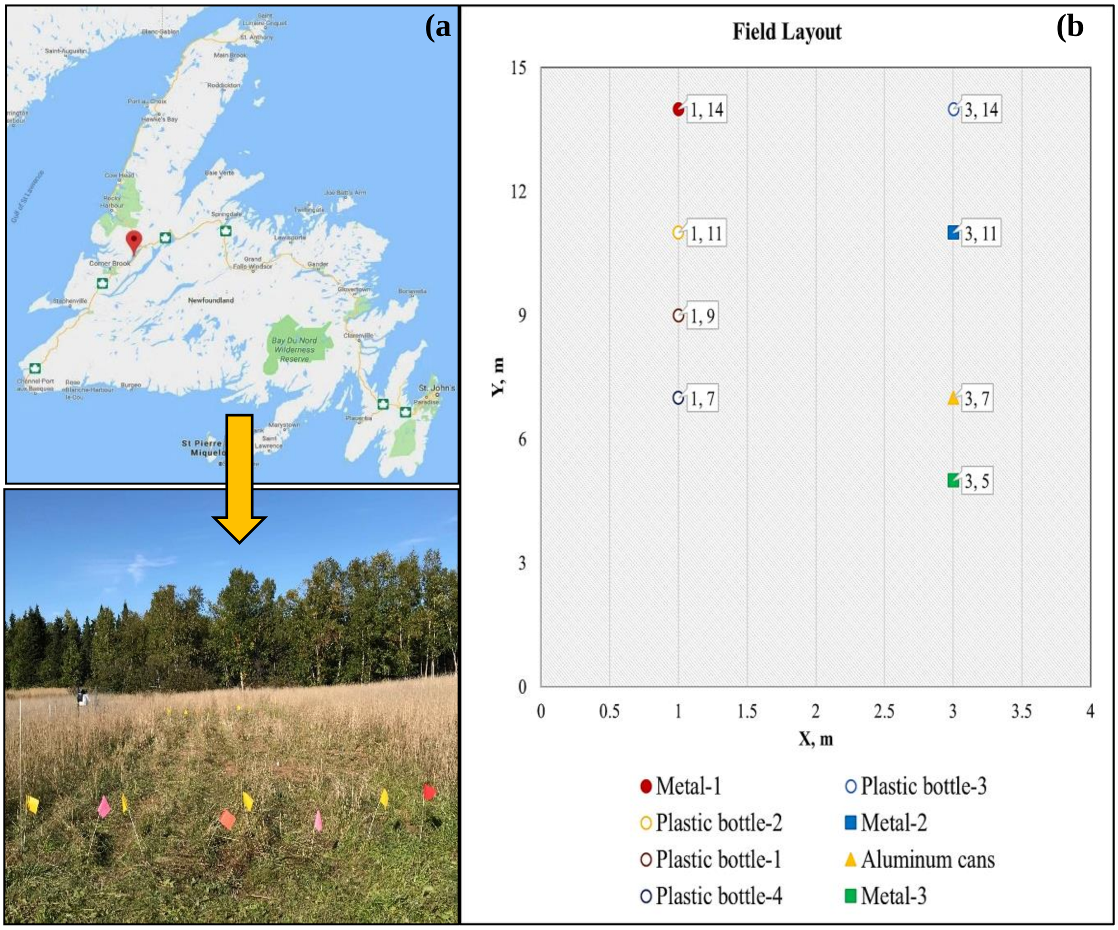

Figure **3.1**: Study location of the research field at PBRS (a), experiment layout with buried targets and coordinates (b).

3.4.2 Experimental Plot

An experimental plot (Figure **3.1**b) was selected and marked in a grass field of the PBRS on September 22, 2017. The following materials were selected and randomly buried: hollow metal pieces, beverage Aluminum cans filled with salt water, and plastic bottles filled with salt water and tap water, as shown in following Table 3.1.

Table 3.1: Information of buried targets

Buried Targets	**Buried depth (cm)**	**x, y Coordinate (m, m)**	**Size of the targets**	**Other details**
Plastic bottles – 1	30	1, 9	2 L	Tap water
Plastic bottles – 2	30	1, 11	2 L	12 mS/m
Metal – 1	35	1, 14	Ø 18 x 30 cm^3	Cylindrical
Metal – 2	40	3, 11	30 x 15 x 10 cm^3	Rectangular
Aluminum cans	45	3, 7	473 mL x 8	9 mS/m
Plastic bottles – 3	45	3, 14	3 L & 2 L	3 mS/m
Plastic bottles – 4	50	1, 7	710 mL x 3	9 mS/m
Metal – 3	80	3, 5	30 x 15 x 10 cm^3	Rectangular

3.4.3 Multi-coil EMI Sensor

The multi-coil EMI probe operates at a fixed frequency of 30 kHz with three coil separations. The instrument has one transmitter coil (Tx) and three receiver coils (Rx) with fixed offsets of 0.32 m, 0.71 m, and 1.18 m. Operating sensor height is approximately 20 cm from the ground surface (Altdorff et al., 2018) in order to maximize the depth of exploration. The sensor is well adapted to outside temperatures between -10℃ and +50℃ and the temperature stability is ±1 mS/m per 10℃ change in temperature (GF-Instruments, 2011). The multi-coil EMI surveys were done in one direction (individual parallel transects) over the experimental plot.

3.4.4 Multi-frequency EMI Sensor

The multi-frequency EMI sensor is a handheld, digital, and broadband electromagnetic sensor. A fixed coil separation between Tx and Rx is 1.67 m and there is a bucking coil at ~1m from Tx to cut off the primary field from the Rx (Minsley et al., 2012; Simon et al., 2015). Typically, frequencies have to be specified and selected by users. Up to ten frequencies can be used simultaneously. However, since the power provided by the internal battery is distributed equally among the selected frequencies, the strength of each frequency signal is reduced as more frequencies are selected, consequently lowering the resolution. Free-air calibration (or 'zero') and amplitude calibration have been done at the factory and stored in the multi-frequency sensor software. Three factory-calibrated frequencies were selected for the multi-frequency EMI surveys. An approximately 1 m sensor height was maintained for the bi-directional surveys. All grid lines were parallel to each other.

3.4.5 Electromagnetic Induction Surveys

All EMI surveys were carried with line spacing of 0.5 m in order to develop high-resolution MS_a maps. Three EMI survey sets were completed using both instruments. The first survey (Survey-1) was on September 22, 2017, before burying the targets; the second survey (Survey-2) was on September 22, 2017, after burying the targets; and the third survey (Survey-3) was on October 03, 2017. The MS_a were measured by both the VCP and HCP coil orientations of both instruments. Both instruments were warmed up for approximately 20–30 min at the beginning of all EMI surveys, as suggested by several authors (Altdorff et al., 2018; Santos and Porsani, 2011; Von Hebel et al., 2014).

The MS_a measurements from 0 m to 4 m distance on the Y-axis, where the undisturbed soil was present, were used to estimate background means in order to compare with the buried areas' data. Interpolated MS_a absolute deviation maps were created using absolute deviation for each data point from the background mean. Table **3.3** shows the number of data used for the calculation and the background means. The ordinary block kriging interpolating technique was used to create maps using Surfer11 (Golden Software Inc., USA) that illustrate clear observation of buried targets. Only MS_a measurements of HCP_{C3} were different from other coil separations of the multi-coil sensor. Therefore, the raw MS_a map is shown for the stated situation for more detailed interpretations of HCP_{C3}.

3.4.6 GPR Survey

A parallel study was carried out using different GPR frequencies by another graduate student at the same research field. Some of those GPR measurements were taken as supporting data for EMI interpretation in my study. Six GPR grid surveys were carried out using 250, 500, and 1000 MHz center frequency transducers of the PulseEKKO Pro GPR system (Sensors and Software Inc., Canada). Each grid survey contains nine GPR transects which were coincided with EMI grid lines. The data processing was done using the corresponding software. Reflection from a sub-surface point reflector (*i.e.* buried target) could trace out a hyperbola in a GPR radargram. The shape of the hyperbola is influenced by the depth and material of the target and the matrix (Maas and Schmalzl, 2013). Depth to the buried targets was estimated by manually fitting the corresponding hyperbolas. The estimated depth and the actual depth were compared in fitted line plots of a regression analysis.

3.4.7 Depth Sensitivity of EMI

Multi-coil and multi-frequency EMI sensors can be used to characterize detail for vertical layering (Saey et al., 2012). The depth sensitivity varies like geometrically or frequency soundings by changing ICS or frequencies, respectively. Generally, 'skin depth' is a standard measure for depth sensitivity of frequency sounding EMI sensors. The skin depth (δ) is the depth where the primary EM wave is attenuated by a factor of 1/e, or to about 37% of the original amplitude (Spies, 1989). However, when conditions are less than ideal, skin depth underestimates the DS of the EMI data, and overestimates in environmentally noisy or geologically complex areas (Bongiovanni et al., 2008; Huang, 2005).

$$\delta = \sqrt{\frac{1}{\sigma\mu\pi f}} \qquad \text{Eq. 3.1}$$

where σ is the conductivity of the medium, μ is the magnetic permeability, and f is a frequency of the primary EM wave.

The theoretical DS models were developed for relative response (RR) and cumulative response (CR) of the induced signals (secondary field) of the EMI sensors (McNeill, 1980). The relative response (RR) describes the contribution of an induced signal from a thin layer at different depths, and the cumulative response (CR) is the volume of integration between a certain depth and infinite depth. These models have different equations for quadrature (EC_a) component (McNeill, 1980; Saey et al., 2015; Wait, 1962) and in-phase (MS_a) component (Keller and Frischknecht, 1966; Simpson et al., 2009) of induced responses.

The EC_a – DS models are more popular than MS_a because of the sign-changes on the HCP coil orientation and ensuing difficult interpretations of the MS_a depth response model. Some researchers have used the same equation of the EC_a depth model for the MS_a depth model (Santos and Porsani, 2011). Effective depth measurements (effective DS) of most of the EMI instruments follow geometry-sounding techniques. The effective depth determined where 70% of the CR comes from on the EC_a depth model. Callegary et al. (2007) came up with a better explanation for the model of EC_a associated with McNeill's approximations.

Table **3.2**: Theoretical effective depths for EC_a depth model of both multi-coil and multi-frequency

Inter-coil separation (m)	Coil orientation	Effective depth (cm)
Multi-coil EMI		
0.32 (C1)	VCP_{C1}	25
	HCP_{C1}	50d
0.71 (C2)	VCP_{C2}	50s
	HCP_{C2}	100
1.18 (C3)	VCP_{C3}	90
	HCP_{C3}	180
Multi-frequency EMI		
1.67 (C4)	VCP_{C4}	125
	HCP_{C4}	250

s, shallower; d, deeper; C1 to C4, inter-coil separation

The CR(z) is a fraction of the secondary magnetic field, which is generated between a considered normalized depth, z (where the depth is divided by s – inter-coil separation), and infinite depth. CR is zero at infinity and reaches 1 when z is very small. However, contribution of the air for negative z (between senor and ground surface) is negligible, since most of the responses measured at a depth > z (Callegary et al., 2007). For example, the CR value at 0.3 (30%) in the X-axis for VCP and HCP modes measure responses at depths > 0.75*s* and >1.5*s*, respectively. In other words, 70% of CR accounted between 0*s*–0.75*s* and 0*s*–1.5*s* for VCP and HCP mode of operations. Therefore, in general, the effective depths for EC_a measurements are defined as 0.75*s* and 1.5*s* for VCP and HCP modes of operations, respectively (Callegary et al., 2007; Doolittle and Brevik, 2014; McNeill, 1980). However, these effective depths are different for MS_a depth models. Table **3.2** shows effective depth based on EC_a depth models for the multi-coil and multi-frequency EMI sensors.

Relative and cumulative response models of EC_a (Figure **3.2**) for a homogeneously conductive environment, below a normalized depth of *z*, for both coil orientations are given by Eq. 3.2–3.5 (McNeill, 1980):

$$RR_{VCP} = 2 - \frac{4z}{(4z^2+1)^{\frac{1}{2}}} \quad \text{Eq. 3.2}$$

$$RR_{HCP} = \frac{4z}{(4z^2+1)^{\frac{3}{2}}} \quad \text{Eq. 3.3}$$

$$CR_{VCP} = (4z^2+1)^{\frac{1}{2}} - 2z \quad \text{Eq. 3.4}$$

$$CR_{HCP} = \frac{1}{(4z^2+1)^{\frac{1}{2}}} \quad \text{Eq. 3.5}$$

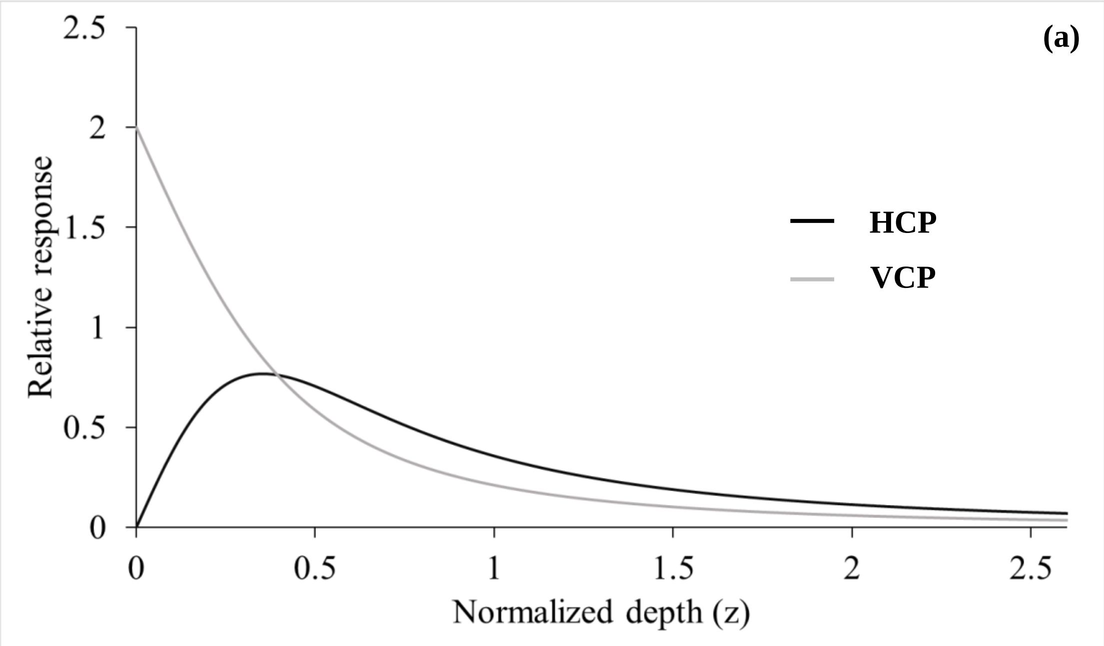

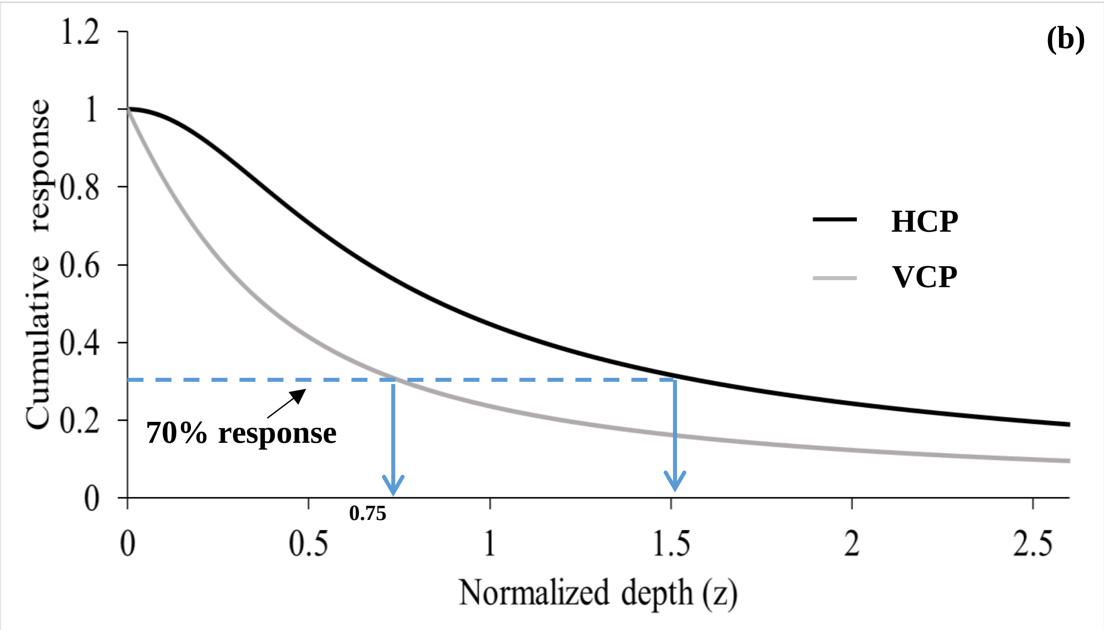

Figure **3.2**: Typical depth sensitivity responses of EC_a depth model: (a) relative response and (b) cumulative response for the function of normalized depth (z)

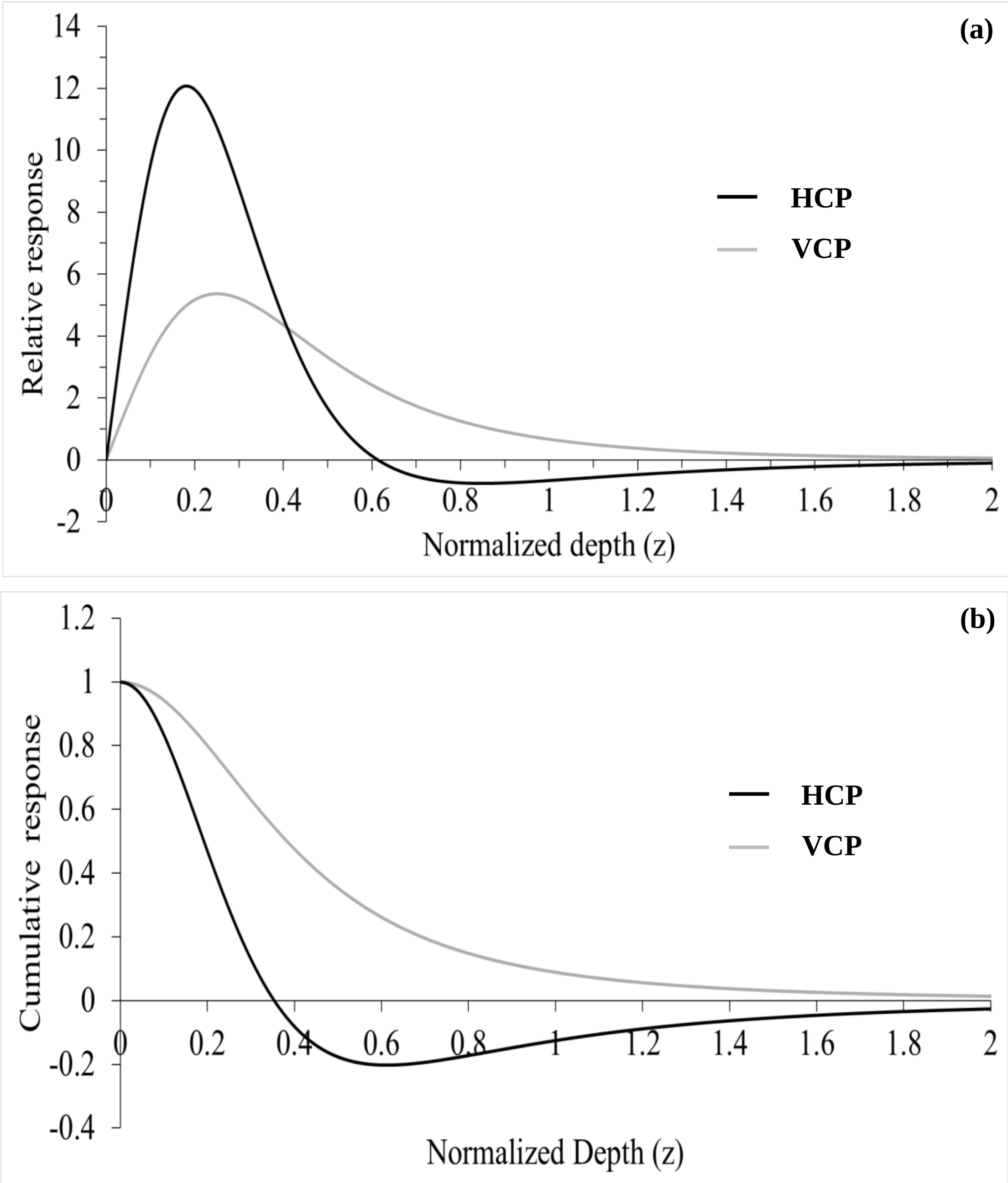

Figure **3.3**: Typical depth sensitivity responses of MS_a depth model: (a) relative response and (b) cumulative response for the function of normalized depth (*z*)

Eq. 3.6–3.9, give relative and cumulative response models, respectively, of MS_a (Figure **3.3**), for a homogeneously conductive environment, below a normalized depth of *z*, for both VCP and HCP coil orientations (Keller and Frischknecht, 1966):

$$RR_{VCP} = \frac{12(z)}{s(4z^2+1)^{\frac{5}{2}}} \qquad \text{Eq. 3.6}$$

$$RR_{HCP} = \frac{12z(3-8z^2)}{s(4z^2+1)^{\frac{7}{2}}} \qquad \text{Eq. 3.7}$$

$$CR_{VCP} = \frac{1}{(4z^2+1)^{\frac{3}{2}}} \qquad \text{Eq. 3.8}$$

$$CR_{HCP} = \frac{1-8z^2}{(4z^2+1)^{\frac{5}{2}}} \qquad \text{Eq. 3.9}$$

Measured data were undergone series of analyses. Descriptive statistical analysis was performed in order to characterize quality of field data measurements from both instruments. Line graphs were created to show raw MS_a data distribution along with one transect (at 3 m on X-axis). Finally, interpolated maps were created from absolute deviation MS_a data to clearly exhibit anomalies from buried objects.

3.5. Results and Discussion

3.5.1 Multi-coil EMI Survey

Descriptive statistics for the multi-coil EMI data are summarized in Table **3.3**. The coefficient of variations (CV) of MS_a varied for Survey-1 from 1.0% to 3.3%, in Survey-2 from 4.8% to 15.4%, and for Survey-3 from 3.7% to 15.2%. The higher CV ranges of Survey-2 and Survey-3 were caused by strong responses from buried metal targets influencing MS_a. Moreover, the means of both surveys look closer to the values of Survey-1 (Table **3.3**). Negative MS_a were observed in the HCP mode of the largest coil separation (C3) after the targets were buried.

Figure **3.4** and **3.5** show line graphs that exhibit distribution of raw MS_a measurements from the multi-coil device for all 3 surveys, for both the VCP and HCP coil orientations on a 15 m transect, where three metal targets were buried. Three key observations can be noticed in both figures:

(i) Only VCP_{C1} (Figure **3.4**a) shows higher variability of MS_a along the transect from 0 to 15 m, including survey-1.

(ii) Three metal targets were identified in the transect. Figure **3.4**c and **3.5**b clearly reveal the presence of metal-3 target, which was buried at 80 cm depth below the surface.

(iii) Only the HCP_{C3} coil orientation (Figure **3.5**c) shows reversal anomalies.

Inferred from the observations (i), higher MS_a variability in the shallowest depth EMI data might be due to highly heterogeneous shallow soil. The anomalies from the targets are very low compared to other coil separations. From observation (ii), the strong anomalous responses (compared to the background) revealed three metal targets buried at depths 80 cm (metal-3), 45 cm (aluminum cans), and 40 cm (metal-2) along the 0 to 15 m transect. The interpretation of the last two observations can be achieved with the help of the theoretical DS models of MS_a. Figure **3.6** and **3.7** show ordinary block kriging interpolated maps of MS_a that show all four small metal targets in the experimental plot.

3.5.1.1 VCP Coil Orientation and Interpretation

Typically, the effective DS from MS_a measurements are lower than the EC_a (Table **3.2** and **3.4**) (Simpson et al., 2009). The theoretical models of MS_a (Figure **3.9**) show that exploration of DS increases with inter-coil separation (ICS). The VCP_{C1} shows only three metal targets with weak responses, and also showed that 90% of the CR was obtained within the 30 cm depth Table **3.4**. Therefore, targets from 35 – 45 cm depth were detected by VCP_{C1}. All four metal targets were detected by the VCP_{C2} and VCP_{C3} coils, and the fourth metal, which was buried at 80 cm depth, was sensed weakly. The observed strength of anomalies from the metal targets diminishes from shallower to deeper layers. The temporal stability on MS_a measurements of the buried targets can be seen in Figure **3.6** and APPENDIX 4, for short (after 10 days) and long-term (after 9 months) stability of EMI readings, respectively. The field MS_a data of the VCP coil configuration could be clearly supported by the theoretical MS_a depth models.

Table **3.3**: Descriptive statistics of MS_a of multi-coil EMI sensor with respect to survey days

EMI surveys	**Total No. of data**	**Mean**	**SD**	**CV**	**Min**	**Max**	**No. data for background mean**	**Background mean**
Survey-1 (Sept 22)								
VCP_{C1}	428	1.98	0.06	3.03	1.85	2.16	116	1.98
VCP_{C2}	428	2.43	0.06	2.47	1.96	2.56	116	2.44
VCP_{C3}	428	2.41	0.08	3.32	1.60	2.57	116	2.41
HCP_{C1}	414	1.95	0.02	1.03	1.90	2.05	113	1.95
HCP_{C2}	414	2.50	0.06	2.40	2.38	2.84	113	2.48
HCP_{C3}	414	2.78	0.08	2.88	2.59	3.79	113	2.77
Survey-2 (Sept 22)								
VCP_{C1}	415	1.97	0.10	5.08	1.75	2.28	115	1.97
VCP_{C2}	415	2.48	0.18	7.26	2.23	3.69	115	2.43
VCP_{C3}	415	2.54	0.26	10.24	2.21	3.77	115	2.43
HCP_{C1}	414	1.86	0.09	4.84	1.76	2.81	115	1.85
HCP_{C2}	414	2.44	0.13	5.33	2.29	3.27	115	2.39
HCP_{C3}	414	2.66	0.41	15.41	-0.95	2.96	115	2.70
Survey-3 (Oct 03)								
VCP_{C1}	444	1.92	0.07	3.65	1.78	2.31	120	1.92
VCP_{C2}	444	2.29	0.18	7.86	2.15	3.53	120	2.23
VCP_{C3}	444	2.33	0.25	10.73	2.14	3.71	120	2.22
HCP_{C1}	421	1.95	0.08	4.10	1.90	2.68	116	1.93
HCP_{C2}	421	2.54	0.14	5.51	2.39	3.51	116	2.48
HCP_{C3}	421	2.70	0.41	15.19	-1.41	3.27	116	2.74

MS_a (ppt) data were used for descriptive statistics; SD, standard deviation; CV, coefficient of variation (%); Min, Minimum; Max, Maximum

Table **3.4**: Descriptive analysis of MS_a depth model of multi-coil and multi-frequency sensors

EMI configurations	70% CR from VCP	Positive peak in RR	Sign-changing point in RR	Sign-changing point in CR	Negative Peak in RR	Negative Peak in CR	90% CR, from VCP
Multi-coil EMI							
VCP_{C1}	20	8	-	-	-	-	30
VCP_{C2}	40	18	-	-	-	-	65
VCP_{C3}	65	30	-	-	-	-	110
HCP_{C1}		**6**	20	**12**	27	20	
HCP_{C2}		**13**	43	**26**	60	43	
HCP_{C3}		**21**	72	**42**	100	72	
Multi-frequency EMI							
VCP	90	42	-	-	-	-	160
HCP		**30**	103	**60**	145	103	

All values are representing depth below the surface in cm; CR – Cumulative Response; RR – Relative Response.

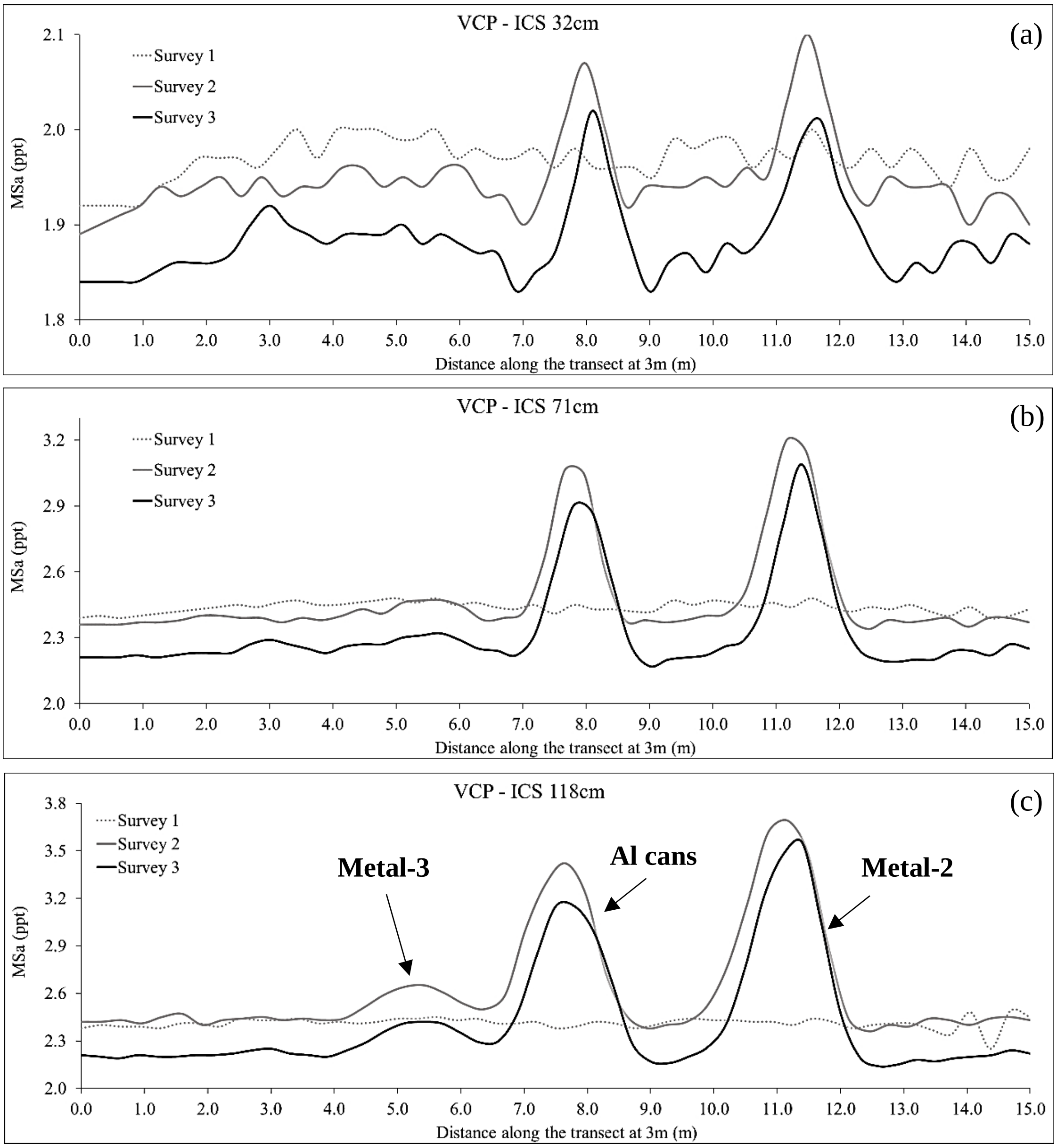

Figure **3.4**: Variability of MS_a of the vertical coplanar (VCP) mode on a transect at 3 m (x-axis) for all 3 surveys of multi-coil EMI sensor: (a) ICS 32 cm; (b) ICS 71 cm; (c) ICS 118 cm.

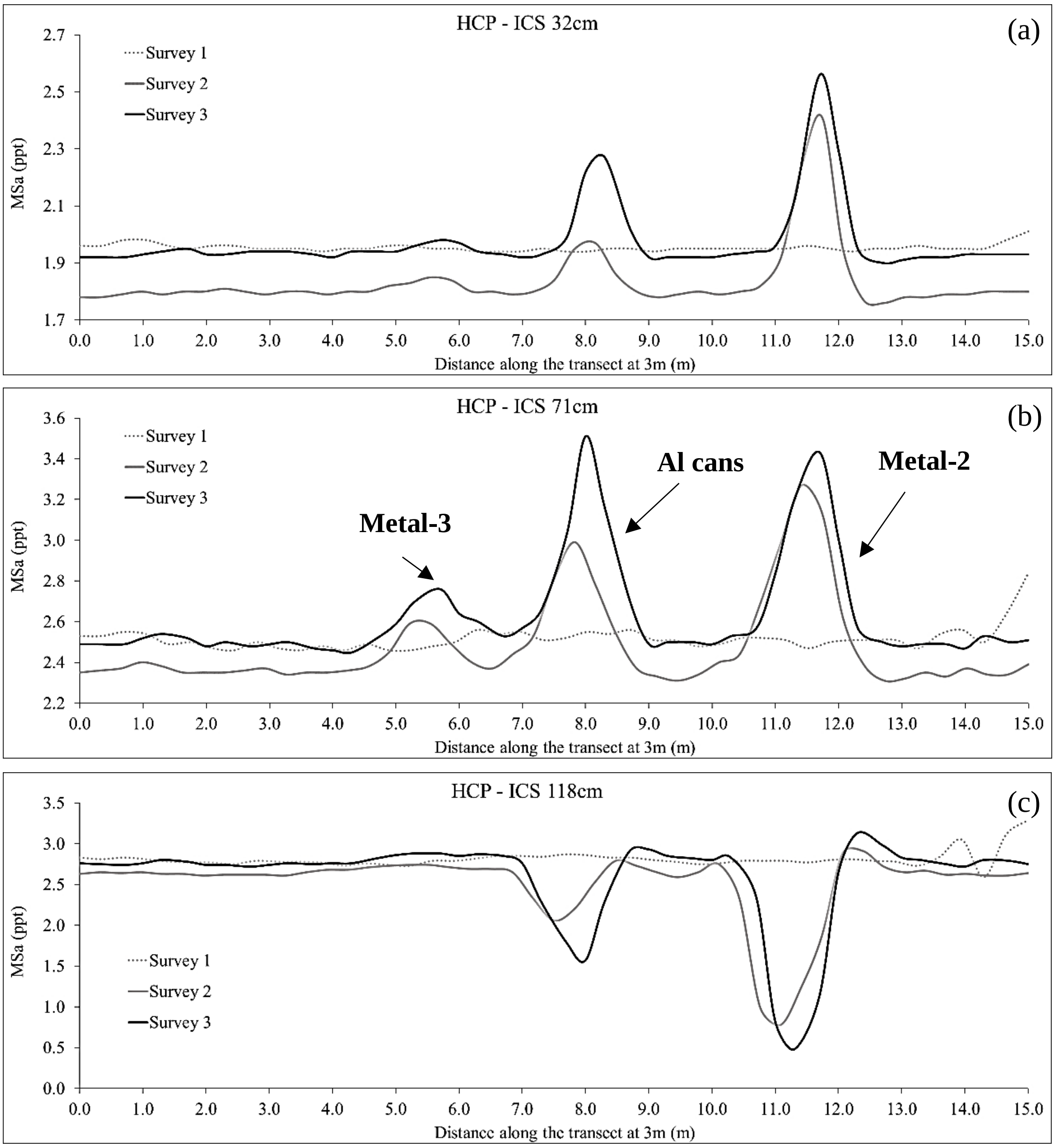

Figure **3.5**: Variability of MS_a of horizontal coplanar (HCP) mode on a transect at 3 m (x-axis) for all 3 surveys of multi-coil EMI sensor: (a) ICS 32 cm; (b) ICS 71 cm; (c) ICS 118 cm.

All targets were located below the depth of the peak response on the relative response (RR) model. The RR declined from the peak and its 90% cumulative response (CR) was reached at depths of 30cm for C1, 65cm for C2, and 110 cm for C3 coil pairs of the VCP orientation. These characteristics could explain that the shallowest buried target induced the strongest anomaly, while the signal response reduces with depth, for the VCP coil orientation (Figure **3.6** b & c).

3.5.1.2 HCP Coil Configuration and Interpretation

The interpretation of MS_a measurements from the HCP mode is more complicated than for the VCP mode (Benech et al., 2016; Noh et al., 2016; Saey et al., 2013; Simpson et al., 2010, 2009; Thiesson et al., 2011). In my results, only the HCP_{C2} coil pair was able to clearly sense the target (metal-3) at the 80 cm depth, while the other two coils showed very weak responses. The strength of the anomalies on the HCP_{C1} of survey-2 and survey-3 decreased from the shallowest target to the deeper, where a similar response was observed in the VCP coils' orientation. However, the theoretical DS model of the HCP is different from the VCP. Two observations could be noticed from the HCP DS model of MS_a (Figure **3.9**):

(i) Negative MS_a anomalies, or MS_a values less than the background, were observed within an area where a few conductive targets were buried. That specific depth was identified as the *sign-changing point* from positive to negative in the CR depth curve: the negative MS_a data were produced when targets were located in between the surface and the *sign-changing point*. Positive measurements were recorded when the targets were located below that specific depth point (*i.e. sign-changing points* in the CR depth curve are 12 cm for C1, 26 cm for C2, and 42 cm for C3).

(ii) The strength of the MS_a anomaly increases towards the *sign-changing point* in the RR depth curve and its strength reduces after that specific depth (*i.e. sign-changing points* in the RR curve are 20 cm for C1, 43 cm for C2 and 72 cm for C3).

Several logical relationships could be seen between the CR and RR of MS_a theoretical depth curves. The depth of the negative peak in CR curve and *sign-changing point* in RR curve are shown to be similar values. A depth of the *sign-changing point* in CR is double of the positive peak in RR curve (Table **3.4**).

HCP_{C1}: All targets were located below the *sign-changing point* in the CR (12 cm) as well as in the RR (20 cm) curves. Therefore, positive MS_a values and a decreasing trend in strength of anomaly could be observed from a shallower to a deeper target.

HCP_{C2}: All four metal targets were clearly identified through the HCP_{C2} coil pair. All targets were located below the *sign-changing point* (26 cm); consequently, all MS_a values were positive. The *sign-changing point* of the HCP_{C2} in the RR curve is 43 cm, and, therefore, the two targets buried at depths 40 cm and 45 cm were closer to the critical depth point (43 cm), hence complex to interpret. When considering the two targets buried at 35 cm and 40 cm depths, the increasing trend in the strength of anomaly was observed towards the critical point at 43 cm, and the other two targets, which were buried at 45 cm and 80 cm depths, showed a decreasing trend in the strength of anomaly after the critical point (43 cm).

HCP_{C3}: It shows some negative MS_a measurements in the shallow targets (Figure **3.8**). A clear indication was given for the HCP_{C3} only. The shallowest metal target (at 35 cm), located above the *sign-changing point* in CR (42 cm), produced negative MS_a values. The target at 40 cm sometimes showed positive values too, because it was located near the critical *sign-changing point*. The results revealed that only the deepest target showed highly positive MS_a measurements compared to the background or nearly to the background values, and others exhibited lower than background MS_a values. According to the guideline developed here, the behavior of the anomaly's strength is true even for the HCP_{C3} coil orientation. The *sign-changing point* in the RR curve is 72 cm, and the MS_a of three shallow metallic targets increases towards that point, from negative to positive.

Thiesson et al. (2011) noticed the negative values of in-phase responses of the HCP coil orientation. They mentioned a criterion to identify when the in-phase response of HCP turns to negative responses: when $h>0.45L$, where *h* is the depth of the conductive or magnetic thin layer, and *L* is the ICS of the EMI sensor. This would explain that the deeper targets produce negative values and the shallower targets do not. If compared with the criterion based on my results (the developed guideline), approximately similar values were observed for the multi-coil EMI sensor. However, the concept of negative MS_a is opposite to the above criterion. These guidelines versus (vs.) Thiesson et al.'s (2011) criteria are: for C1, 12 vs. 14 cm; for C2, 26 vs. 32 cm; and for C3, 42 vs. 53 cm for HCP coil orientation.

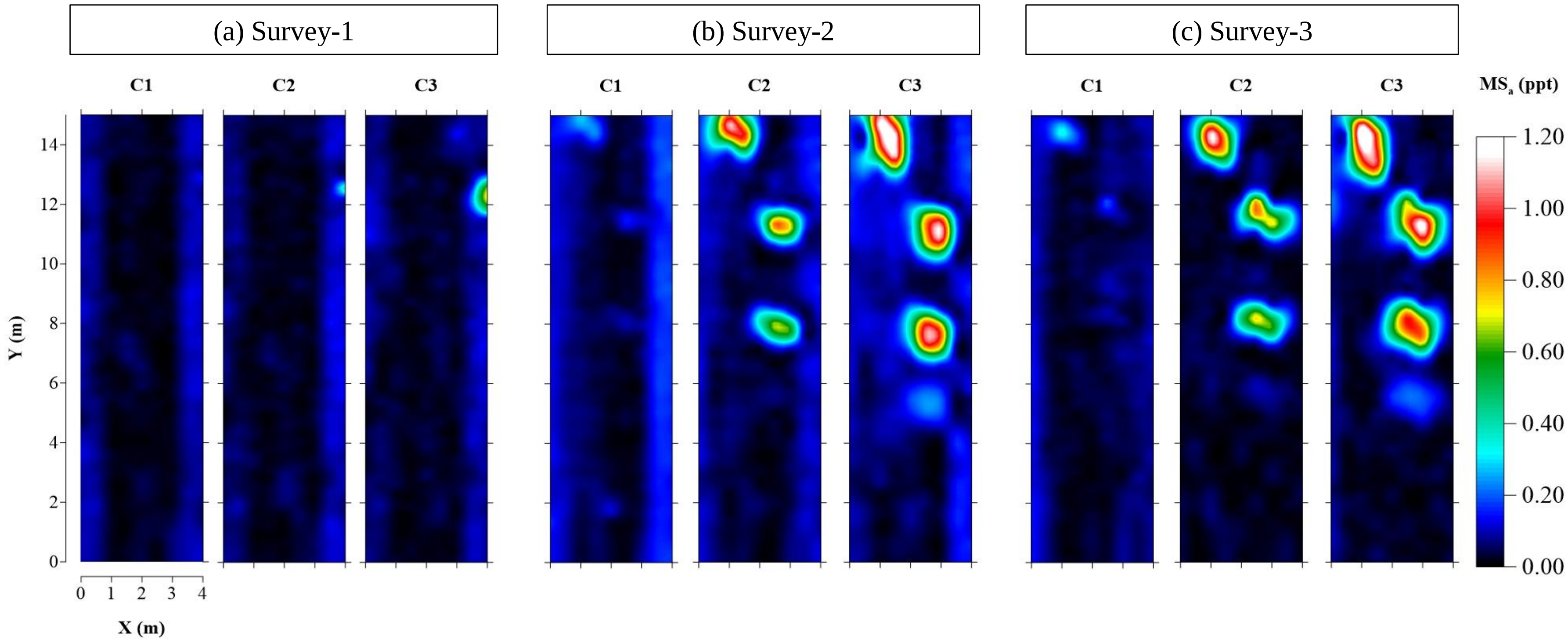

Figure **3.6**: Absolute deviation of MS_a of the VCP coil orientation by multi-coil EMI sensor: (a) Survey-1; (b) Survey-2; (c) Survey-3.

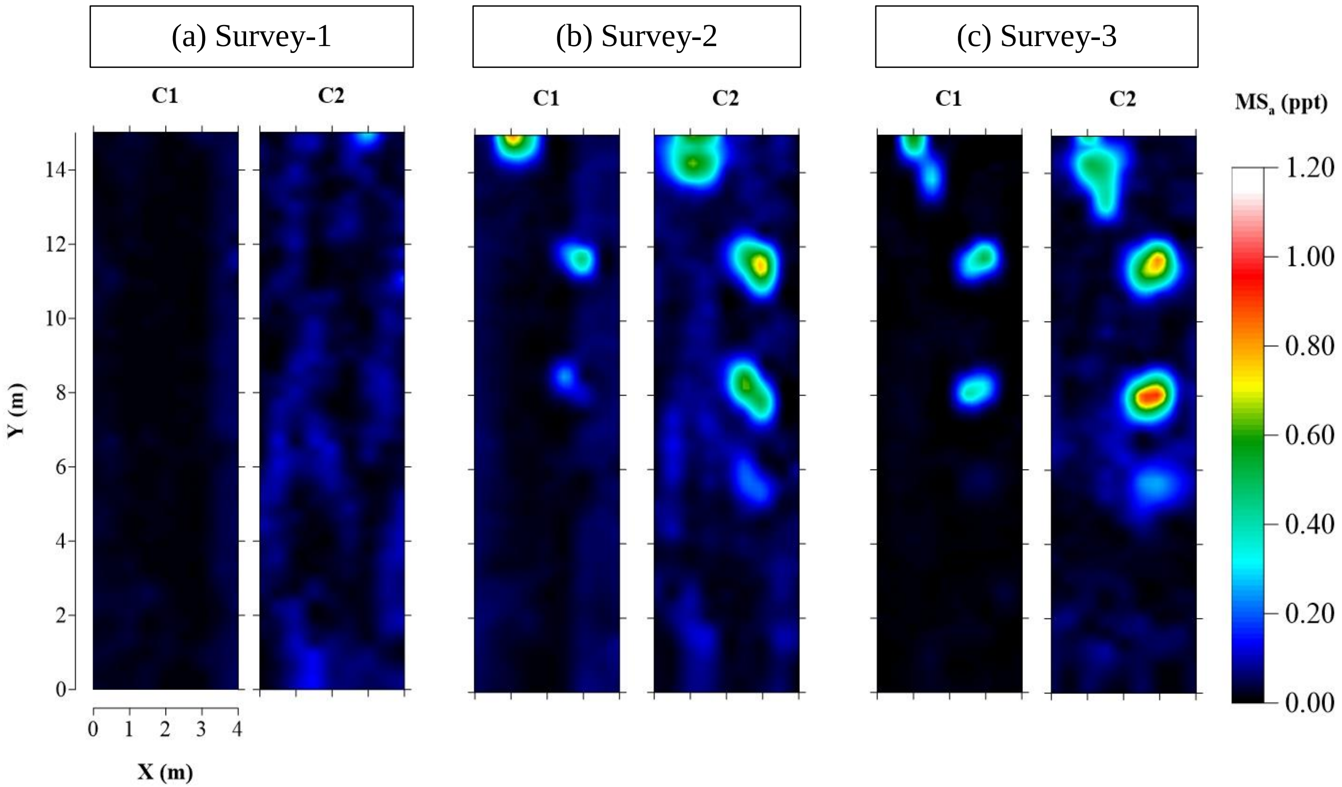

Figure **3.7**: Absolute deviation of MS_a of C1 and C2 of the HCP coil orientation by Multi-coil EMI sensor: (a) Survey-1; (b) Survey-2; (c) Survey-3.

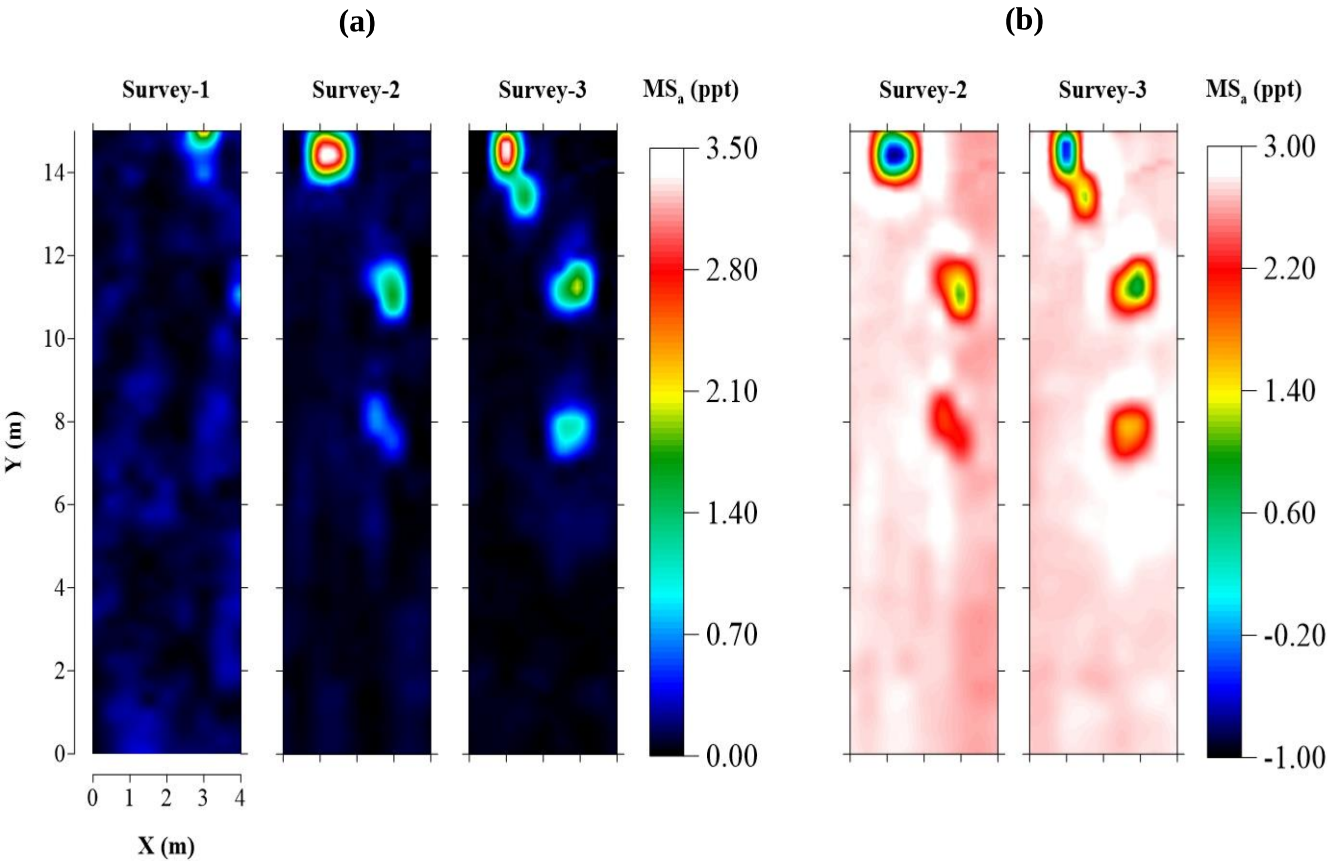

Figure **3.8**: Absolute deviated (a) and raw (b) MS_a data for the HCP-C3 of multi-coil EMI sensor.

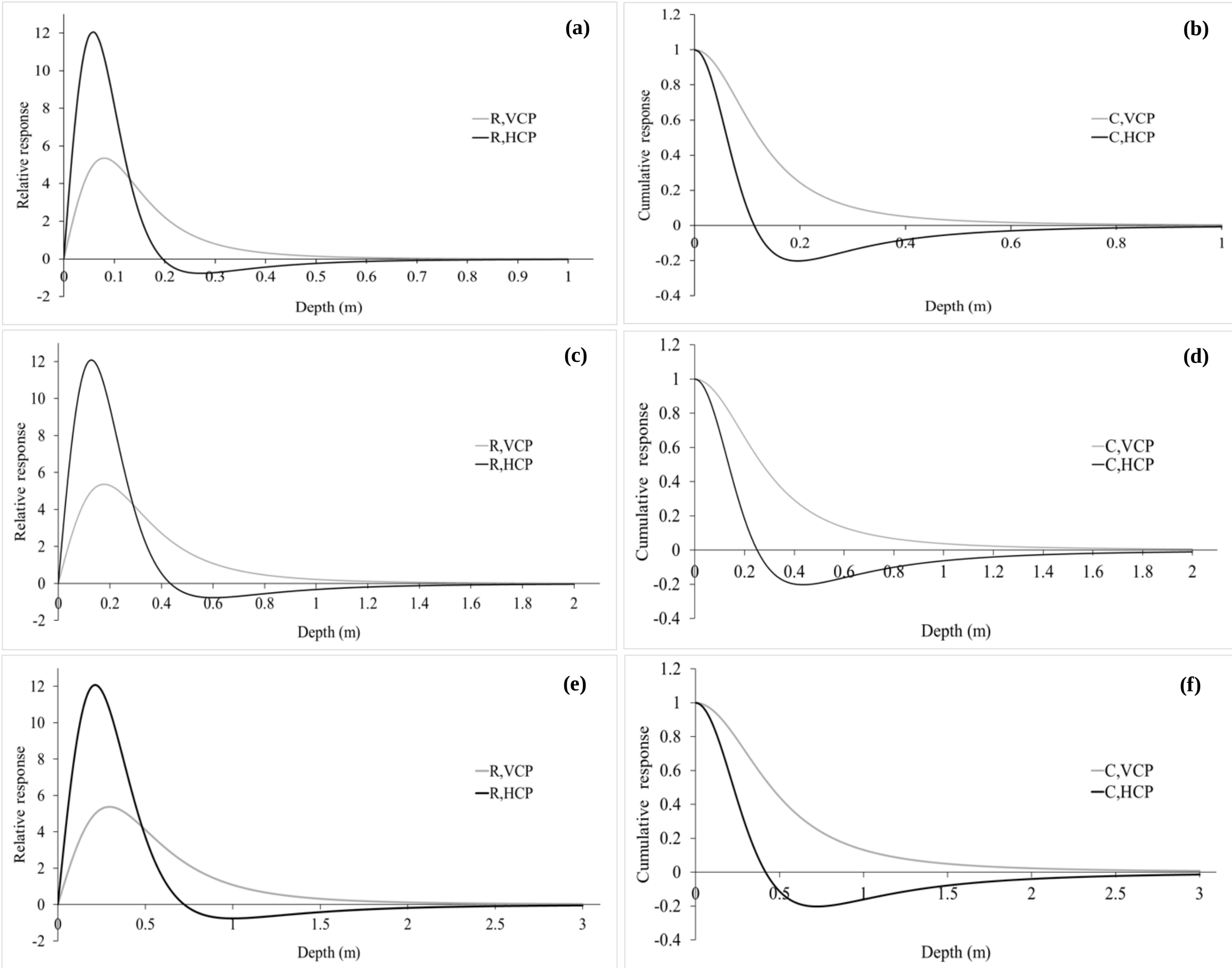

Figure **3.9**: Relative response (RR) and cumulative response (CR) DS models of MS_a as a function of depth: a-b, C1; c-d, C2; e-f, C3 of multi-coil EMI sensor

3.5.2 Multi-frequency EMI Survey

Descriptive statistics of frequencies 18 kHz, 38 kHz, 49 kHz, and 80 kHz of both coil orientations' measurements are displayed in Table **3.5**. From all EMI surveys, only the 80 kHz frequency of the VCP and HCP coils measured negative values of MS_a. CV% ranges for Survey-1 were 10.5%–32.6%, Survey-2 were 11.3%–32.3%, and Survey-3 were, 9.1%–21.1%. There was not much CV% difference displayed between measurements before and after the targets were buried. The mean of 80 kHz in all surveys was negative for both the VCP and the HCP coil orientations.

Preliminary analysis showed that all ordinary block kriging interpolated maps were not appropriate to discuss the measured multi-frequency EMI data, so a specific colour scale was selected for further investigation. Therefore, it is very challenging to interpret the multi-frequency EMI results with respect to our interested targets. Overall, only three metal targets were identified with weak anomalies (Figure **3.10 – 3.12**). The VCP coil pair showed a fairly precise anomaly on the target buried at the 35 cm depth. Also, an increasing trend of anomaly strength could be seen from a lower frequency to a higher frequency (Figure **3.11**a).

Frequencies 18 kHz and 38 kHz of the HCP coil orientation detected three metal targets buried at the depths of 35, 40, and 45 cm. The other two frequencies (49 kHz and 80 kHz) with the HCP mode show only two targets (at depths of 35 and 40 cm). The shallowest target produced lower MS_a values than the background soils for the HCP model of all frequencies (Figure **3.11**b and **3.12**b). The overall results of the multi-frequency EMI sensor provided fewer details (anomaly strength and DS) of small buried targets, and even those were uncertain when compared to the multi-coil sensor.

These results suggested that either selected frequencies of the multi-frequency EMI device or the sensor are not suitable to detect small metallic targets in shallow soils.

Moreover, theoretical DS models of MS_a did not support the measured MS_a data in this particular experimental location. An additional processing technique is needed to improve the performance of the multi-frequency sensor in order to identify subsurface metal targets from surrounding soil properties.

Table **3.5**: Descriptive statistics of MS_a of the multi-frequency EMI with respect to the survey days

EMI surveys	Total No. of data	Mean	SD	CV	Min	Max	No. data for background mean	Background mean
Survey-1 (Sept 22)								
VCP 18 kHz	893	5.67	0.87	15.34	3.18	7.83	240	5.24
VCP 38 kHz	893	7.24	1.00	13.81	4.76	9.45	240	6.78
VCP 49 kHz	938	9.20	0.97	10.54	6.62	11.40	251	8.92
VCP 80 kHz	938	-21.27	1.04	N/A	-24.20	-19.10	251	-21.55
HCP 18 kHz	916	7.94	2.57	32.37	0.78	11.40	246	6.75
HCP 38 kHz	916	8.71	2.84	32.61	0.84	13.00	246	7.37
HCP 49 kHz	910	14.11	2.31	16.37	7.17	17.00	246	12.90
HCP 80 kHz	910	-25.88	2.36	N/A	-33.20	-23.00	246	-27.05
Survey-2 (Sept 22)								
VCP 18 kHz	992	5.14	0.68	13.23	2.82	6.96	267	4.97
VCP 38 kHz	992	6.65	0.75	11.28	3.71	8.69	267	6.44
VCP 49 kHz	957	6.88	0.80	11.63	3.92	8.74	257	6.81
VCP 80 kHz	957	-24.11	0.90	N/A	-27.10	-21.27	257	-24.22
HCP 18 kHz	962	9.90	2.55	25.76	2.84	13.45	258	8.82
HCP 38 kHz	962	11.51	2.78	24.15	3.71	15.53	258	10.34
HCP 49 kHz	929	8.24	2.66	32.28	1.09	12.05	250	6.63
HCP 80 kHz	929	-32.83	2.65	N/A	-40.34	-28.51	250	-34.31
Survey-3 (Oct 03)								
VCP 18 kHz	920	7.49	0.76	10.15	5.30	9.88	248	7.43
VCP 38 kHz	920	9.33	0.85	9.11	6.47	11.50	248	9.29
VCP 49 kHz	927	10.69	1.02	9.54	8.35	13.25	250	10.44
VCP 80 kHz	927	-19.94	1.06	N/A	-22.69	-17.41	250	-20.15
HCP 18 kHz	906	13.74	2.85	20.74	5.35	17.84	245	12.37
HCP 38 kHz	906	15.89	3.35	21.08	2.38	20.31	245	14.56
HCP 49 kHz	929	18.35	2.65	14.44	10.48	21.81	250	17.56
HCP 80 kHz	929	-21.98	2.88	N/A	-32.96	-18.10	250	-22.62

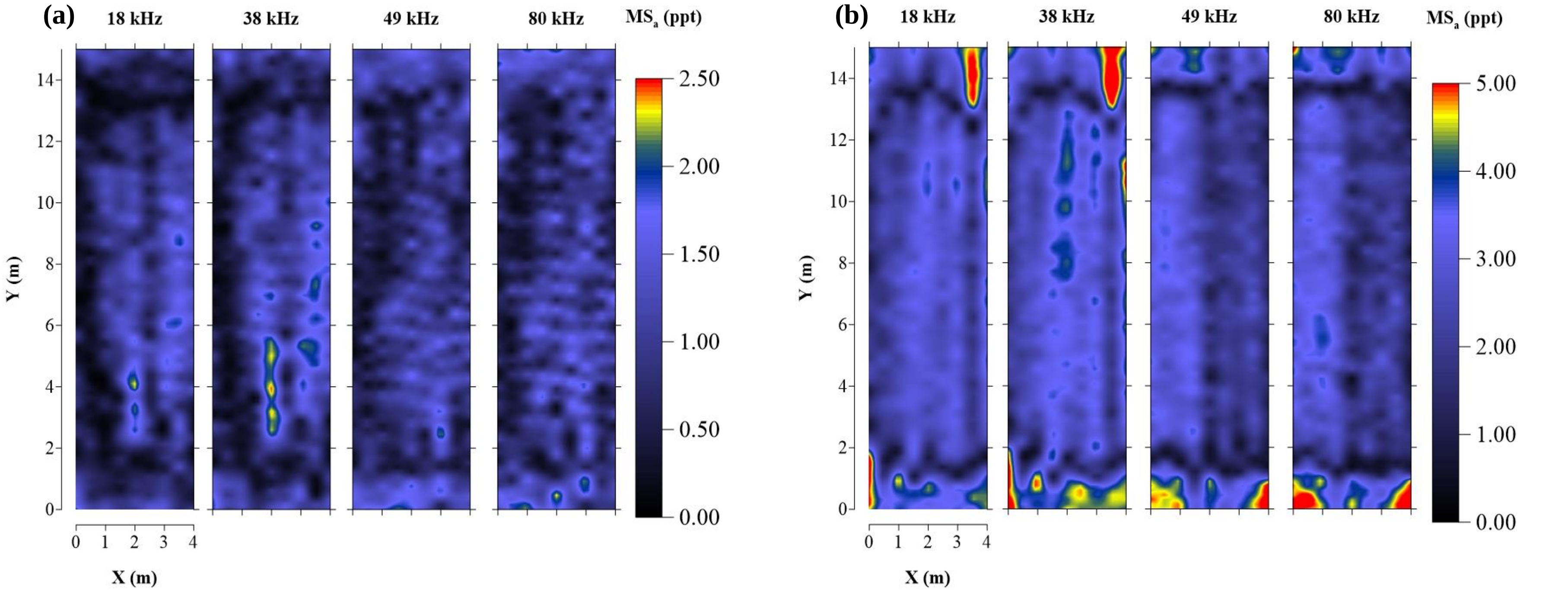

Figure **3.10**: Absolute deviation of MS_a of multi-frequency EMI for Survey-1: (a) VCP and (b) HCP coil pairs.

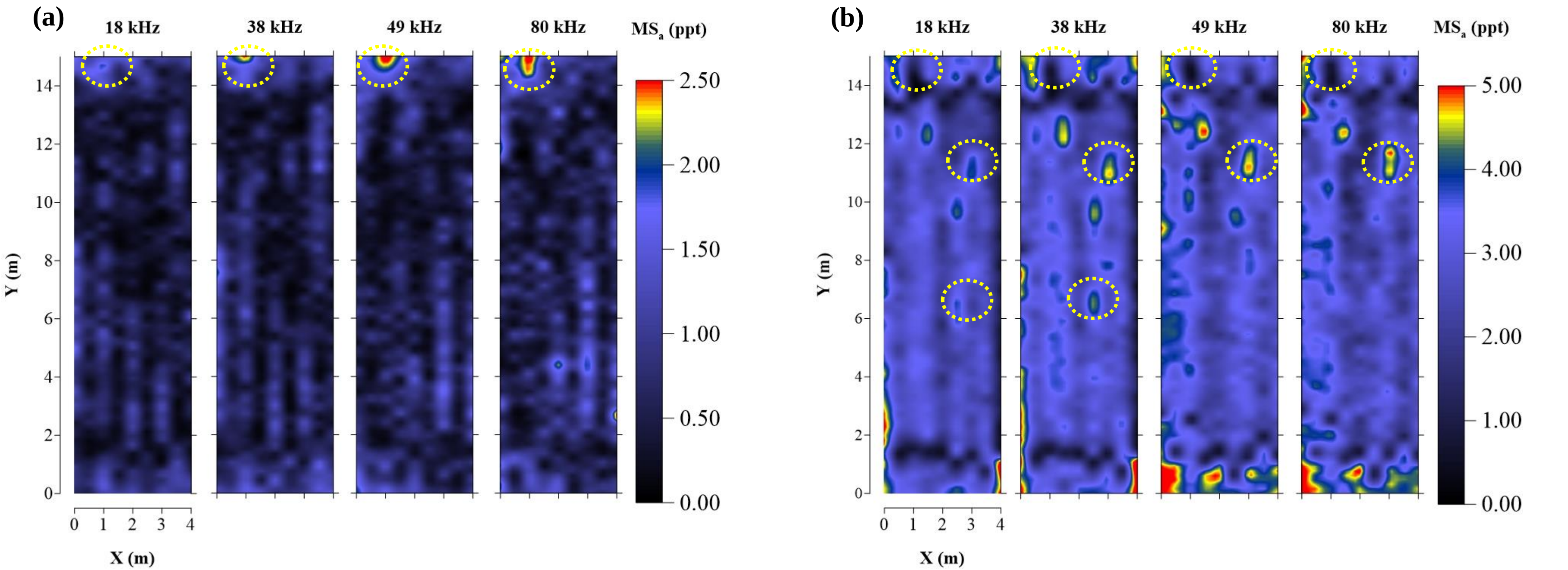

Figure **3.11**: Absolute deviation of MS$_a$ of multi-frequency EMI for Survey-2: (a) VCP and (b) HCP coil pairs. Dotted circles show some buried locations

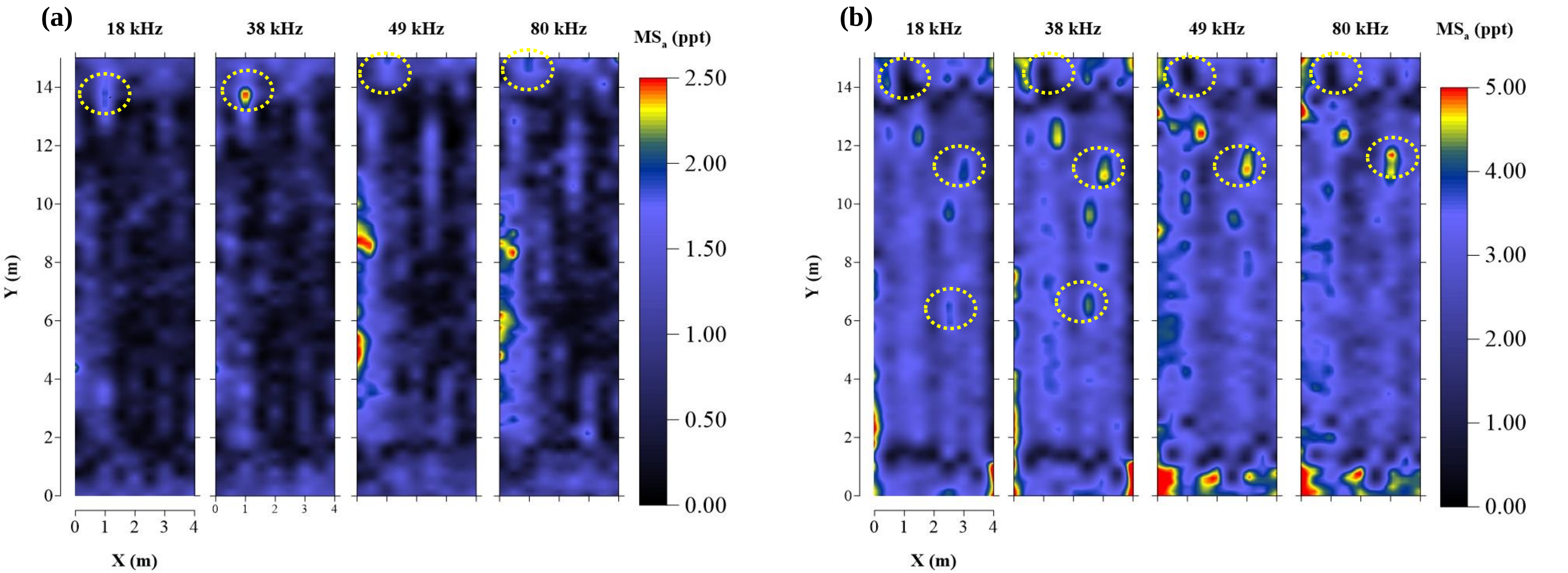

Figure **3.12**: Absolute deviation of MS_a of multi-frequency for Survey-3: (a) VCP and (b) HCP coil pairs. Dotted circles show some buried locations

3.5.3 GPR Data Analysis

The actual depth of all buried targets, including plastic bottles and metals, were detected by the GPR method. The GPR method gives more precise DS measurements than EMI sensors, as expected. The DS of the GPR is entirely dependent on wave velocity in the subsurface and the frequency used. Table **3.6** shows the GPR surveys with three different frequencies and measured actual depths of buried targets. A relationship between the actual depth of the reflector and the measured depth of the corresponding hyperbola were fitted using a linear regression model (Table **3.7**). Figure **3.13** shows reflections from all metallic and non-metallic (plastic) buried targets clearly. Therefore, EMI and GPR combined integrated analysis is more meaningful when the depth of the target is uncertain with EMI alone.

Table **3.6**: Actual depth vs GPR estimated depth of buried targets for 6 GPR surveys

Buried Target	**Actual Depth (m)**	**GPR Estimated Depth (m)**					
		D1F2	**D2F1**	**D2F2**	**D2F3**	**D3F1**	**D4F2**
Plastic bottles – 1	0.30	0.30	0.31	0.33	0.33	0.38	0.29
Plastic bottles – 2	0.30	0.27	0.27	0.27	0.32	0.28	0.27
Metal – 1	0.35	0.34	0.40	0.29	0.35	0.42	0.30
Metal – 2	0.40	0.36	0.39	0.36	0.38	0.38	0.39
Al Cans	0.45	0.38	0.43	0.38	0.44	0.52	0.45
Plastic bottles – 3	0.45	0.46	0.34	0.41	0.45	0.47	0.51
Plastic bottles – 4	0.50	0.44	0.54	0.46	0.45	0.45	0.43
Metal – 3	0.80	0.67	0.73	0.71	0.71	0.70	0.71

D1-D4, Days, F1-1000 MHz, F2-500 MHz, F3-250 MHz

Table **3.7**: Summary of fitted line plot results for the relationship between actual depth and GPR estimated depth

	D1F2	**D2F1**	**D2F2**	**D2F3**	**D3F1**	**D4F2**
Standard error of estimate (m)	0.027	0.056	0.028	0.013	0.050	0.046
Coefficient of determination (R^2) %	96.0	87.9	96.5	99.1	86.3	91.4
***P*<0.005**	0.000	0.001	0.000	0.000	0.001	0.000

D1-D4, Days, F1-1000 MHz, F2-500 MHz, F3-250 MHz

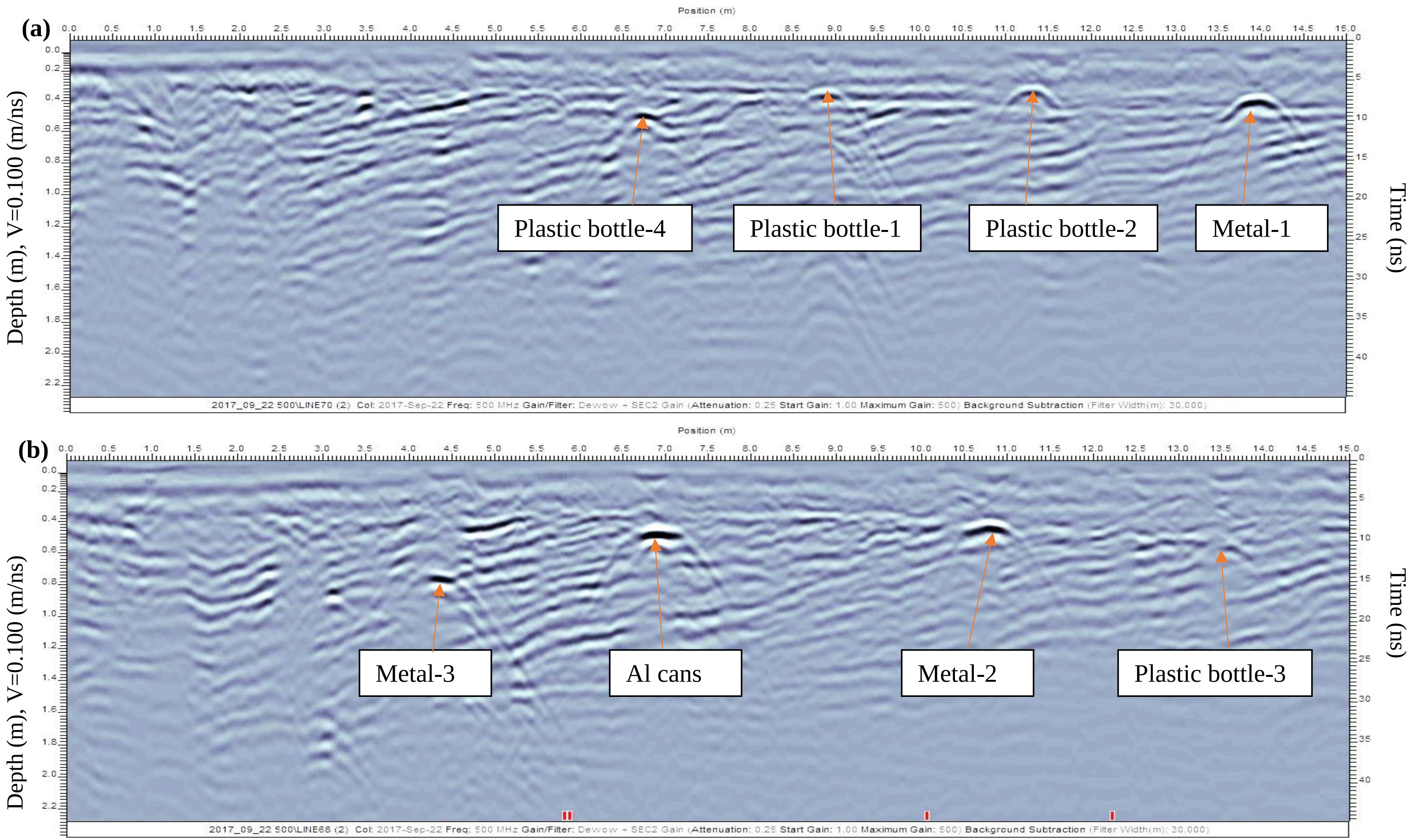

Figure **3.13**: 500 MHz GPR survey carried out (Oct 24, 2017) along the two transects where the targets were buried. (a) transect at 1 m in X axis (b) transect at 3 m in X axis

3.6. Conclusions

Multi-coil and multi-frequency EMI sensors were used to investigate depth sensitivity (DS) of MS_a in shallow soil. The multi-coil sensor provided better performance in respect to detecting small metallic targets compared to the multi-frequency probe, in the tested Podzolic soil. All buried metal targets were detected in all six integral depth layers through the multi-coil EMI surveys, while only three metal targets could be recognized through the multi-frequency EMI surveys. Characterization of MS_a anomalies from three inter-coil separations of the multi-coil were assessed with theoretical DS models. However, the multi-frequency sensor failed to evaluate theoretical DS behavior with these small targets.

The *sign-changing* behavior (negative values of MS_a) of the HCP coil orientation was observed only in the HCP_{C3} of the multi-coil EMI sensor, and as well in both coil orientation surveys of 80 kHz frequency of the multi-frequency. The HCP mode of operations is more complicated compared to the VCP mode.

In all EMI surveys, there were no observations of the plastic bottles filled with salt water and tap water. However, all plastics were identified from the GPR survey data. Integrated EMI and GPR techniques were successfully applied to investigate depth sensitivity analysis using small buried metallic and non-metallic targets.

Negative anomalies will be a good indicator to identify metallic targets in shallow soils. There is a potential application of the MS_a to detect metallic targets (either iron or aluminum) in a shallow soil, as revealed from this experiment. The developed DS guidelines were more suitable for both coil orientations of the multi-coil EMI sensor. From this experiment, DS of by the multi-frequency sensor is still inconclusive for different frequencies, but it may have potential if further processing techniques are applied.

3.7. References

Allred, B.J., Ehsani, M.R., Saraswat, D., 2005. The impact of temperature and shallow hydrologic conditions on the magnitude and spatial pattern consistency of electromagnetic induction measured soil electrical conductivity. Trans. Am. Soc. Agric. Eng. 48, 2123–2135. https://doi.org/10.13031/2013.20098

Allred, B.J., Fausey, N.R., Peters, L., Chen, C., Daniels, J.J., Youn, H., 2004. Detection of buried agricultural drainage pipe with geophysical methods. Appl. Eng. Agric. 20, 307–318. https://doi.org/10.13031/2013.16067

Altdorff, D., Bechtold, M., van der Kruk, J., Vereecken, H., Huisman, J.A., 2016. Mapping peat layer properties with multi-coil offset electromagnetic induction and laser scanning elevation data. Geoderma 261, 178–189. https://doi.org/10.1016/j.geoderma.2015.07.015

Altdorff, D., Galagedara, L., Nadeem, M., Cheema, M., Unc, A., 2018. Effect of agronomic treatments on the accuracy of soil moisture mapping by electromagnetic induction. Catena 164, 96–106. https://doi.org/10.1016/j.catena.2017.12.036

Annan, A.P., 2003. Ground Penetrating Radar Principles, Procedure & Applications. Mississauga, ON. https://doi.org/10.1016/B978-0-444-53348-7.00016-8

Badewa, E., Unc, A., Cheema, M., Kavanagh, V., Galagedara, L., 2018. Soil Moisture

Mapping Using Multi-Frequency and Multi-Coil Electromagnetic Induction Sensors on Managed Podzols. Agronomy 8, 224. https://doi.org/10.3390/agronomy8100224

Barrowes, B.E., Douglas, T.A., 2016. Evaluation of Electromagnetic Induction (EMI) Resistivity Technologies for Assessing Permafrost Geomorphologies.

Benech, C., Dabas, M., Simon, F. -x., Tabbagh, A., Thiesson, J., 2016. Interpretation of shallow electromagnetic instruments resistivity and magnetic susceptibility measurements using rapid 1D/3D inversion. Geophysics 81, E103–E112. https://doi.org/10.1190/geo2014-0549.1

Bevan, B., Rinita, D., 2003. Magnetic Susceptibility Sounding. Weems, VA. https://doi.org/10.13140/RG.2.2.10891.28962

Boaga, J., 2017. The use of FDEM in hydrogeophysics: A review. J. Appl. Geophys. 139, 36–46. https://doi.org/10.1016/j.jappgeo.2017.02.011

Bongiovanni, M. V., Bonomo, N., de la Vega, M., Martino, L., Osella, A., 2008. Rapid evaluation of multifrequency EMI data to characterize buried structures at a historical Jesuit Mission in Argentina. J. Appl. Geophys. 64, 37–46. https://doi.org/10.1016/j.jappgeo.2007.11.006

Callegary, J.B., Ferré, T.P.A., Groom, R.W., 2007. Vertical Spatial Sensitivity and Exploration Depth of Low-Induction-Number Electromagnetic-Induction Instruments. Vadose Zo. J. 6, 158–167. https://doi.org/10.2136/vzj2006.0120

Corwin, D.L., 2005. Geospatial Measurements of Apparent Soil Electrical Conductivity for Characterizing Soil Spatial Variability, in: Soil-Water-Solute Process

Characterization: An Integrated Approach. CRC Press, Boca Raton, FL, pp. 639–672. https://doi.org/10.1201/9781420032086.ch18

Dalan, R.A., 2008. A Review of the Role of Magnetic Susceptibility in Archaeogeophysical Studies in the USA: Recent Developments and Prospects. Archaeol. Prospect. 15, 1–31. https://doi.org/10.1002/arp

Dalan, R.A., Banerjee, S.K., 1998. Techniques of Soil Magnetism. Geoarchaeology 13, 3–36.

De Smedt, P., Saey, T., Lehouck, A., Stichelbaut, B., Meerschman, E., Islam, M.M., Van De Vijver, E., Van Meirvenne, M., 2013. Exploring the potential of multi-receiver EMI survey for geoarchaeological prospection: A 90ha dataset. Geoderma 199, 30–36. https://doi.org/10.1016/j.geoderma.2012.07.019

Delefortrie, S., Hanssens, D., De Smedt, P., 2018. Low signal-to-noise FDEM in-phase data: Practical potential for magnetic susceptibility modelling. J. Appl. Geophys. 152, 17–25. https://doi.org/10.1016/j.jappgeo.2018.03.003

Doolittle, J.A., Brevik, E.C., 2014. The use of electromagnetic induction techniques in soils studies. Geoderma 223, 33–45. https://doi.org/10.1016/j.geoderma.2014.01.027

Drive, C., 2007. Ground Penetrating Radar: Theory and Applications, Cardiovascular Imaging. Elsevier. https://doi.org/10.1016/B978-1-4160-5009-4.50004-2

Fitterman, D. V, Labson, V.F., 2005. 10. Electromagnetic Induction Methods for Environmental Problems, in: Butler, D.K. (Ed.), Near-Surface Geophysics. Society of Exploration Geophysicists, Oklahoma, U.S.A, pp. 301–356.

https://doi.org/10.1190/1.9781560801719.ch10

Huang, H., 2005. Depth of investigation for small broadband electromagnetic sensors. Geophysics 70, 135–142. https://doi.org/10.1190/1.2122412

Huang, H., Won, I.J., San Filipo, B., 2003. Detecting buried nonmetal objects using soil magnetic susceptibility measurements, in: Proceedings of SPIE. pp. 1181–1188. https://doi.org/10.1117/12.485952

Hubbard, S.S., Linde, N., 2011. Hydrogeophysics, Treatise on Water Science. https://doi.org/10.1016/B978-0-444-53199-5.00043-9

Huisman, J.A., Hubbard, S.S., Redman, J.D., Annan, A.P., 2003. Measuring soil water content with ground penetrating radar. Vadose Zo. J. 2, 476–491. https://doi.org/10.2113/2.4.476

Jol, H.M., 2009. Ground Penetrating Radar Theory and Applications. Elsevier, Oxford.

Kadiolu, S., Daniels, J.J., 2008. 3D visualization of integrated ground penetrating radar data and EM-61 data to determine buried objects and their characteristics. J. Geophys. Eng. 5, 448–456. https://doi.org/10.1088/1742-2132/5/4/008

Keiswetter, D.A., Won, I.J., 1997. Multifrequency Electromagnetic Signature of the Cloud Chamber, Nevada Test Site. J. Environ. Eng. Geophys. 2, 99–103. https://doi.org/10.4133/JEEG2.2.99

Keller, G. V, Frischknecht, F.C., 1966. Electrical methods in geophysical prospecting. Pergamon Press, New York.

Kirby, G.E., 1988. Soils of the Pasadena-Deer Lake area, Newfoundland [WWW Document]. URL http://sis.agr.gc.ca/cansis/publications/surveys/nf/nf17/nf17_report.pdf (accessed 11.8.17).

Linford, N.T., 1998. Geophysical Survey At Boden Vean, Cornwall, Including an Assessment of the Microgravity Technique for the Location of Suspected Archaeological Void Features. Archaeometry 40, 187–216. https://doi.org/10.1111/j.1475-4754.1998.tb00833.x

Maas, C., Schmalzl, J., 2013. Using pattern recognition to automatically localize reflection hyperbolas in data from ground penetrating radar. Comput. Geosci. 58, 116–125. https://doi.org/10.1016/j.cageo.2013.04.012

McNeill, J.D., 1980. Electromagnetic Terrain Conductivity Measurement at Low Induction Numbers, Technical note TN-06. Mississauga, ON.

McNeill, J.D., Bosnar, M., 1999. Application of dipole–dipole electromagnetic systems for geological depth sounding, Technical Note TN-31. Mississauga, ON.

Minsley, B.J., Smith, B.D., Hammack, R., Sams, J.I., Veloski, G., 2012. Calibration and Filtering Strategies for Frequency Domain Electromagnetic Data Calibration and fi ltering strategies for frequency domain electromagnetic data. J. Appl. Geophys. 80, 56–66. https://doi.org/10.1016/j.jappgeo.2012.01.008

Moghadas, D., André, F., Slob, E.C., Vereecken, H., Lambot, S., 2010. Joint full-waveform analysis of off-ground zero-offset ground penetrating radar and electromagnetic induction synthetic data for estimating soil electrical properties. Geophys. J. Int. 182, 1267–1278. https://doi.org/10.1111/j.1365-246X.2010.04706.x

Noh, K., Oh, S., Seol, S.J., Lee, K.H., Byun, J., 2016. Analysis of anomalous electrical conductivity and magnetic permeability effects using a frequency domain controlled-source electromagnetic method. Geophys. J. Int. 204, 1550–1564. https://doi.org/10.1093/gji/ggv537

Rubin, Y., Hubbard, S.S., 2005. Hydrogeophysics, Vasa.

Saey, T., De Smedt, P., Delefortrie, S., Van De Vijver, E., Van Meirvenne, M., 2015. Comparing one- and two-dimensional EMI conductivity inverse modeling procedures for characterizing a two-layered soil. Geoderma 241, 12–23. https://doi.org/10.1016/j.geoderma.2014.10.020

Saey, T., De Smedt, P., Meerschman, E., Islam, M.M., Meeuws, F., Van De Vijver, E., Lehouck, A., Van Meirvenne, M., 2012. Electrical conductivity depth modelling with a multireceiver EMI sensor for prospecting archaeological features. Archaeol. Prospect. 19, 21–30. https://doi.org/10.1002/arp.425

Saey, T., Delefortrie, S., Verdonck, L., De Smedt, P., Van Meirvenne, M., 2014. Integrating EMI and GPR data to enhance the three-dimensional reconstruction of a circular ditch system. J. Appl. Geophys. 101, 42–50. https://doi.org/10.1016/j.jappgeo.2013.11.004

Saey, T., Note, N., Gheyle, W., Stichelbaut, B., Bourgeois, J., Van Eetvelde, V., Van Meirvenne, M., 2016. EMI as a non-invasive survey technique to account for the interaction between WW I relicts and the soil environment at the Western front. Geoderma 265, 39–52. https://doi.org/10.1016/j.geoderma.2015.11.020

Saey, T., Van Meirvenne, M., De Smedt, P., Neubauer, W., Trinks, I., Verhoeven, G., Seren, S., 2013. Integrating multi-receiver electromagnetic induction measurements into the interpretation of the soil landscape around the school of gladiators at Carnuntum. Eur. J. Soil Sci. 64, 716–727. https://doi.org/10.1111/ejss.12067

Santos, V.R.N., Porsani, J.L., 2011. Comparing performance of instrumental drift correction by linear and quadratic adjusting in inductive electromagnetic data. J. Appl. Geophys. 73, 1–7. https://doi.org/10.1016/j.jappgeo.2010.10.004

Sasaki, Y., Kim, J.-H., Cho, S.-J., 2010. Multidimensional inversion of loop-loop frequency-domain EM data for resistivity and magnetic susceptibility. Geophysics 75, 213–223. https://doi.org/10.1093/gji/ggv354

Simon, F.-X., Moffat, I., 2015. Identification of shapes and uses of past landscapes through EMI survey, in: Sarris, A. (Ed.), Best Practices of Geoinformatic Technologies for the Mapping of Archaeolandscapes. Archaeopress, Oxford, pp. 25–34.

Simon, F.-X., Sarris, A., Thiesson, J., Tabbagh, A., 2015. Mapping of quadrature magnetic susceptibility/magnetic viscosity of soils by using multi-frequency EMI. J. Appl. Geophys. 120, 36–47. https://doi.org/10.1016/j.jappgeo.2015.06.007

Simon, F.-X., Tabbagh, A., Thiesson, J., Donati, J.C., Sarris, A., 2014. Complex Susceptibility Measurement Using Multi-frequency Slingram EMI Instrument, in: Near Surface Geoscience 2014-20th European Meeting of Environmental and Engineering Geophysics. ATHENES, Greece.

Simpson, D., Van Meirvenne, M., Lück, E., Rühlmann, J., Saey, T., Bourgeois, J., 2010. Sensitivity of multi-coil frequency domain electromagnetic induction sensors to map soil magnetic susceptibility. Eur. J. Soil Sci. 61, 469–478.

https://doi.org/10.1111/j.1365-2389.2010.01261.x

Simpson, D., van Meirvenne, M., Saey, T., Vermeersch, H., Bourgeois, J., Lehouck, A., Cockx, L., Vitharana, U.W.A., 2009. Evaluating the multiple coil configurations of the EM38DD and DUALEM-21S sensors to detect archaeological anomalies. Archaeol. Prospect. 16, 91–102. https://doi.org/10.1002/arp.349

Spies, B.R., 1989. Depth of investigation in electromagnetic sounding methods. GEOPHYSICS 54, 872–888. https://doi.org/10.1190/1.1442716

Tang, P., Chen, F., Jiang, A., Zhou, W., Wang, H., Leucci, G., de Giorgi, L., Sileo, M., Luo, R., Lasaponara, R., Masini, N., 2018. Multi-frequency Electromagnetic Induction Survey for Archaeological Prospection: Approach and Results in Han Hangu Pass and Xishan Yang in China. Surv. Geophys. 1–18. https://doi.org/10.1007/s10712-018-9471-5

Thiesson, J., Rousselle, G., Simon, F.X., Tabbagh, A., 2011. Slingram EMI prospection: Are vertical orientated devices a suitable solution in archaeological and pedological prospection? J. Appl. Geophys. 75, 731–737. https://doi.org/10.1016/j.jappgeo.2011.10.002

Von Hebel, C., Rudolph, S., Mester, A., Huisman, J.A., Kumbhar, P., Vereecken, H., Van Der Kruk, J., 2014. Three-dimensional imaging of subsurface structural patterns using quantitative large-scale multiconfiguration electromagnetic induction data. Water Resour. Res. 50, 2732–2748. https://doi.org/10.1002/2013WR014864

Witten, A.J., Levy, T., Adams, R.B., Won, I.J., 2000. Geophysical Surveys in the Jebel

Hamrat Fidan, Jordan. Geoarchaeology 15, 135–150. https://doi.org/10.1002/(SICI)1520-6548(200002)15:2<135::AID-GEA2>3.0.CO;2-M

Chapter 4: General Summary and Conclusions

This thesis explored the uses of the multi-coil and the multi-frequency EMI sensors in western Newfoundland Podzolic soils. EC_a and MS_a are the two main components measured from the EMI sensors, and both, in particular, were used in my two research studies. Both research studies were conducted at the PBRS, managed by the Department of Fisheries and Land Resources, of the Government of Newfoundland and Labrador, Canada.

Spatiotemporal characterization of soil EC_a variability is essential for agricultural or shallow soil investigations. EMI-EC_a is a proxy of soil's physiochemical properties, and the significance of the properties were assessed through a study. Study-1 (Chapter-2) showed the relationship between EC_a and soil properties under wet and dry conditions, which were established by geostatistical and multivariate statistical approaches, including variogram analyses, PCA, and MLR. The results revealed that investigated significant soil properties on EC_a measurements are: silt, SMC, CEC, EC_w , and sand. Besides, better coil separations, frequencies, and coil orientations were determined for the sandy loam soil. VCP–C3 and HCP–C2 are the most suitable coil separations of the multi-coil EMI sensor, while VCP–49kHz for the multi-frequency is appropriate to investigate soil variability under wet conditions. Spatiotemporal variability of EC_a were illustrated via interpolated maps, which are easy to understand when discussing soil variability over a field scale. The first study inferred that the multi-coil is the more suitable EMI sensor, compared to the multi-frequency, to investigate spatiotemporal variability of EC_a as a proxy of soil properties in the shallow (agricultural) soils in western Newfoundland.

Study-2 (Chapter-3) described the depth sensitivity (DS) analysis of the multi-coil and multi-frequency EMI sensors using small buried targets. The *sign-changing* behavior of some MS_a (negative) measurements of the HCP coil orientation, and the theoretical MS_a DS models of EMI, were difficult to interpret with field measurements. Therefore, I investigated the DS of EMI sensors using small buried targets and assessed it with theoretical DS models of MS_a and validated it with integrated EMI and GPR analyses.

MS_a data were used for mapping and detecting metallic targets. The results revealed that multi-coil EMI probe clearly sensed all four metallic targets from all three coil separations and in both coil orientations. However, only three of the metal targets were identified from the multi-frequency EMI measurements with weak anomalies. The multi-coil sensor is the more accurate and reliable sensor to detect small metallic targets in shallow soils compared to the multi-frequency. To illustrate, a guideline was developed under Chapter-3, to understand and evaluate the negative MS_a values of the HCP of the multi-coil EMI with the theoretical DS models. Finally, I concluded that the multi-coil EMI sensor shows better accuracy predicting the depth of targets than the multi-frequency sensor in the shallow soils of the tested field.

4.1. Recommendations for Future Works

The following recommendations are suggested for further studies,

- Measurements of soil physiochemical properties of deeper soil may develop strong correlations with EMI-EC_a data, since the multi-frequency measures deeper volumes of soil.
- Terrain indices, such as slope and topography of the field, should be considered on EMI survey measurements.
- Regular soil sampling intervals can achieve prediction of more precise SMC variability with EMI surveys throughout the growing season.
- Depth sensitivity analyses and spatiotemporal variability of EMI-EC_a on different soils are needed for soil science studies to improve precision agriculture management on the island portion of Newfoundland and Labrador.
- Systematically bury the metallic targets in 10 cm increments in depth, with the distance between targets higher than the longest ICS of the EMI instruments. These might be useful to gain more understanding about the theoretical DS models.
- Do the same DS analysis of EMI with buried targets for different kinds of soils, such as clay, loamy, and sandy soils. It may better expose the variability of MS_a contrast between background soil and the targets.

APPENDIX 1 Descriptive Analysis of Raw EC_a Data Measured by Both EMI Sensors

Descriptive statistics of raw EC_a (mS/m) data collected on October 13, 2017

Variable	Count	Mean	SD	CV	Min	Max
Multi-frequency EMI						
VCP–18kHz	2525	0.005	< 0.000	0.130	0.005	0.005
VCP–38kHz	2562	2.835	0.698	24.630	0.910	5.880
VCP–49kHz	2525	14.304	0.630	4.410	12.590	16.800
HCP–18kHz	2502	0.005	< 0.000	0.090	0.005	0.005
HCP–38kHz	2548	4.483	0.655	14.600	3.200	7.060
HCP–49kHz	2502	11.748	0.560	4.760	10.640	14.170
Multi-coil EMI						
VCP–C1	1019	-1.274	0.528	-41.420	-2.230	8.510
VCP–C2	1019	2.434	0.312	12.800	1.640	4.110
VCP–C3	1019	2.514	0.341	13.580	0.640	3.620
HCP–C1	1044	-0.350	0.494	-141.210	-1.140	7.650
HCP–C2	1044	3.168	0.336	10.610	1.640	4.670
HCP–C3	1044	3.031	0.360	11.890	1.770	4.090

Shaded variables corresponding to negative values and outliers; SD – standard deviation; CV – coefficient of variation; Min – minimum; Max – maximum;

APPENDIX 2 Experimental Variogram With Pairs of Samples

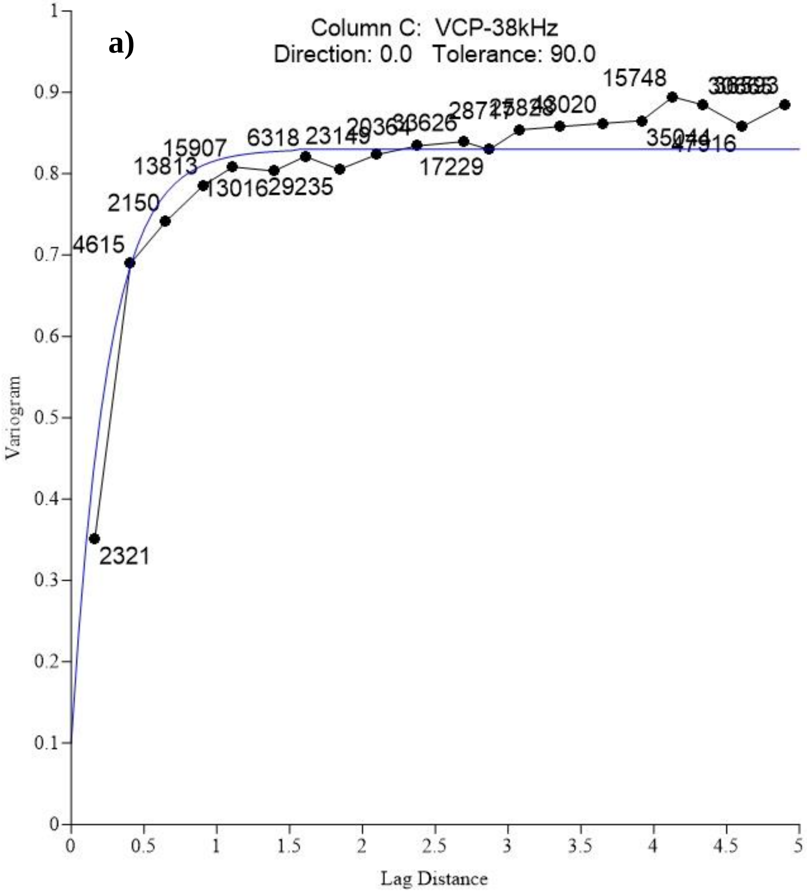

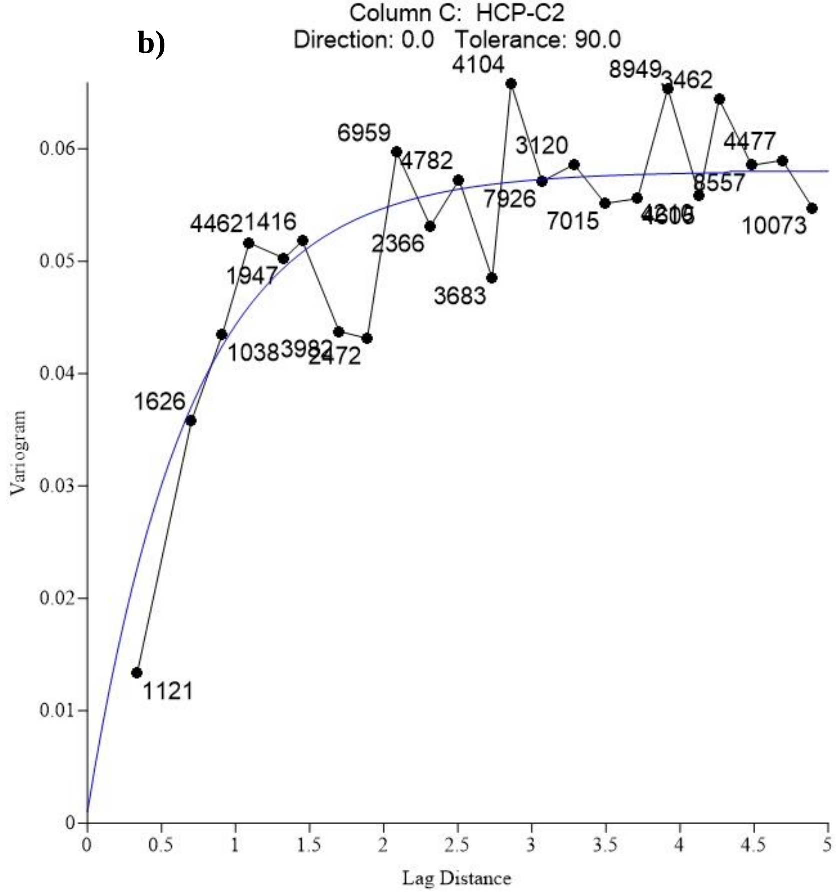

Experimental variogram depicted from multi-frequency EMI data (VCP-38 kHz) fitted with spherical model (a), and multi-coil EMI data (HCP-C2) fitted with exponential model (b).

APPENDIX 3 Temporal EC_a Measurements of Multi-coil EMI Sensor

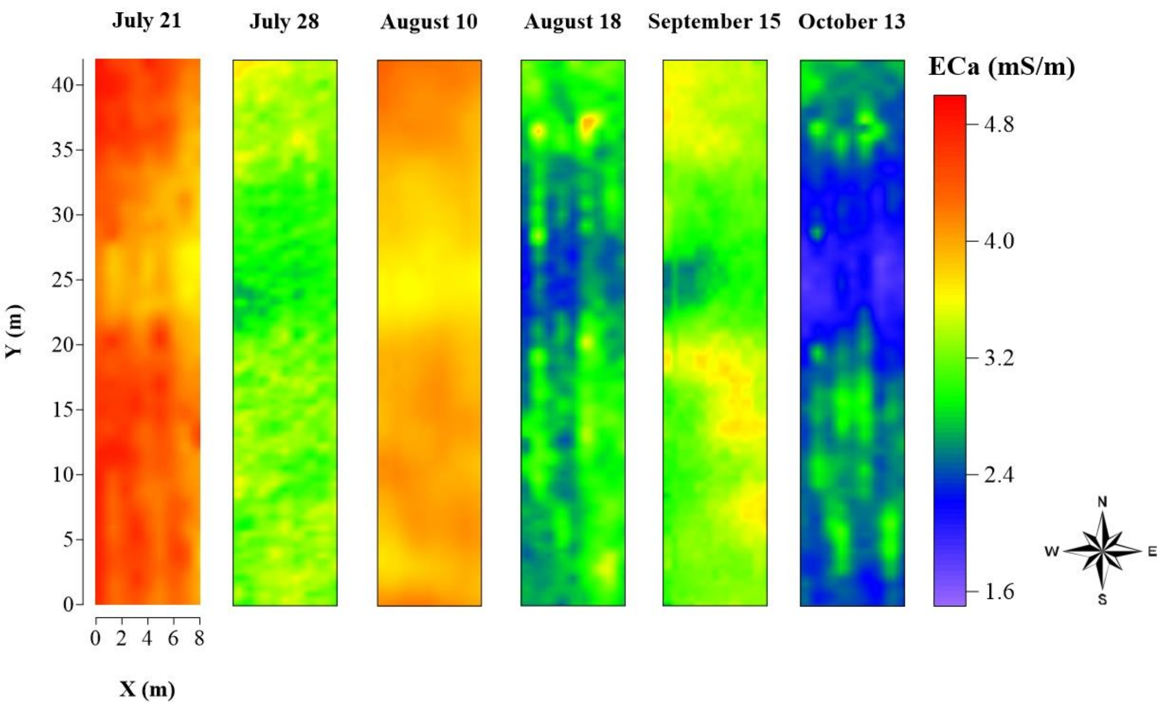

VCP-C2

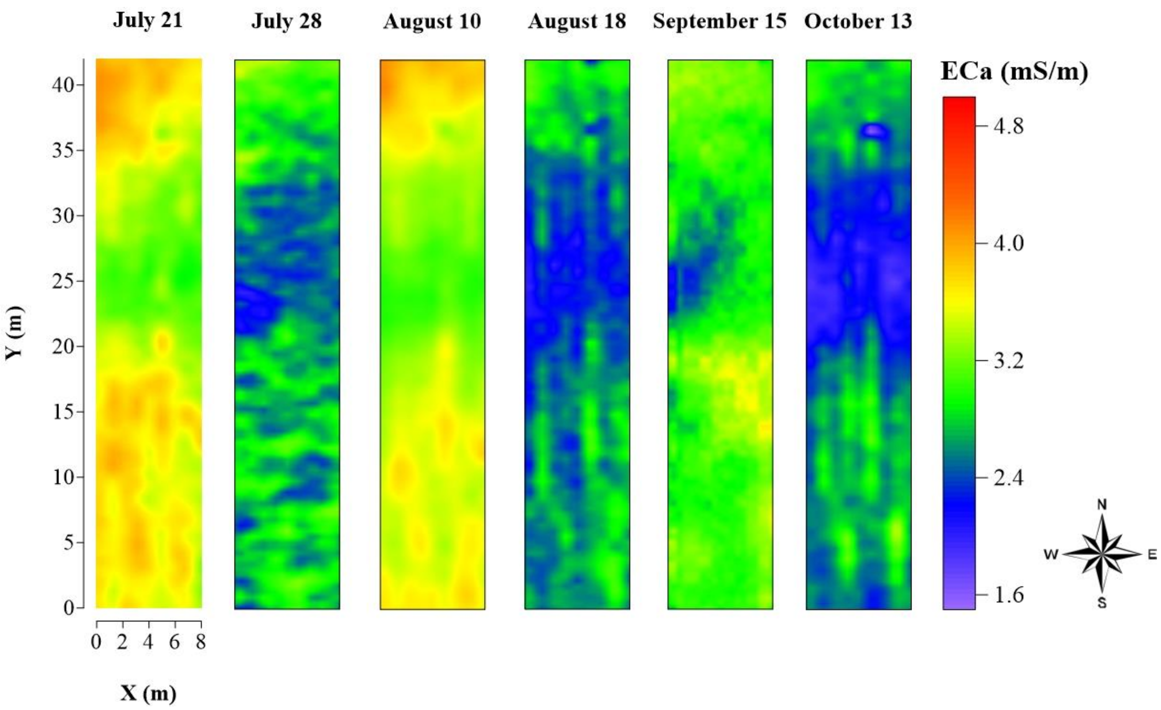

VCP-C3

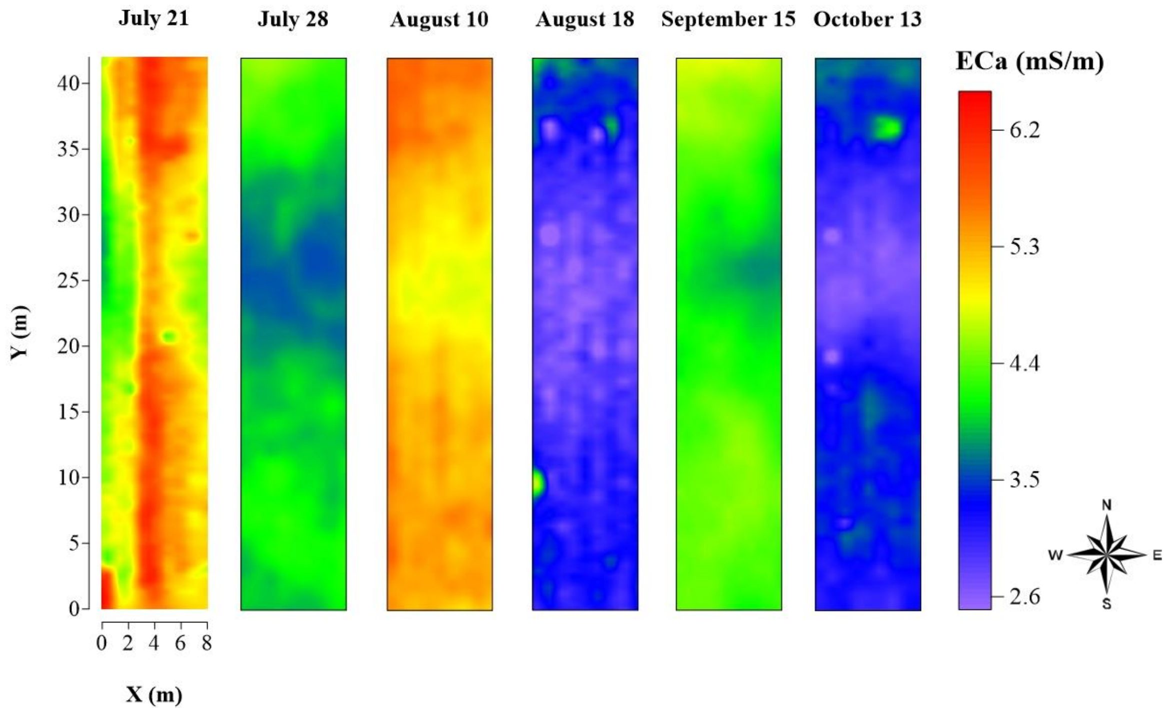
July 21
July 28
August 10
August 18
September 15
October 13
ECa (mS/m)
6.2
5.3
4.4
3.5
2.6
Y (m)
0
5
10
15
20
25
30
35
40
0 2 4 6 8
X (m)
N
W
E
S

HCP-C2

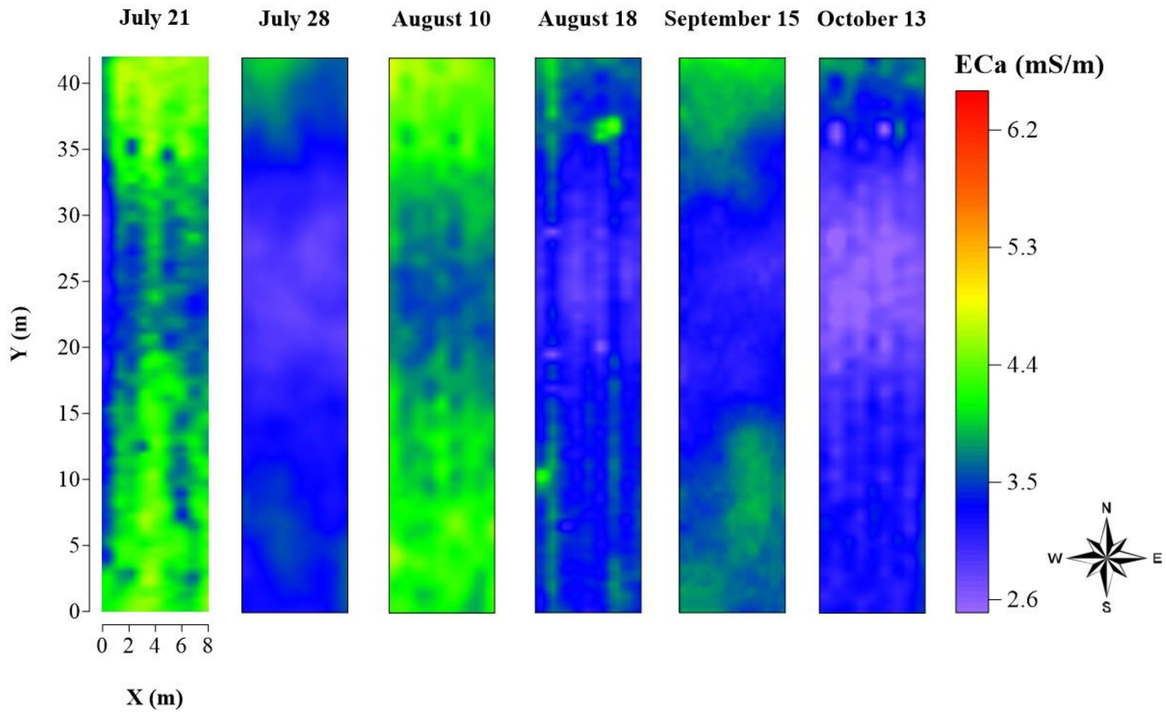
July 21
July 28
August 10
August 18
September 15
October 13
ECa (mS/m)
6.2
5.3
4.4
3.5
2.6
Y (m)
0
5
10
15
20
25
30
35
40
0 2 4 6 8
X (m)
N
W
E
S

HCP-C3

APPENDIX 4 Absolute Deviation MS_a Maps of VCP Coil Orientation by Multi-coil EMI Sensor: 20th of June 2018

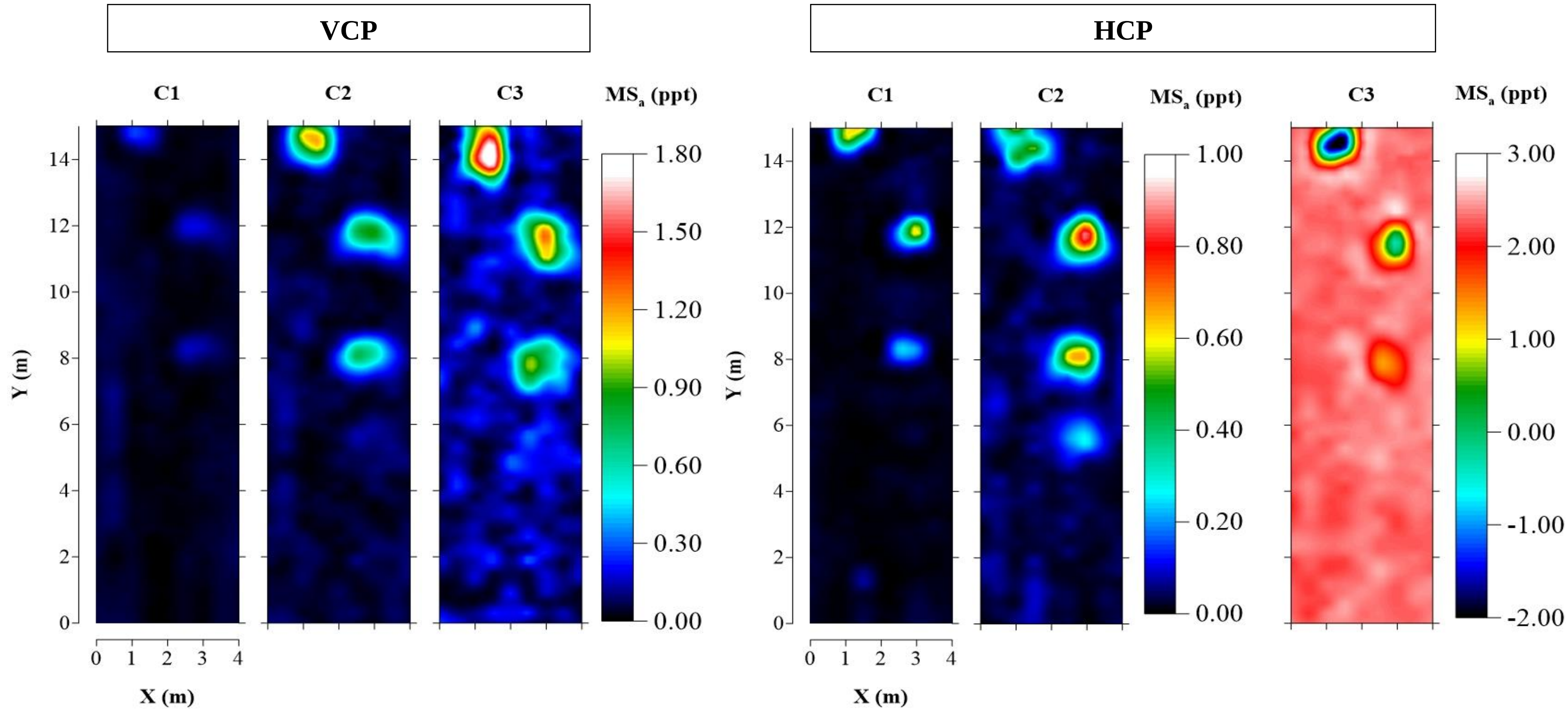

VCP and HCP mode of operation of multi-coil EMI sensor on 20th of June 2018, HCP_{C3} shows raw MS_a data and other maps are created from absolute deviation from background mean of MS_a

APPENDIX 5 Theoretical depth model of MS_a: RR of both sensors and actual depth of buried metallic targets

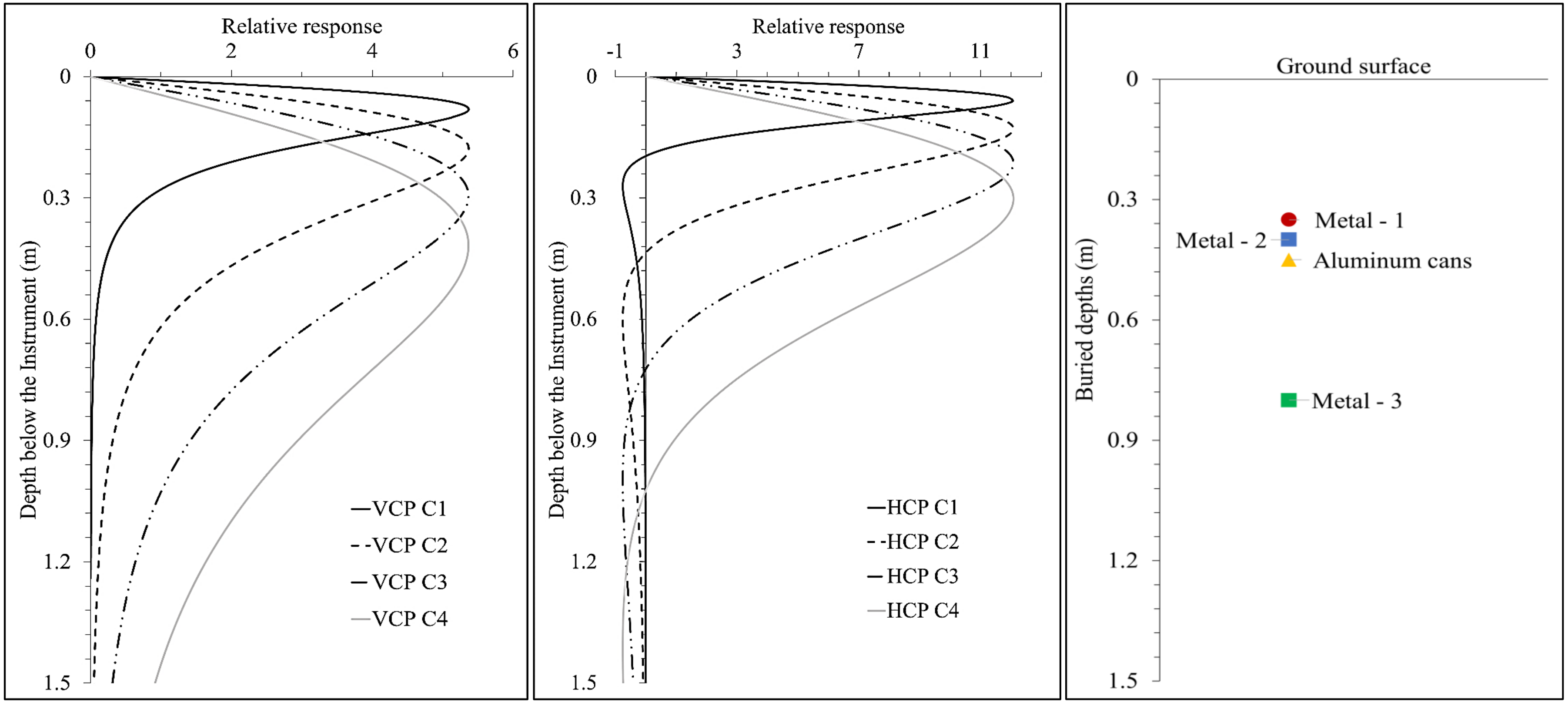

C1-C3, coil separations of multi-coil EMI sensor; C4 is a coil separation of multi-frequency EMI sensor

APPENDIX 6 Theoretical Depth Model of MS_a: CR of Both Sensors and Actual Depth of Buried Metallic Targets

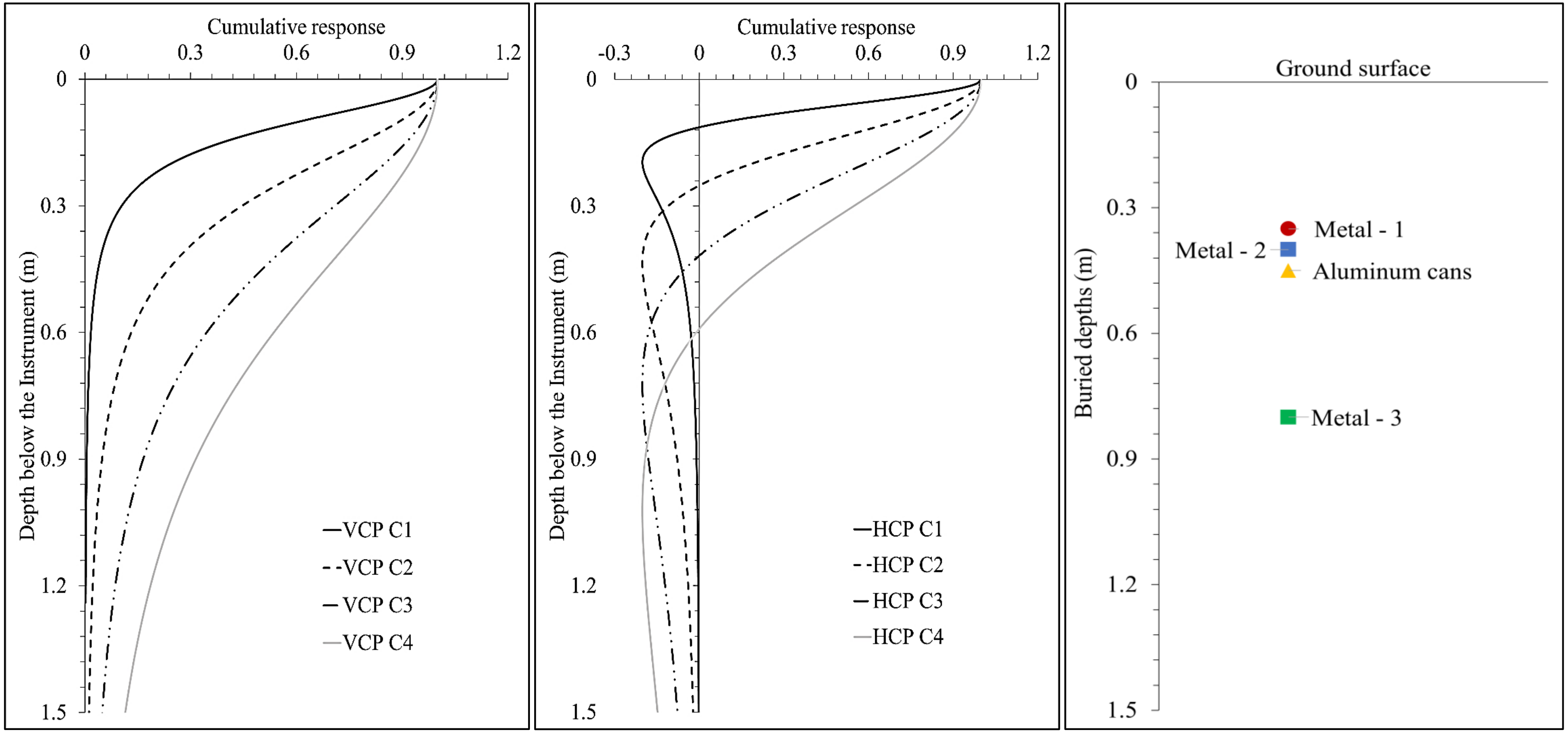

C1-C3, coil separations of multi-coil EMI device; C4 is a coil separation of multi-frequency EMI device